

**International  
Journal of  
Engineering  
Technologies  
(IJET)**

**Printed ISSN: 2149-0104  
e-ISSN: 2149-5262**

**Volume: 1  
No: 2  
June 2015**

**© Istanbul Gelisim University Press, 2015**  
Certificate Number: 23696  
All rights reserved.

*International Journal of Engineering Technologies is an international peer-reviewed journal and published quarterly. The opinions, thoughts, postulations or proposals within the articles are but reflections of the authors and do not, in any way, represent those of the Istanbul Gelisim University.*

**CORRESPONDENCE and COMMUNICATION:**

Istanbul Gelisim University Faculty of Engineering and Architecture  
Cihangir Mah. Şehit P. Onb. Murat Şengöz Sk. No: 8  
34315 Avcılar / Istanbul / TURKEY  
**Phone:** +90 212 4227020 **Ext.** 221  
**Fax:** +90 212 4227401  
**e-Mail:** [ijet@gelisim.edu.tr](mailto:ijet@gelisim.edu.tr)  
**Web site:** <http://ijet.gelisim.edu.tr>  
<http://dergipark.ulakbim.gov.tr/ijet>


**Printing and binding:**

Anka Matbaa  
Sertifika No: 12328  
Tel: +90 212 5659033 - 4800571  
e-Posta: [ankamatbaa@gmail.com](mailto:ankamatbaa@gmail.com)

**International Journal of Engineering Technologies (IJET) is included in:**



**International Journal of Engineering Technologies (IJET) is indexed  
by the following service:**

Organization	URL	Starting Date	Feature
 OpenAIRE The OpenAIRE2020 Project	<a href="https://www.openaire.eu/">https://www.openaire.eu/</a>	2015	Open Access



**INTERNATIONAL JOURNAL OF ENGINEERING TECHNOLOGIES (IJET)**

**International Peer-Reviewed Journal**

**Volume 1, No 2, June 2015, Printed ISSN: 2149-0104, e-ISSN: 2149-5262**

**Owner on Behalf of Istanbul Gelisim University**

Rector Prof. Dr. Burhan AYKAÇ

**Editor-in-Chief**

Prof. Dr. İlhami ÇOLAK

**Associate Editors**

Dr. Selin ÖZÇİRA

Dr. Mehmet YEŞİLBUDAK

**Layout Editor**

Seda ERBAYRAK

**Proofreader**

Özlemnur ATAOL

**Copyeditor**

Evrin GÜLEY

**Contributor**

Ahmet Şenol ARMAĞAN

**Cover Design**

Tarık Kaan YAĞAN

## **Editorial Board**

Professor İlhami COLAK, Istanbul Gelisim University, Turkey

Professor Dan IONEL, Regal Beloit Corp. and University of Wisconsin Milwaukee, United States

Professor Fujio KUROKAWA, Nagasaki University, Japan

Professor Marija MIROSEVIC, University of Dubrovnik, Croatia

Prof. Dr. Şeref SAĞIROĞLU, Gazi University, Graduate School of Natural and Applied Sciences, Turkey

Professor Adel NASIRI, University of Wisconsin-Milwaukee, United States

Professor Mamadou Lamina DOUMBIA, University of Québec at Trois-Rivières, Canada

Professor João MARTINS, University/Institution: FCT/UNL, Portugal

Professor Yoshito TANAKA, Nagasaki Institute of Applied Science, Japan

Dr. Youcef SOUFI, University of Tébessa, Algeria

Prof.Dr. Ramazan BAYINDIR, Gazi Üniversitesi, Turkey

Professor Goce ARSOV, SS Cyril and Methodius University, Macedonia

Professor Tamara NESTOROVIĆ, Ruhr-Universität Bochum, Germany

Professor Ahmed MASMOUDI, University of Sfax, Tunisia

Professor Tsuyoshi HIGUCHI, Nagasaki University, Japan

Professor Abdelghani AISSAOUI, University of Bechar, Algeria

Professor Miguel A. SANZ-BOBI, Comillas Pontifical University /Engineering School, Spain

Professor Mato MISKOVIĆ, HEP Group, Croatia

Professor Nilesh PATEL, Oakland University, United States

Assoc. Professor Juan Ignacio ARRIBAS, Universidad Valladolid, Spain

Professor Vladimir KATIC, University of Novi Sad, Serbia

Professor Takaharu TAKESHITA, Nagoya Institute of Technology, Japan

Professor Filote CONSTANTIN, Stefan cel Mare University, Romania

Assistant Professor Hulya OBDAN, Istanbul Yildiz Technical University, Turkey

Professor Luis M. San JOSE-REVUELTA, Universidad de Valladolid, Spain

Professor Tadashi SUETSUGU, Fukuoka University, Japan

Associate Professor Zehra YUMURTACI, Istanbul Yildiz Technical University, Turkey

Dr. Rafael CASTELLANOS-BUSTAMANTE, Instituto de Investigaciones Eléctricas, Mexico

Assoc. Prof. Dr. K. Nur BEKIROGLU, Yildiz Technical University, Turkey

Professor Gheorghe-Daniel ANDREESCU, Politehnica University of Timisoara, Romania

Dr. Jorge Guillermo CALDERÓN-GUIZAR, Instituto de Investigaciones Eléctricas, Mexico

Professor VICTOR FERNÃO PIRES, ESTSetúbal/Polytechnic Institute of Setúbal, Portugal

Dr. Hiroyuki OSUGA, Mitsubishi Electric Corporation, Japan

Associate Professor Serkan TAPKIN, Istanbul Gelisim University, Turkey

Professor Luis COELHO, ESTSetúbal/Polytechnic Institute of Setúbal, Portugal

Professor Furkan DINCER, Mustafa Kemal University, Turkey

Professor Maria CARMEZIM, ESTSetúbal/Polytechnic Institute of Setúbal, Portugal

Associate Professor Lale T. ERGENE, Istanbul Technical University, Turkey

Dr. Hector ZELAYA, ABB Corporate Research, Sweden

Professor Isamu MORIGUCHI, Nagasaki University, Japan

Associate Professor Kiruba SIVASUBRAMANIAM HARAN, University of Illinois, United States

Associate Professor Leila PARSA, Rensselaer Polytechnic Institute, United States

Professor Salman KURTULAN, Istanbul Technical University, Turkey

Professor Dragan ŠEŠLIJA, University of Novi Sad, Serbia

Professor Birsen YAZICI, Rensselaer Polytechnic Institute, United States

Assistant Professor Hidenori MARUTA, Nagasaki University, Japan

Associate Professor Yilmaz SOZER, University of Akron, United States

Associate Professor Yuichiro SHIBATA, Nagasaki University, Japan

Professor Stanimir VALTCHEV, Universidade NOVA de Lisboa, (Portugal) + Burgas Free University, (Bulgaria)

Professor Branko SKORIC, University of Novi Sad, Serbia

Dr. Cristea MIRON, Politehnica University in Bucharest, Romania

Dr. Nobumasa MATSUI, MHPS Control Systems Co., Ltd, Japan

Professor Mohammad ZAMI, King Fahd University of Petroleum and Minerals, Saudi Arabia

Associate Professor Mohammad TAHA, Rafik Hariri University (RHU), Lebanon

Assistant Professor Kyungnam KO, Jeju National University, Republic of Korea

Dr. Guray GUVEN, Conductive Technologies Inc., United States

Dr. Tuncay KAMAŞ, Eskişehir Osmangazi University, Turkey

## **From the Editor**

Dear Colleagues,

On behalf of the editorial board of International Journal of Engineering Technologies (IJET), I would like to share our happiness to publish the second issue of IJET. My special thanks are for members of editorial board, editorial team, referees, authors and other technical staff.

Please find the second issue of International Journal of Engineering Technologies at <http://dergipark.ulakbim.gov.tr/ijet>. We invite you to review the Table of Contents by visiting our web site and review articles and items of interest. IJET will continue to publish high level scientific research papers in the field of Engineering Technologies as an international peer-reviewed scientific and academic journal of Istanbul Gelisim University.

Thanks for your continuing interest in our work,

**Professor ILHAMI COLAK**  
**Istanbul Gelisim University**  
[icolak@gelisim.edu.tr](mailto:icolak@gelisim.edu.tr)

---

<http://dergipark.ulakbim.gov.tr/ijet>  
**Printed ISSN: 2149-0104**  
**e-ISSN: 2149-5262**

International Journal of  
Engineering Technologies  
**IJET**



# Table of Contents

	Page
<i>From the Editor</i>	vii
<i>Table of Contents</i>	ix
<u>Analysis on Meeting the Electric Energy Demand With Small Wind Turbine in Turkey</u>	
<i>Haci Sogukpinar, İsmail Bozkurt</i>	51-55
<u>Application of Soft Computing Models to Daily Average Temperature Analysis</u>	
<i>Mustafa Göçken, Aslı Boru, Ayşe Tuğba Dosdoğru, Nafiz Berber</i>	56-64
<u>In-Situ Measurement Via E/M Impedance Spectroscopy Technique Using Shear Horizontal Piezoelectric Wafer Active Sensors</u>	
<i>Tuncay Kamaş</i>	65-71
<u>Single Phase Series Active Filter Load Compensation for Aircraft Applications</u>	
<i>Mohammad H. Taha</i>	72-77
<u>Original Solution for Structural and Functional Rehabilitation of Masonry Buildings</u>	
<i>Kubilay Kaptan</i>	78-82
<u>Calculation of Aerodynamic Performance Characteristics of Airplane Wing and Comparing with the Experimental Measurement</u>	
<i>Haci Sogukpinar, İsmail Bozkurt</i>	83-87
<u>Seismic Fragility Curves for 1 and 2 Stories R/C Buildings</u>	
<i>Muhammed Tekin, Ali Gürbüz</i>	88-94

**International Journal of Engineering Technologies, IJET**

**e-Mail:** [ijet@gelisim.edu.tr](mailto:ijet@gelisim.edu.tr)

**Web site:** <http://ijet.gelisim.edu.tr>  
<http://dergipark.ulakbim.gov.tr/ijet>

# Analysis on Meeting the Electric Energy Demand with Small Wind Turbine in Turkey

Hacı Sogukpinar\*†, Ismail Bozkurt\*\*

\*Department of Energy Systems Engineering, Faculty of Technology, University of Adiyaman, Adiyaman 02040, Turkey

\*\* Department of Mechanical Engineering, Faculty of Engineering, University of Adiyaman, Adiyaman 02040, Turkey

hsogukpinar@adiyaman.edu.tr, ibozkurt@adiyaman.edu.tr

†Corresponding Author; Hacı Sogukpinar, Department of Energy Systems Engineering, Faculty of Technology, University of Adiyaman, Adiyaman 02040, Turkey, Tel: +90 416 223 38 00/2840, hsogukpinar@adiyaman.edu.tr

*Received: 27.05.2015 Accepted: 08.06.2015*

**Abstract-** Wind energy is one of the most important renewable energy sources in terms of huge potential. Turkey has adequate wind energy potential to generate its own electricity. Together with the technological developments of wind turbine, generating electricity from wind energy is becoming increasingly common in Turkey and around the world. In this study, Turkey's wind energy potential and a small wind turbine to meet the electricity needs of a home were analysed economically. Installation height of the wind turbine is lower compared to other large turbine so wind speed can be slightly lower. Therefore smaller generator with larger wind turbine blade was scheduled to be assembled to meet the electricity needs for a house in Turkey. Cost of a system is about \$ 6,576 and this system can pay for itself in 10 years.

**Keywords** Wind energy, wind turbine, economic analysis

## 1. Introduction

Wind turbine is one of the important renewable technologies. Wind technology is approaching maturity and has demonstrated the capability to play a significant role in the world's future energy demand [1]. Turkey is a country with rich wind potential. Investments that are related with wind energy are growing rapidly with government support. After 2005 installed wind power capacity in Turkey has started to increase so fast. In 2005 total installed capacity in Turkey reached only 20.1 MW and 3762.10 MW by 2014 [2]. There are many studies on wind turbine and its economic analysis in the literature. Ozerdem et. al. [3] studied the technical and economic feasibility of wind farms in Izmir, Turkey. The method was applied to a potential wind farm site located in Izmir, Turkey. Akdag and Guler [4] investigated the wind energy development, new wind power plant license applications and wind electricity generation cost analyses in Turkey. Li et. al. [5] suggested a methodology to accurately evaluate the economic viability of a micro wind turbine on a case-by-case basis. The methodology was used to demonstrate the realistic economic analysis of a number of micro wind turbines available in Ireland. Mostafaeipour [6] analysed the economic evaluation and applications of three small wind turbines to install some small wind turbine models for the sustainable development of Kerman. Mohammadi and Mostafaeipour [7] evaluated the economic feasibility of electricity generation using six different wind turbines with rated powers ranging from 20 to 150 kW in city of Aligoodarz situated in the west part of Iran. Brusca [8] investigated the implementation of a new statistical based

methodology for energetic and economic evaluation of wind turbine systems without using anemometric measurements for specific installation sites. Mostafaeipour et. al. [9] assessed wind energy potential for the city of Zahedan in south east part of Iran. It was recommended to install Proven 2.5 kW model wind turbine in the region which is the most cost efficient option. Groth and Vogt [10] investigated residents of wind farm locations as a whole and independently as groups to identify what, if any similarities and differences exist between the residents' perceptions. Grieser et. al. [11] investigated the location-specific attractiveness of small wind turbines. The scenarios for different types of small wind turbines were analysed to assess the economic viability various storage system options, support schemes, and specific urban surroundings for the case of Germany.

In this study, the economic possibility of meeting the electric energy demand with small wind turbine was analysed in Turkey. Furthermore, the wind energy potential in Turkey was summarized as well as the economic evaluation of utilizing small scale wind turbines.

## 2. Materials and Methods

Turkey is dependent on foreign fossil fuels and it holds significant amounts of energy-related imports. About \$ 60 billion energy related trade deficit poses a serious problem in the economy. Therefore, in terms of compensating the growing needs of energy, wind energy is very important among alternative resources. Turkey has significant potential

in terms of economic wind potential. The average annual wind speed distribution overall height of 50 m around Turkey is given in Figure 1.

As shown in Figure 1, Aegean coast is seen as having significant potential in terms of wind. Wind power plant installation continues to be concentrated in this region. The economic value of wind across the country is in the coastline of Aegean and Marmara regions, in the Mediterranean region surrounding area of Hatay, coast line of Sinop in the black sea region, and there is local winds caused by the mountainous structure in the inner region. Wind energy potential in Turkey is given in Table 1.

For the high economic value of wind, the total potential is 47,849 MW in the country. As considering the total power of installed plants in the country is 60,000 MW, the total wind potential is almost competent to meet the requirements. The total installed capacity of wind power plants across the country in 2005 was around 20 MW. With the launch of government support after 2005, installations have gained speed and in the first year 31 MW of power plants installation was taken place. In later years installations have continued rising acceleration. As of December 2014, the total installed capacity had increased to 3762 MW.

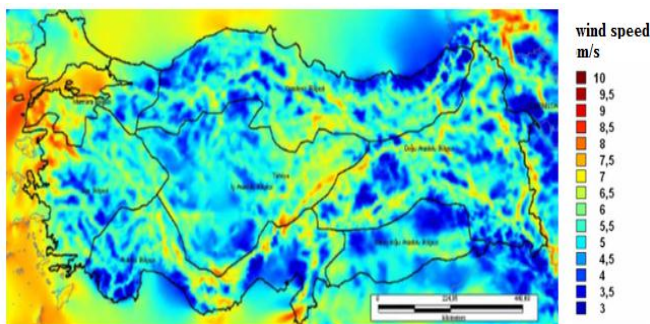


**Fig. 1.** The wind map of Turkey [2]

**Table 1.** Wind powers with respect to wind speed distribution in Turkey [2].

The average annual wind speed (m/s)	Power density (W/m <sup>2</sup> )	Capacity (MW)
7.0-7.5	400-500	29,259.36
7.5-8.0	500-600	12,994.32
8.0-9.0	600-800	5,399.92
>9.0	>800	195.84
	<b>Total</b>	<b>47,849.00</b>
	<b>Onshore (MW)</b>	<b>37,836.00</b>
	<b>Offshore (MW)</b>	<b>10,013.00</b>

Also, the total power of the wind turbines is around 1200 MW which are in the construction phase. The total capacity of wind turbines in the country's 2020 target is expected to be increased to 20,000 MW. Turkey is increasingly turning to renewable energy resources to improve its energy security, and seeks to provide 30% of its electricity from renewable energy by 2023 [12]. Total annual installed capacity has been 500 MW since 2010 and it is expected to be 1000 MW after 2015. 75 % of installations in the country are located in the Aegean and Marmara. Total wind potential for wind speeds between 6,6 and 7 m/s is 83.906 MW at 50 m height. If this potential can be converted to the production, Turkey provides both its needs and rise to the position of energy exporting countries and \$ 60 billion doesn't leave from the country annually. Turkey generates its electricity generally through thermal power plants powered with the natural gas. The country has very few natural gas resources and almost entirely imported. An electricity production cost per kWh in the country is given in Table 2 according to 2015 data.

Referring to Table 2, nuclear power plant in terms of production costs constitutes the highest value. However, considering the country in terms of gaining the installation of this technology will bring many technological achievements. When the wind energy compared with fossil fuels it has serious advantages? Because wind energy system doesn't need any fuel except wind, not producing any waste and government supports makes wind power more attractive. Another important event is now increasing the threat of global warming due to CO<sub>2</sub> emissions. Associated with this situation, The Kyoto Protocol was signed in 1996 and entered into force in 2005. Many countries committed to reduce greenhouse gas emissions to a certain extent in this protocol. Fossil fuels per unit of electricity (kWh) emit approximately 860 g of CO<sub>2</sub>, 210 g SO<sub>2</sub> and 3 g NO<sub>x</sub> to the atmosphere. In mind that the annual consumption for a house is 3600 kWh and if it is supplied from wind energy, in the range of 2880-3420 kg of CO<sub>2</sub> doesn't release into the atmosphere. If this installation built throughout the city at 1000 home, 3,000 tons of CO<sub>2</sub> do not release into the atmosphere every year. This will give chance to the new generations to leave a cleaner world.

**Table 2.** Comparison of cost wind energy with other energy sources [2]

Energy Source	Balanced Unit Energy Cost Range (\$ cent/kWh)
Coal	4,8 - 5,5
Naturel Gas	3,9 - 4,4
Hydropower	5,1 - 11,3
Biomass	5,8 - 11,6
Nuclear	11,1 - 14,5
<b>Wind (*)</b>	<b>4,0 - 6,0</b>

(\*) The Federal Production Tax Credit (PTC) Excluded.

### 3. Results and Discussion

In this study, the economic cost analysis was performed for a home demand procurement by a wind turbine. Taking into account regional differences, the average consumption of a house in Turkey is given in Table 3. A fully equipped home was taken into account in calculating the consumption.

According to the Table 3, daily consumption of a house is about 9 kWh. However, the additional 1.3 kWh consumption for other uses were taken into account and total consumption becomes 10 kWh. Taking into account in the case of daily wind fluctuation, over 50 % of the total consumption was added to daily consumption and finally daily total is thought to be 15 kWh. Wind turbine is in the class of a micro-turbine and it can be installed on the roof of the house or in the garden. To do so, it is suitable to be mounted on a pole at about 8-10 m in height. Installation height of the wind

**Table 3.** The average consumption diagram of a house

Electrical appliances	Power (Watt)	Used Days	Used hours	Annual consumption (kWh)
Refrigerator (400 liters, A+ energy class)	42	365	24	365
Air conditioning (A+ energy class) cooling mode	2200	70	8	1232
Vacuum cleaner	1000	104	0.5	52
LCD TV	100	365	5	182.5
Laptop	75	240	4	72
Washing machine AAA (cotton 60 ° C)	2000	208	0.75	312
Iron	1000	104	2	208
Hairdryer	400	365	0,3	43.8
bulb (CFC - 5 pieces)	50	365	5	91
Electric furnace	2500	52	1.5	195
Toaster	1000	52	1.2	62.4
mixer	100	52	0.16	1
Cooker Hood	150	365	0.66	36.1
Dish-washing machine	1200	260	1	315
Phone charger	4	300	2	2.4
Other uses	1300	365	1	480
<b>Total</b>				3650
<b>Daily total</b>				10

turbine is lower compared to other large turbine therefore wind speed can be slightly lower. Therefore smaller generator with larger wind turbine blade was scheduled to be assembled. The turbine was expected to operate with capacity factor of 0.3 therefore 2 kW generator is enough to meet the needs of a house. Aluminium was used in blade production. Because aluminium can be processed by the local industry conditions all over the country. 2.5 m radius of the blade was designed for this case study. Maximum power can be converted by a wind turbine is calculated with the help of equation (1).

$$P = \frac{1}{2} c_p \rho A v^3 \quad (1)$$

Where,  $c_p$  is power coefficient,  $\rho$  is density of airflow,  $A$  is swept area of rotor,  $v$  is free wind speed.

Turbine generates at full capacity at the wind speed of 7-8 m/s ( $c_p$  is 0.4). In this design, rotor is required to do 30-50 revolutions per minute. As a result, the generator starts production in 240 rpm and produce full power in 400 rpm. Thus one gearbox is needed to increase revolution eight to fifteen fold. The gearbox and alternator are domestic production can be bought anywhere in Turkey. To prevent complete discharge of the gel batteries or to control charging, one charge control unit is needed. 10 pieces 150 Ah gel batteries are needed to store the generated electricity. In this way, it may store 18 kWh of electricity. One smart 4000 W inverter is necessary to run electrical appliances at home. If the stored electricity is not enough, extras can be used from the grid. The working diagram of system is given in Figure 2. Materials necessary for the establishment of the system and price list are given in Table 4. The price is valid in Turkey and prices can vary in other countries. A total of \$ 6,576 is required for installation of the system. Consuming monthly 300 kWh of electricity, total bill amount for a family (taken into account the data of April 2015) is \$ 46. The annual electricity price turns out to be \$ 554. However, annual inflation is taken into consideration; share price becomes a little more expensive than a year before. If the price does not rise, \$ 5,538 is paid as a total bill in ten year. However, there is a range of 6-10 % annual inflation in Turkey conditions. Considering annual inflation reflected to the electricity bill is 4 %, 10 year total electricity bill becomes \$ 10,508. If the annual inflation rate is 10 % then total bill rises to \$ 13,001.

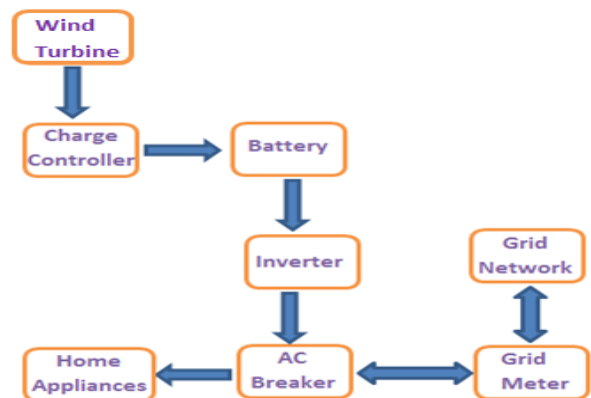


**Fig. 2.** System operation scheme

**Table 4.** System component price list

Item list	Amount	Unit price (\$)	Total price (\$)
Rotor	1	767	767
Alternator	1	769	769
Gearbox	1	462	462
Full sine inverter 4000W	1	770	770
150 A gel batteries	10	288.5	2885
Charging control unit	1	154	154
Mast and installation	1	769	769
<b>Total</b>			<b>6,576</b>

Given that annual inflation reflected as 4 % share of electricity bills, total bill becomes \$ 9,615 with the most optimistic estimate in 10 year. A total of \$ 3,846 is to be spent on maintenance for 10 years. Taking into account to replace old and deteriorating parts, maintenance cost is kept as high as possible. In this case, money invested is paying off in 10 years. If the system is considered to provide 20 years of service, case is made quite lucrative. Latest calculations indicate that this installation will profit after the first 10 years.

#### 4. Conclusion

Energy is the most important issues in today's world. Energy has become an integral part of people's daily lives. So the countries spend the most of the money on energy issue. Producing their own energy makes the country more powerful than other countries. The main reasons of the wars of the last 30 years are energy related. In terms of energy, foreign-dependent economy of the country is being shaken and investigates ways to generate its own energy. Turkey is a poor country in terms of fossil fuel resources. However, it has significant potential in terms of renewable energy resources. It has the potential to meet all the electricity needs only from wind energy. However, the transformation generates a profit if done through indigenous technology and resources. Otherwise, for the imported wind turbine, 7-8 years of production costs have to pay in advance to foreign countries. The domestic wind power system is thus important to produce fully native in the country. On the other hand impact of global warming, all countries all over the world are making significant strides in renewable energy. Otherwise, we may not find a habitable world in the near future.

In this study, Turkey wind energy potential was investigated. Turkey has a total 47,849 MW wind power potential in wind speed of 7 m/s and over. This value is enough to meet all the needs of the country's nominal demand. The total potential is around 83,906 MW for the wind speed from 6,5 to 7 m/s.

Finally, economic analysis was conducted for 2 kW micro wind turbine. Rotor blades were made of aluminium. The goal here is to be able to manufacture this rotor in all industrial organizations across the country. Paying attention to the use of domestic component in all systems to prevent national capital going out and to prevent or reduce the budget deficit. The rotors, alternators, gearbox, inverter, charge control unit and gel battery are provided from domestic producers. Cost of a system is about \$ 6,576 and this system can pay for itself in 10 years. Such individual installation can be done in other countries but installation costs can vary in terms of workmanship and materials. Governments incentives for the installation of such systems should be established or encouraging publications should be made. Renewable energy sources have become a necessity for a sustainable future.

#### References

- [1] L. Staudt, Wind Energy, Future Energy Improved, Sustainable and Clean Options for our Planet, Elsevier, 2008, pp. 93, 95–110, chapter 6.
- [2] TWEA, Turkey Wind Energy Association, “Türkiye Rüzgâr Enerjisi Potansiyeli”, <http://www.eie.gov.tr>, 2015.
- [3] B. Ozerdem, S. Ozer, M. Tosun, “Feasibility study of wind farms: A case study for Izmir, Turkey”, Journal of Wind Engineering and Industrial Aerodynamics, vol. 94, pp. 725–743, 2006.
- [4] S.A.Akdag, Ö. Güler, “Evaluation of wind energy investment interest and electricity generation cost analysis for Turkey”, Applied Energy, vol. 87, pp. 2574–2580, 2010.
- [5] Z. Li, F. Boyle, A. Reynolds, “Domestic application of micro wind turbines in Ireland: Investigation of their economic viability”, Renewable Energy, vol. 41, pp. 64–74, 2012.
- [6] A. Mostafaeipour, “Economic evaluation of small wind turbine utilization in Kerman, Iran”, Energy Conversion and Management, vol. 73, pp. 214–225, 2013.
- [7] K. Mohammadi, A. Mostafaeipour, “Economic feasibility of developing wind turbines in Aligoodarz, Iran”, Energy Conversion and Management, vol. 76, pp. 645–653, 2013.
- [8] S. Brusca, “A new statistical based energetic-economic methodology for wind turbine systems evaluation”, Energy Procedia, vol. 45, pp. 180 – 187, 2014.
- [9] A. Mostafaeipour, M. Jadidi, K. Mohammadi, A. Sedaghat, “An analysis of wind energy potential and economic evaluation in Zahedan, Iran”, Renewable and Sustainable Energy Reviews, vol. 30, pp. 641–650, 2014.
- [10] T.M. Groth, C. Vogt, “Residents' perceptions of wind turbines: An analysis of two townships in Michigan”, Energy Policy, vol. 65, pp. 251–260, 2014.

- [11]B. Grieser, Y. Sunak, R. Madlener, “Economics of small wind turbines in urban settings: An empirical investigation for Germany”, Renewable Energy, vol. 78, pp. 334-350, 2015.
- [12]GWEC (Global Wind Energy Association). (2014). Global Wind Report, [http:// www.gwec.net/](http://www.gwec.net/)

# Application of Soft Computing Models to Daily Average Temperature Analysis

Mustafa Göçken \*†, Aslı Boru\*, Ayşe Tuğba Dosdoğru\*\*, Nafiz Berber\*\*\*

\*Adana Science and Technology University, Industrial Engineering Department, Adana, Turkey

\*\*Gaziantep University, Industrial Engineering Department, Gaziantep, Turkey

\*\*\*Orcan Natural Gas Wholesale and Distribution Company Limited, Hatay, Turkey

mgocken@adanabtu.edu.tr, aboru@adanabtu.edu.tr, dosdogru@gantep.edu.tr

† Corresponding author; Mustafa Gocken, Industrial Engineering Department, Adana Science and Technology University,

Yeşiloba Yerleşkesi, Yeşiloba mah., Öğretmenler Bulvarı,

46278 sok., No: 3, 01180, Seyhan/ADANA, Tel.: 0 (322) 455 0000 – 2226;

Fax: 0 (322) 455 00 09, Email: mgocken@adanabtu.edu.tr

*Received: 02.04.2015 Accepted: 12.06.2015*

**Abstract-** Providing critical information about daily life, weather forecasting has important role for human being. Especially, temperature forecasting is rather important because it affects not only people but also other atmospheric parameters. Various techniques have been used for analysis of the dynamic behaviour of weather. This ranges from simple observation of weather to using computer technology. In this study, ANFIS (Adaptive Network Based Fuzzy Inference System), ANN (Artificial Neural Network) and MRA (Multiple Regression Analysis) have been applied for weather forecasting. To judge the forecasting capability of the proposed models, the graphical analysis and the indicators of the accuracy of Mean Absolute Deviation (MAD), Mean Square Error (MSE), Root-Mean Squared Error (RMSE), Mean Absolute Percent Error (MAPE), Determination Coefficient ( $R^2$ ), Index of Agreement (IA), Fractional Variance (FV), Coefficient of Variation (CV, %) are given to describe models' forecasting performance and the error. The results show that ANFIS exhibited best forecasting performance on weather forecasting compared to ANN and MRA.

**Keywords** Weather forecasting, ANFIS, ANN, MRA.

## 1. Introduction

Weather is a description of instant conditions of the atmosphere at a particular time. Weather directly and indirectly affects our daily life because it affects the main ingredients of life on Earth such as soil, water etc. To ensure quality life, weather parameters should be analysed carefully. For these reasons, many people are applied their own model to predict these parameter. Over the many years, the state of the cloud, wind direction, intensity of the stars, and many other observational factors are used to take precautions. In this way, they save lives, money and time in both local and global area. However, this prediction doesn't provide sufficient information because weather is affected by number of variables. For this purpose, meteorological services carried out challenging operational tasks to understand weather [1] and so many types of models are prepared to solve mystery of weather. Presenting a linear relationship between input data and output data is one of the most popular one. One of the simple models to present linear relationship

is Multiple Linear Regression (MLR). Paras and Mathur [2] used MLR to develop a model for weather forecasting. In the study, data collected from a particular station and then applied to estimate weather conditions. Some statistical indicators such as moving average are also processed to extract the hidden information of the time series. Abatzoglou et al. [3] presented general structure of seasonal temperature and precipitation trends by using MLR models. The result of the study shows that MLR models explained between 22% and 54% of the interannual variance in seasonal temperature. The other powerful model is ANN that is an important alternative tool to conventional models in weather forecasting. ANN has a reasonable forecasting accuracy and minimum forecasting error. The properties of ANN are well suited to the problem of weather forecasting under temporal and spatial variability [4]. Abhishek et al. [5] presented applicability of ANN and developed nonlinear predictive models for weather analysis. In the study, MSE is used as a measure of the forecasting accuracy. The results show that this study can be helpful to concentrate on the trend of



weather over a long period of time in a particular station and area. In same manner, Dombaycı and Gölcü [6] used ANN in daily temperature forecasting and evaluated ANN accuracy using FV and RMSE. Smith et al. [7] used ANN to forecast air temperature based on near real-time data. Smith et al. [8] developed an enhanced ANN for air temperature forecasting including larger training set sizes, seasonal input terms, increased lag lengths, and varying the size of the network. Şahin [9] modelled monthly mean air temperature based on remote sensing and ANN. Hayati, and Mohebi [10] utilized ANN for one day ahead forecasting of an important weather parameter and used MAE to evaluate ANN model. Kaur and Singh [11] used ANN to forecast the minimum temperature for Chandigarh city. Previous studies presented that weather forecasting with ANN are very encouraging and forecasting can be made with high degree of accuracy. In addition to ANN, combining ANN and fuzzy logic called ANFIS is used in many application of the weather forecasting. Quality of a weather forecasting is increased by fuzziness that characterizes the scattering of real data around the prognosis [12]. Also, the human thinking and reasoning are easily described using fuzzy logic in the mathematical framework. Thus, fuzzy logic is principle of many systems and ANFIS is one of them. ANFIS reasonably forecast a large class of functions and it presents dynamic behaviour of atmospheric conditions in a clear way. Tektaş [13] used ANFIS and Auto Regressive Moving Average models for weather forecasting in Turkey. The performance comparisons of ANFIS and ARIMA models due to MAE, RMSE,  $R^2$  presented that ANFIS yields better results. Daneshmand et al. [14] used ANFIS for modelling and forecasting the monthly minimum temperature. Research results indicated that the ANFIS can forecast the monthly minimum temperature in the particular station. Oyediran and Adeyemo [15] used ANFIS and Multi-Layer Perceptron to represent characteristic of metrological data sets. It is found that ANFIS model has an ability to yield better results than the Multi-Layer Perceptron model. Also, ANFIS clearly analysed more compact and natural internal representation of the temperature, rainfall, wind, and relative humidity. It is seen that researchers continue to develop finer models for increasing accuracy in forecasting. In this study, ANFIS, ANN, and MRA have been applied for weather forecasting.

## 2. Preprocessing

Selection of input variables is a fundamental task. The task of selecting input variables is largely dependent on the discovery of relationships within the available data to identify suitable predictors of the model output. Using too much unnecessary input data may overload the system, reducing the calculation speed and at times worsen the results of the forecasting system [16]. In literature, many researchers have applied trial and error according to their experiences to determine input variables. Similarly, we used trial and error method. On the other hand, researchers should be careful in this step. Defining what constitutes an optimal set of input variables is significant in designing forecasting models. Identification of an optimal set of input variables will lead to a more accurate, efficient, cost-effective, and

more easily interpretable models [16]. We are interested in quantifying the strength and direction of a presumed relationship between input variables and temperature. In these cases, we can use a measure of association known as a correlation to determine the characteristics of this relationship. This complex relationship between input variables and temperature is shown in Fig. 1-4. For this purposes, we used the Pearson product-moment correlation coefficient that is the most common statistical calculation. Usually known as the “Pearson  $r$ ” or simply “ $r$ ,” this statistic is a measure of the covariance of the two variables divided by the product of their standard deviation. The higher the absolute value of the correlation coefficient, the stronger the correlation between the two weather parameters. Note that a positive correlation indicates an increasing linear relationship, while a negative correlation indicates a decreasing linear relationship [17]. It may take on a range of values from -1 to 0 to +1, where the values are absolute and nondimensional with no units involved. The strength of the correlation is not dependent on the direction or the sign. Thus,  $r=0.40$  and  $r=-0.40$  are equal in the degree of association of the measured variable [18]. For a correlation coefficient, we are interested in how two variables vary with respect to each other. There are two important assumptions of the Pearson correlation coefficient: first, it can be used only with interval or ratio data and second, the data must be normally distributed. Also, it should be noted that no matter how strong the correlation coefficient, we cannot say that one variable cause the other.

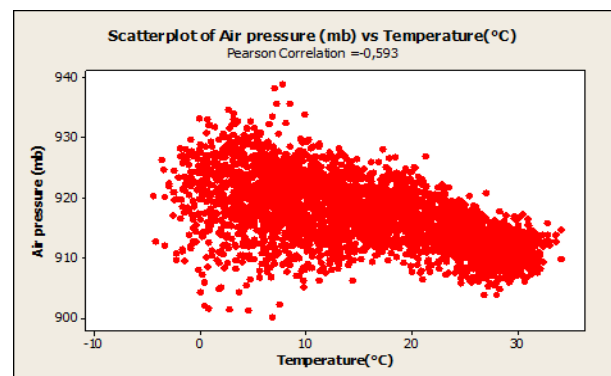


Fig. 1. The scatter plot of air pressure-temperature.

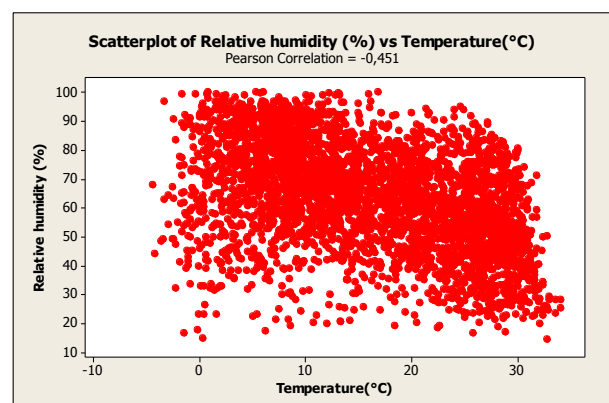


Fig. 2. The scatter plot of relative humidity-temperature.

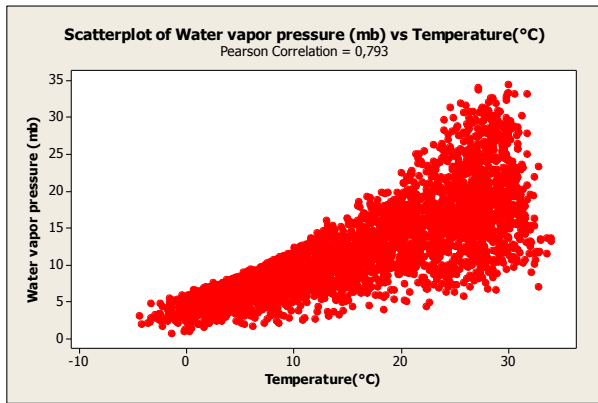


Fig. 3. The scatter plot of water vapour pressure-temperature.

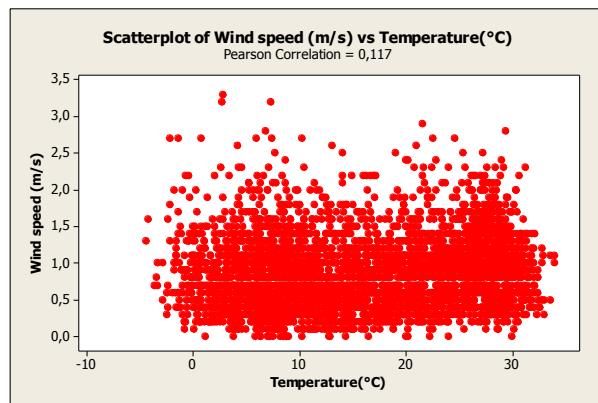


Fig. 4. The scatter plot of wind speed-temperature.

We can only report the strength and direction of the relationship [19]. The scatter plot is useful to illustrate the concept of correlation and to visualize the relationship between the input variables. In this study, scatter plots are generated for the correlations -0.593, -0.451, 0.793, and 0.117 that are the Pearson product-moment correlation coefficient. That is, the higher the correlation in either positive direction or negative direction, the more linear the association between two variables and the more obvious the trend in a scatter plot. The scatter plot of water vapour pressure and temperature shows approximately linear trend but others are not clear as water vapour pressure and temperature. It is also seen that temperature and air pressure are negatively correlated. This means that as the temperature decreases, the air pressure increases, and as the temperature increases, the air pressure decreases. In same manner, humidity is negatively correlated with temperature. The wind speed is slightly correlated with temperature. Data are daily average values for Gaziantep between 01/01/2001 and 31/12/2010 and obtained from General Directorate of Meteorology. The number of data which are 18260 is sufficient to apply ANFIS, ANN, and MRA for weather forecasting. Details about data are given in Table 1.

Table 1. Descriptive Statistics of the input variables and output variable

	N	Mean	Std. Deviation	Minimum	Maximum
Air pressure	3652	916,7691	5,51781	900,10	938,70
Water vapor pressure	3652	12,1347	6,31326	0,70	34,30
Humidity	3652	63,7321	18,28262	14,30	100,00
Wind speed	3652	0,8661	0,48689	0,00	3,30
Temperature	3652	15,9233	9,29021	-4,40	34,00

### 3. ANFIS

ANFIS has a potential to capture the benefits of ANN and fuzzy logic in a single model. Linguistic information is utilized from the fuzzy logic. The learning capability and parameter optimization is taken from ANN. Also, ANN learning rules are applied to identify and set the parameters and structure of a Fuzzy Inference System (FIS). Basically, ANFIS design includes two steps. First step is the design of the premise parameters and the other step is consequent parameter training. ANFIS keeps the premise parameters fixed and estimates them in a forward pass and then in a backward pass by keeping fixed the consequent parameters [20]. ANFIS has adaptable structure and includes developed data analysing technique such as numerical classification and constructing a rule. Hence, all rules formed for weather forecasting can be appointed by ANFIS [21]. The basic structure of FIS defines the number and type of the membership functions used in the fuzzy rules, and a reasoning mechanism of FIS. Note that FIS does not have a learning algorithm for parameter estimation but it is able to employ rules and knowledge that are represented with linguistic expressions [22]. Let  $U$ , a subset of  $R$ , be the universe discourse, where  $U = \{u_1, u_2, \dots, u_n\}$ , in which the possible linguistic values  $f_{A(t)}$  of fuzzy sets  $A(t)$  are defined, where  $f_{A(t)}$  denotes the membership function of the fuzzy set  $A(t)$ ,  $f_{A(t)}: U \rightarrow [0,1]$ , and the  $A(t)$  can be seen as a linguistic variable which is a collection of  $f_{A(t)}(u_1), f_{A(t)}(u_2), \dots, f_{A(t)}(u_n)$ .  $F = \{A(t), t = 1, 2, \dots\}$  is called a fuzzy time series defined on  $U$ . Assume the temperature on the first day is 39, denoted as Temperature (1)=39, while the temperature on the second day is 34, denoted as Temperature (2)=34, and the temperature on day  $t$  is 39.5, denoted as Temperature (t)=39.5 (Fig. 5). Following the fuzzification process, each of these temperature values would then obtain a linguistic value; for example,  $A(1)$ ="Very high temperature",  $A(2)$ ="High temperature",  $A(t-1)$ ="High temperature",  $A(t)$ ="Very high temperature".



**Fig. 5.** Illustrative example of linguistic expressions.

Thus, the  $F$  is a fuzzy time series definition on  $U$ , and  $F = \{\text{"Very high"}, \text{"High"}, \dots, \text{"High"}, \text{"Very high"}\}$  [23]. Input-output mapping smoothly constructed by using ANFIS serves as a basis for building the set of fuzzy if-then rules to generate the input output pairs [21]. Based on FIS, ANFIS uses the fuzzy rule base as the model structure to transform the original rules into fuzzy rules one by one. Hence, by the fuzzy clustering of data or other clustering analysis, huge amounts of data can be transformed into fuzzy rule bases, thus reducing parameter computation and data storage requirements. In addition, expert experience and knowledge can be transformed into inference rules to compensate for the lack of a data-based description of the system [24]. Therefore, the main contribution of ANFIS in the modeling process is the fuzzy if-then rules, in which the membership function parameters are estimated with the learning algorithm of ANN. Using the learning capability of ANN, the fuzzy rules are automatically generated and the parameters are optimized [22]. To give two fuzzy if-then rules example, the two rules is given for a first order Sugeno model as follow [25]:

Rule 1: If  $v$  is  $V_1$  and  $d$  is  $D_1$  then  $f_1 = p_1v + q_1d + r_1$  (1)

Rule 2: If  $v$  is  $V_2$  and  $d$  is  $D_2$  then  $f_2 = p_2v + q_2d + r_2$  (2)

In Eq. (1) and Eq. (2),  $p_1, p_2, q_1, q_2, r_1$  and  $r_2$  are linear parameters and  $V_1, V_2, D_1$  and  $D_2$  are non-linear parameters. A circle indicates a fixed node whereas a square indicates an adaptive node i.e. the parameter are changed during adaptation or training and  $O_{j,i}$ , denotes the output of the  $i^{\text{th}}$  node in layer  $j$ . The entire system structure consists of five layers (Fig. 6).

### Layer 1

Each node ' $i$ ' in this layer generates a membership grades of a linguistic label. It is the fuzzy layer, in which  $v$  and  $d$  are the input of nodes.  $V_1, V_2, D_1$ , and  $D_2$  are linguistic labels used in the fuzzy theory for dividing the membership functions. The membership relationship between the output and input functions of this layer can be expressed as given in Eq. (3) and Eq. (4):

$$O_{l,i} = \mu_{V_i}(v) \quad i = 1, 2 \quad (3)$$

$$O_{l,j} = \mu_{D_j}(d) \quad j = 1, 2 \quad (4)$$

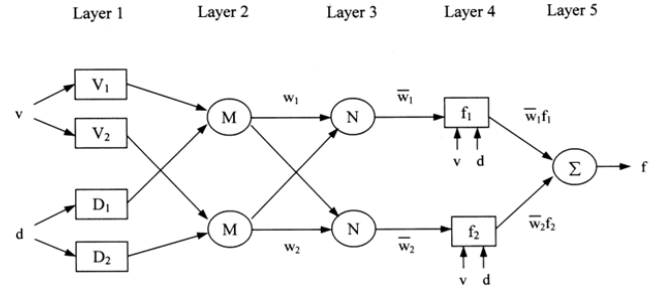


**Fig. 6.** Basic ANFIS structure.

where  $O_{l,i}$  and  $O_{l,j}$  denote the output functions and  $\mu_{V_i}(v)$ ,  $\mu_{D_j}(d)$  denote the membership functions. The membership function which represents a fuzzy set is usually denoted by  $\mu_{V_i}(v)$  and  $\mu_{D_j}(d)$ . For an element  $d$  and  $v$ , the value  $\mu_{V_i}(v)$  and  $\mu_{D_j}(d)$  is called the membership degree of  $d$  and  $v$  in the fuzzy set. The membership degree  $\mu_{V_i}(v)$  and  $\mu_{D_j}(d)$  quantifies the grade of membership of the element  $d$  and  $v$  to the fuzzy set. If the value is 0,  $d$ , and  $v$  are not a member of the fuzzy set. If the value is 1,  $d$ , and  $v$  are member of the fuzzy set. Lastly, if value is between 0 and 1, fuzzy members only partially belong to the fuzzy set [26]. In this study, each input parameters are divided into seven scale on the membership function; very low, low, little low, medium, little high, high and very high. Thus, the triangular membership function is employed;  $\mu_{V_i}(v)$  is given in Eq. (5):

$$\mu_{V_i}(v) = \max\left[\min\left(\frac{v-a_i}{b_i-a_i}, \frac{c_i-v}{c_i-b_i}\right), 0\right] \quad (5)$$

where  $a_i, b_i$ , and  $c_i$  are the parameters of the membership function, governing the triangular membership functions accordingly. Triangular shape membership function is one of the most suitable membership functions to forecast temperature because it requires less computing time.

### Layer 2

Each node in this layer calculates the 'firing strength' of each rule via multiplication (Eq. (6)):

$$O_{2,i} = w_i = \mu_{V_i}(v) \mu_{D_i}(v) \quad i = 1, 2, \dots \quad (6)$$

where  $O_{2,i}$  denotes the output of the layer 2.

### Layer 3

The  $i^{\text{th}}$  node of this layer calculates the ratio of the  $i^{\text{th}}$  rule's strength to the sum of all rules' firing strengths (Eq. (7)):

$$O_{3,i} = \bar{w}_i = \frac{w_i}{(w_1 + w_2)} \quad i = 1, 2, \dots \quad (7)$$

For convenience, output of this layer  $O_{3,i}$  will be called 'normalized firing' strength.

#### Layer 4

Every node 'i' in this layer is a square node with a node function as given in Eq. (8).

$$O_{4,i} = \bar{w}_i f_i = \bar{w}_i (p_i v + q_i d + r_i) \quad i = 1, 2, \dots \quad (8)$$

where  $O_{4,i}$  denotes the layer 4 output. In this layer,  $p_i$ ,  $q_i$ , and  $r_i$  are called linear parameter or consequent parameters.

#### Layer 5

The single node in this layer is a fixed node, which computes the overall output as the summation of all incoming signals (Eq. (9)):

$$O_{5,i} = \sum_i \bar{w}_i f_i = \frac{\sum_i w_i f_i}{\sum_i w_i} \quad i = 1, 2, \dots \quad (9)$$

In ANFIS structure, first and fourth layers are adaptive layers. The modifiable parameters are so-called premise parameters in the first layer and consequent parameters in the fourth layer [25].

In this paper, MATLAB is used to create ANFIS and it contains all the ANFIS information such as ANFIS editor, membership function editor, rule editor and so on. To create fuzzy inference system, either Mamdani or Sugeno type systems can be used but ANFIS has only support Sugeno type system. For this reason, Sugeno type system is used intentionally in the study. The main difficulty of the ANFIS model is related to the number of input variables. If ANFIS inputs exceed five, the computational time and rule numbers will increase, so ANFIS will not be able to model output with respect to inputs [27]. Therefore, we used four input variables. Most literature on forecasting show that triangular shape membership function is one of the most suitable membership functions to forecast temperature because it requires less computing time. Hence, we used triangular membership function and each input parameters are divided into seven scale on the membership function; very low, low, little low, medium, little high, high and very high. In ANFIS, 2401( $7^4$ ) rules are created for 4 inputs and 7 membership function defined for each input. A simple interpretation of one rule is "If air pressure is the first membership function associated with air pressure and if vapour pressure is the first membership function associated with vapour pressure, and if humidity is the first membership function associated with humidity, and if wind speed is the first membership function associated with wind speed, then output 1 should be the membership function associated with output 1 with weight 1.

#### 4. ANN

ANN is a computational network and simulates the networks of neurons of biological central nervous system [28]. One of the most important features of ANN is that it

performs a large number of numerical operations in parallel. These operations involve simple arithmetic operations as well as nonlinear mappings and computation of derivatives. Almost all data stored in the network are involved in recall computation at any given time [29]. ANN has an ability to learn nonlinear problem with training that provide sufficiently accurate online response and to model unknown data relationship. Simple model of ANN has three set of rules: multiplication, summation, and activation. Artificial neuron is the basic building block of every ANN and affect system performance directly. The inputs are weighted in the model and every input value is multiplied with individual weight. Sum function (sums all weighted inputs and bias) is applied in the middle section of artificial neuron. Finally, weighted inputs and bias is passing through activation function that is also called transfer function [30]. Basic working principle of ANN is seen in Fig. 7. Also, simplicity of artificial neuron model is given in Eq. (10).

$$y_i(k) = F. \left( \sum_{i=0}^m (w_i(k).x_i(k) + b) \right) \quad (10)$$

Where:

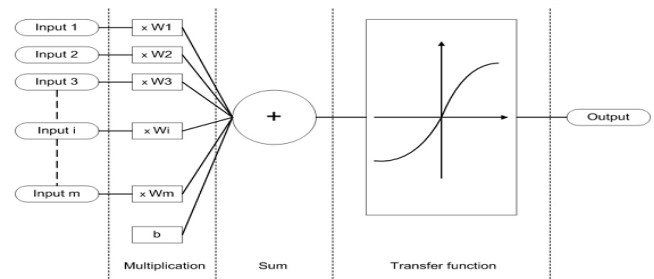


Fig. 7. Working principle of an artificial neuron [30].

- $x_i(k)$ ,  $w_i(k)$ , and  $y_i(k)$  represent input value, weight value, and output value in discrete time  $k$  where  $i$  goes from 0 to  $m$  respectively,
- $b$  is bias,
- $F$  is a transfer function.

Each connection of input layer has an independent weight,  $w$  attached to it. The input parameters are fed through the input nodes to the next level where each of the input values are multiplied by the relevant weight on each connection to create a weighted input value [30]. In ANN, the input parameters that are air pressure (mb), water vapour pressure (mb), relative humidity (%), and wind speed (m/s) are fed through the input nodes to the next level where each of the input values are multiplied by the relevant weight on each connection to create a weighted input value. Then, system continues by determining the number of hidden layers and nodes. Although there have been some suggestions related to these decisions, a standard model does not exist. Generally these crucial decisions are determined by

trial and error method. One hidden layer is generally enough for most applications.

As a remark, notice that a larger number of hidden neurons in general would yield better learning capability of the ANN until the overfit phenomenon occurs [31]. Choi [31] presented that 20 hidden neurons can be used in ANN because the value of the MSE is lowest when compared with other number of the hidden neurons (2, 10, 15, 25, 30, 100). Therefore, we used one hidden layer and 20 hidden neurons in ANN structure. In ANN, 15% of the original data are divided randomly to use as validation and test data sets. 70% of the original data are used for training. The process of training the network is the adjustment of the weights to produce the desired response to the given inputs. In ANN, an input–output pair is selected from the training set and the selected inputs are used to calculate output. Then, error that is the difference between the network output and the desired output is found. This training cycle is repeated until the error reduces to an acceptable value [6].

## 5. MRA

MRA is one of the simple statistical tools that are used for weather forecasting. One or more variables can be used to forecast another variable of interest. In the model, the input variables are known as independent variables and the variable that is being forecasted is known as the dependent variable [32]. However, the connections between dependent and independent variables are generally not known clearly and hence detail information about solution is not provided. The choice of independent variables is made by the researcher in the experimental design stage. In this study, air pressure (mb), water vapour pressure (mb), relative humidity (%), and wind speed (m/s) are selected as the independent variables and temperature (°C) is selected as the dependent variable. The general form of a regression model for  $k$  independent variables is given in Eq. (11).

$$Y = \beta_0 + \beta_1 X_1 + \beta_2 X_2 + \dots + \beta_k X_k + \epsilon \quad (11)$$

Where  $Y$  is the response variable.  $\beta_0, \beta_1$  to  $\beta_k$  are the regression coefficients.  $\epsilon$  is the error, and  $X_1, X_2, \dots, X_k$  are the independent variables. Based on least squares criterion, the regression coefficients are forecasted by minimizing the sum of the squares of the vertical deviations of each data point to the best-fitting line [33].

## 6. Results and Discussion

We first present scatter plots that are probably the simplest verification tool to provide useful insights in Fig. 8-10. The analyses of scatter plot in proposed models are useful to get a general vision of how well the forecasting model is. The values should lie linearly in a perfect forecasting model. The ordinate and the abscissa should have the same scale, in which case perfection is represented by any point on the 45 degree line for which forecast=observed. If the forecasts were perfect, this line would coincide with the 45 degree line [34]. It could be said that forecasting

performance of the proposed models are remarkable in all models. However, ANFIS and ANN results are more accurate than those of MRA's. In this study, we also used performance indicators to analyse in greater detail. An important aspect of the error indicators used for model evaluations is their capability to discriminate among model results [35]. In the literature, various descriptive statistical indicators are used as helpful tools to describe model's forecasting performance and the error. MAD is the mean of the absolute values of the error between actual and forecast data. The smallest MAD gives the most reliable results when several forecasting models are compared. Hence, the smaller the MAD values the better the forecasting performance. The MAPE is a relative measure which expresses errors as a percentage of the actual data. This is its biggest advantage as it provides as easy and intuitive way of judging the extent, or importance of errors. In addition we can make comparisons involving more than one model since the MAPE of each tells us about the average relative size of their errors [36]. MSE, as its name implies, provides for a quadratic loss function as it squares and subsequently averages the various errors. MSE is especially useful when we are concerned about large errors whose negative consequences are proportionately much bigger than equivalent smaller ones [37]. Besides MSE, RMSE is also useful when large errors are particularly undesirable [38].  $R^2$  estimates the combined dispersion against the single dispersion of the observed and forecasted series. The range of  $R^2$  lies between 0 and 1 which describes how much of the observed dispersion is explained by the forecasting [39]. IA reflects the degree to which the observed variable is accurately forecasted by the input variables. IA is not a measure of correlation or association in the formal sense but rather a measure of the degree to which a model's forecasting are error free. It varies between 0 and 1 where a computed value of 1 indicates perfect agreement between the observation and forecasting, and 0 connotes one of a variety of complete disagreements [40]. FV is a normalization of the mean bias of the sample variances of the observed and forecasted values. CV is also useful to appraise the fit between the observed data and the forecasted outputs. The results of all performance indicators are summarized in Table 2. The results revealed that the forecasting performance of the ANFIS model is better than that of both ANN and MRA models according to all performance indicators. However, the difference between ANFIS and ANN is less than the difference between ANFIS and MRA. The value of the MRA steeply increases which implies that forecasting accuracy dramatically decreases. These indicate that the non-linear ANFIS and ANN models generate a better fit than MRA. One of the most important advantages of ANFIS is that ANFIS integrates ANN and fuzzy logic in a single framework. Thus, it has a potential to capture the benefits of both models. Also, ANFIS reaches to the target faster than ANN. When a more sophisticated system with a huge data is imagined, the use of ANFIS instead of ANN would be more useful to overcome faster the complexity of the problem [41].



**Table 2.** Descriptive statistical performance indicators for proposed models

	ANFIS	ANN	MRA
<b>MAD</b>	1,092	1,31	2,442
<b>MSE</b>	2,158	2,824	9,960
<b>RMSE</b>	1,469	1,680	3,155
<b>MAPE</b>	0,072	0,124	0,238
<b>R<sup>2</sup></b>	0,975	0,966	0,885
<b>IA</b>	0,994	0,991	0,968
<b>FV</b>	0,013	0,021	0,059
<b>(CV, %)</b>	9,224	10,551	19,817

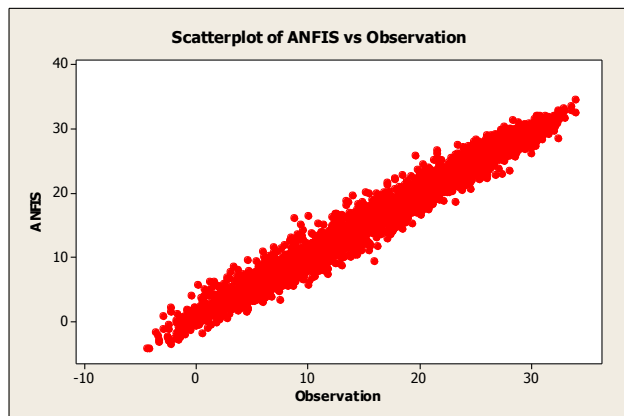


**Fig. 8.** Comparison of observation and forecasting value in 2010 (ANFIS).

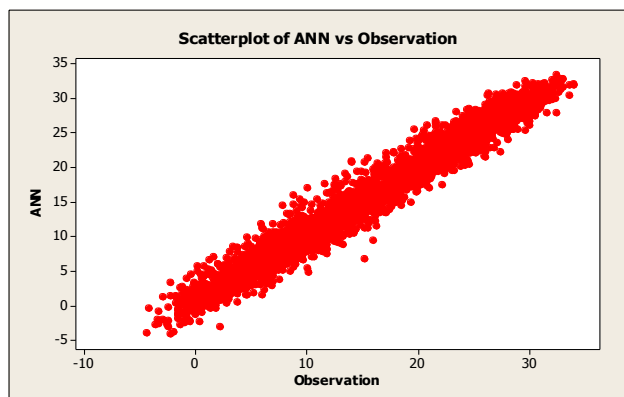


**Fig. 9.** Comparison of observation and forecasting value in 2010 (ANN).

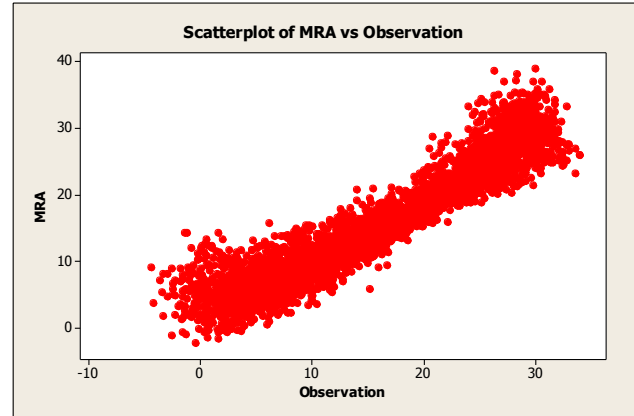


**Fig. 10.** Comparison of observation and forecasting value in 2010 (MRA).

## 7. Conclusion

In this study, 18260 data are used for forecasting daily average temperature of city of Gaziantep by using ANFIS, ANN, and MRA. Every forecasting model is analysed separately and results are compared. Enabling easily configurable forecasting model with given input stands out as a remarkable feature of fuzzy logic. In this study, fuzzy logic is supported by ANFIS Sugeno type system. In FIS structure, 2401 rules are used and triangular membership function is chosen for being more suitable. The other powerful method is ANN that enables to analyse the relationship between the inputs and outputs in forecasting. However, there are a number of different answers to the question of how to define ANN structure. Hence, the determination of the appropriate architecture such as the number of variables, number of layers, and number of neurons in each layer is critical in the design of ANN. We used one hidden layer and 20 hidden neurons in ANN structure. Also, MRA is used for weather forecasting but results are not satisfying as others. Also, the graphical analysis (scatter plot) and statistical performance indicators (MAD, MSE, RMSE, MAPE, R<sup>2</sup>, IA, FV, CV, %) are utilized to judge the forecasting capability of the developed methodology. Specifically, the MAPE performances of each model tells us that the forecasting error of the proposed methods are under approximately 0,238% at the worst case which is acceptable for such a very complex forecasting environment. Also, this limit shows the superiority of the forecasting performances of the proposed methods. Based on the results of the performance indicators, it can conclude that ANFIS produced very small deviations and exhibited superior forecasting performance on weather forecasting compared to both ANN and MRA. The results emphasized that ANFIS can be used conveniently for further weather forecasting studies.

## References

- [1] G. Shrivastava, S. Karmakar, M. K. Kowar, and P. Guhathakurta, Application of Artificial Neural Networks in weather forecasting: A comprehensive literature review,

International Journal of Computer Applications, vol. 51, no. 18, pp. 0975-8887, 2012.

[2] Paras, and S. Mathur, A simple weather forecasting model using mathematical regression, Indian Research Journal of Extension Education Special Issue 1, pp. 161–168, 2012.

[3] J. T. Abatzoglou, D. E. Rupp, and P. W. Mote, Seasonal climate variability and change in the Pacific Northwest of the United States, American Meteorological Society, vol. 27, pp. 2125–2142, 2014.

[4] I. Maqsood, M. R. Khan, and A. Abraham, Weather forecasting models using ensembles of neural networks, Intelligent Systems Design and Applications Advances in Soft Computing, vol. 23, pp. 33–42, 2003.

[5] K. Abhishek, M. P. Singh, S. Ghosh, and A. Anand, Weather forecasting model using Artificial Neural Network, Procedia Technology, vol. 4, pp. 311–318, 2012.

[6] Ö. A. Dombaycı, and M. Gölcü, Daily means ambient temperature prediction using Artificial Neural Network method: A case study of Turkey, Renewable Energy, vol. 34, pp. 1158–1161, 2009.

[7] B. A. Smith, G. Hoogenboom, and R. W. McClendon, Artificial Neural Networks for automated year-round temperature prediction, Computers and Electronics in Agriculture, vol. 68, pp. 52–61, 2009.

[8] B. A. Smith, R. W. McClendon, and G. Hoogenboom, An enhanced Artificial Neural Network for air temperature prediction, World Academy of Science, Engineering and Technology, vol.1 no.7, pp. 80–85, 2005.

[9] M. Şahin, Modeling of air temperature using remote sensing and Artificial Neural Network in Turkey, Advances in Space Research, vol. 50, no. 7, pp. 973–985, 2012.

[10] M. Hayati, and Z. Mohebi, Application of Artificial Neural Networks for temperature forecasting, World Academy of Science, Engineering and Technology, vol.1, no.4, pp. 654–658, 2007.

[11] A. Kaur, and H. Singh, Artificial Neural Networks in forecasting minimum temperature, International Journal of Electronics & Communication Technology, vol. 2, no. 3, pp. 101–105, 2011.

[12] D. Domanska, and M. Wojtylak, Fuzzy weather forecast in forecasting pollution concentrations, Proc. of Chaotic Modeling and Simulation International Conference, pp. 1–8, 2010.

[13] M. Tektaş, Weather forecasting using ANFIS and ARIMA models, Environmental Research, Engineering and Management, vol. 51, pp. 5–10, 2010.

[14] H. Daneshmand, T. Tavousi, M. Khosravi, and S. Tavakoli, Modeling minimum temperature using Adaptive Neuro-Fuzzy Inference System based on spectral analysis of climate indices: A case study in Iran, Journal of the Saudi Society of Agricultural Sciences, vol. 14, pp. 33–40, 2015.

[15] O. F. Oyediran, and A. B. Adeyemo, Performance evaluation of Neural Network MLP and ANFIS models for weather forecasting studies, African Journal of Computing & ICT, vol. 6, no. 1, pp. 147–164, 2013.

[16] R. May, G. Dandy, and H. Maier, Review of input variable selection methods for Artificial Neural Networks, Artificial Neural Networks-Methodological Advances and Biomedical Applications, pp. 19–44, 2011.

[17] N. Sharma, P. Sharma, D. Irwin, and P. Shenoy, Predicting Solar Generation from Weather Forecasts Using Machine Learning, Distributed Generation, Microgrids, Renewables and Storage (IEEE SmartGridComm), pp. 528–533, 2011.

[18] R. Taylor, Interpretation of the correlation coefficient: A basic review, Journal of Diagnostic Medical Sonography, vol. 6, pp. 35–39, 1990.

[19] S. Prion, and K. A. Haerling, Making sense of methods and measurement: pearson product-moment correlation coefficient. Clinical Simulation in Nursing, vol. 10, pp. 587–588, 2014.

[20] Dr G. S. V. P. Raju, V. M. Sumalatha, K. V. Ramani, and K. V. Lakshmi, Solving uncertain problems using ANFIS, International Journal of Computer Applications, vol. 29, no. 11, 2011.

[21] R. Sivakumar, C. Sahana, and P. A. Savitha, Design of ANFIS based estimation and control for MIMO systems, International Journal of Engineering Research and Applications, vol. 2, no. 3, pp. 2803–2809, 2012.

[22] C. Jeong, J. Shin, T. Kim, and J. Heo, Monthly precipitation forecasting with a Neuro-Fuzzy model, Water Resources Management, vol. 26, pp. 4467–4483, 2012.

[23] M. Chen, and B. Chen, Online fuzzy time series analysis based on entropy discretization and a Fast Fourier Transform, Applied Soft Computing, vol.14, pp. 156–166, 2014.

[24] M. Y. Chen, D. R. Chen, M. H. Fan, and T. Y. Huang, International transmission of stock market movements: an Adaptive Neuro-Fuzzy Inference System for analysis of

- TAIEX forecasting, Neural Computing and Applications, vol. 23, pp. 369–378, 2013.
- [25] S. Roy, Design of Adaptive Neuro-Fuzzy Inference System for predicting surface roughness in turning operation, Journal of Scientific and Industrial Research, vol. 64, pp. 653–659, 2005.
- [26] S. Mandal, J. Choudhury, and S. Chaudhuri, In search of suitable fuzzy membership function in prediction of time series data, International Journal of Computer Science Issues, vol. 9, no 3, pp. 293–302, 2012.
- [27] B. Khoshnevisan, S. Rafiee, M. Omid, and H. Mousazadeh, Development of an intelligent system based on ANFIS for predicting wheat grain yield on the basis of energy inputs, Information Processing in Agriculture, vol. 1, pp. 14-22, 2014.
- [28] D. Graupe, Principles of Artificial Neural Networks, Advanced Series on Circuits and Systems, 2st ed., vol. 6, New Jersey: World Scientific, 2007.
- [29] J. M. Zurada, Introduction to Artificial Neural Systems, St. Paul: West Publishing Company, vol. 8, 1992.
- [30] A. Krenker, J. Bester, and A. Kos, Introduction to the Artificial Neural Networks. Artificial Neural Networks: Methodological Advances and Biomedical Applications, First ed., Intech, India, pp 1–18, 2011.
- [31] T. M. Choi, Fashion Branding and Consumer Behaviors: Scientific Models, Imprint: Springer, 2014.
- [32] D. Şchiopu, E. G. Petre, and C. Negoiană, Weather forecast using SPSS statistical methods, Petroleum-Gas University of Ploiesti Bulletin, Mathematics-Informatics-Physics, vol. 61, no. 1, pp. 97–100, 2009.
- [33] Z. Z. Latt, and H. Wittenberg, Improving flood forecasting in a developing country: a comparative study of Stepwise Multiple Linear Regression and Artificial Neural Network, Water Resource Management, vol. 28, pp. 2109–2128, 2014.
- [34] H. R. Stanski, W. R. Burrows, and L. J. Wilson, Survey of common verification methods in meteorology, (Second Edition), World Meteorological Organization, 1989.
- [35] T. Chai, and R. Draxler, Root mean square error (RMSE) or mean absolute error (MAE)? – Arguments against avoiding RMSE in the literature, Geoscientific Model Development, vol. 7, pp. 1247–1250, 2014.
- [36] S. Makridakis, and M. Hibon, Evaluating accuracy (or error) measures, INSEAD, 1995.
- [37] E. Woschnagg, Evaluating forecast accuracy, University of Vienna, Department of Economics, 2004.
- [38] A. Bhatt, D. Pant, and R. Singh, An analysis of the performance of Artificial Neural Network technique for apple classification, AI & Soc. vol. 29, 103–111, 2014.
- [39] P. Krause, D. P. Boyle, and F. Bäse, Comparison of different efficiency criteria for hydrological model assessment, Advances in Geosciences, vol.5, pp. 89–97, 2005.
- [40] C. J. Willmott, On the validation of models. Physical Geography, vol. 2, pp. 194–194, 1981.
- [41] H. Atmaca, B. Cetisli, and H. S. Yavuz, The comparison of fuzzy inference systems and neural network approaches with ANFIS method for fuel consumption data, Second International Conference on Electrical and Electronics Engineering Papers ELECO, 2001.



# In-situ Measurement via E/M Impedance Spectroscopy Technique Using Shear Horizontal Piezoelectric Wafer Active Sensors

Tuncay Kamaş<sup>\*†</sup>

<sup>\*</sup>Department of Mechanical Engineering, Faculty of Engineering and Architecture, Eskişehir Osmangazi University, Meselik Campus Odunpazarı Eskişehir

tkamas@ogu.edu.tr

<sup>†</sup>Corresponding Author; Tuncay Kamaş, Eskişehir Osmangazi University Meselik Campus Engineering and Architecture Faculty M2 Block Mechanical Engineering Dept. C305 Odunpazarı, Eskişehir, Tel: +90 222 239 3750 (3367), tkamas@ogu.edu.tr

*Received:26 .05.2015 Accepted:15.06.2015*

**Abstract-** In this paper, an electromechanical in-situ measurement method is to be developed for determination of some properties of fuel-oils. Electromechanical impedance spectroscopy (EMIS) method is to be utilized in the measurement technique which will be developed. This method uses piezoelectric sensors that work in electromechanical principles as resonator and dynamically determines the characteristics of a medium that the resonator interacts. EMIS method has been mostly used to determine the dynamic changes in elastic properties of solid materials. This method utilizes the shear horizontal piezoelectric wafer active sensor (SH-PWAS) to generate shear horizontal mode standing waves. Piezoelectric wafer active sensors (PWAS), that are to be utilized in this study, have recently been developed as easily manufactured, small in size and weight, and broad banded transducers to utilize in qualitative and quantitative measurement systems.

**Keywords** E/M impedance, shear horizontal, piezoelectricity, fuel

## 1. Introduction

Piezoelectric wafer active sensor (PWAS) is light-weighted, inexpensive, unobtrusive, minimally intrusive sensor requiring low-power [1]. PWAS is made of piezoelectric ceramic with electric field polarization across the electrodes deposited on both surfaces. It has recently been extensively employed in many applications for in-situ structural inspection in fields such as nuclear plants, structural health monitoring (SHM) and non-destructive evaluations (NDE). The SHM methods include techniques through guided wave generation/ transduction and electromechanical impedance spectroscopy (EMIS). EMIS techniques where PWAS is employed as a resonator are used to generate standing waves in local field of a substrate structure. EMIS method has been utilized to determine the local dynamic characteristics of PWAS bonded on a host structure for in-situ ultrasonic. [2]–[4], and [5] utilized the EMIS method for high frequency local modal sensing. Beside these authors, many rigorous modelling attempts exist in the literature regarding different aspects of impedance and admittance spectra of bonded piezoelectric transducers [6]–[10] in the last decade.

Conventional PWAS is thin rectangular or circular wafer that is poled in thickness direction, with electrodes on top and bottom surfaces; those types of PWAS are either used in in-plane or thickness mode [11]. In in-plane mode, applying an electric field in thickness direction  $E_3$  causes the sensor lateral dimensions to increase or decrease, a longitudinal strain will occur  $\varepsilon_1 = d_{13}E_3$  where  $d_{13}$  is the piezoelectric coupling coefficient measured in [m/V]. Thickness mode is a mode that occurs simultaneously with extension mode, but dominates at higher frequencies in MHz, in which strain in the thickness direction will occur  $\varepsilon_3 = d_{33}E_3$ , where  $d_{33}$  is the piezoelectric coupling coefficient in thickness direction [12]. A different mode of oscillation can be achieved when the applied electric field is applied perpendicular to the poling direction; and it is referred as shear mode. For most piezoelectric materials, the coupling coefficients associated with shear mode have the largest value of all coefficients [13]. The higher values of shear coupling coefficients make SH-PWAS superior in actuation and sensing. SH waves are also preferable because the first symmetric mode is non-dispersive, i.e. wave speed is constant at different frequencies. On the other hand, one of the important disadvantages of SH-PWAS is that thicker transducers are

needed to sustain and generate the shear actuation and due to high density of piezo-ceramic materials ( $\approx 7600 \text{ kg/m}^3$  for APC850 piezo-ceramic Navy II type); using of shear mode piezoelectric elements increases the mass of the system considerably.

Kanazawa and Gordon [14] proposed an analytical definition of the resonance frequency shift by purely mechanical analysis which coupled the standing shear wave in the quartz to a damped propagating shear wave in Newtonian fluid i.e.

$$\Delta f = -f_o^{3/2} \sqrt{\eta_L \rho_L / \pi \mu_q \rho_q} \quad (1)$$

and verified by the experimental results in terms of the changes in resonance frequency of the quartz resonator whose one surface is in contact with water that owned varying concentration of glucose and ethanol. In the paper, the boundary layer was identified as the characteristic length of exponentially decaying viscous effects of the liquid on the resonance frequency because the displacement exponentially dies out in the liquid. The approach has been applied for quartz crystal resonators with overlying viscous liquids, thin elastic films and viscoelastic layers [15]–[18]. However the theoretical method derived by Kanazawa & Gordon is only valid for overlying viscous fluid of infinite extent therefore the method analyzes bulk acoustic waves (BAW) which remains the sensor sensitivity low. The sensors utilizing surface acoustic waves (SAW) are superior to the conventional BAW devices in liquid sensor applications since SAW devices can operate at much higher frequencies and more mass sensitive since SAW possesses large attenuation and energy loss due to a mode conversion in the liquid and dissipates due to the viscous effects [15]. Guo & Sun [19] found that shear type SAW is a good candidate for liquid sensing applications. Other alternative to the SAW presented was the shear horizontal (SH) surface wave as seen in Fig. 1.

Kamal et-al. [13] developed a one dimensional analytical model for EMIS of SH-PWAS (Fig. 2) under stress-free boundary condition using the resonator theory with constant electric field assumption as seen in Eq. (2) that defines the E/M admittance of free SH-PWAS. They verified the analytical model by finite element simulation and experimental EMIS measurement as seen in Fig. 3.

$$Y = \frac{\hat{I}}{\hat{V}} = i\omega C \left[ 1 - \kappa_{35}^2 \frac{1}{\phi \cot \phi} \right]^{-1} \quad (2)$$

where  $\kappa_{35}$  is the shear horizontal electromechanical coupling coefficient and can be defined as

$$\kappa_{35} = \sqrt{\frac{d_{35}^2}{\epsilon_{33}^T s_{55}^E}} \quad (3)$$

$\phi$  is the product of the half of the wave number and the characteristic length of PWAS i.e.  $\phi = \gamma l / 2$  and  $C$  is the capacitance of PWAS.

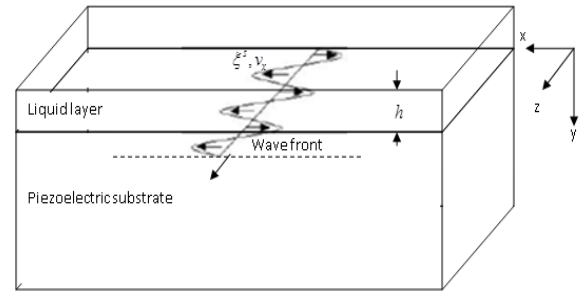


**Fig. 1** Schematic of the propagation of a Shear horizontal (SH) wave along the interface between a piezoelectric substrate and a liquid layer

In this paper, we present one-dimensional analytical model for EMIS of SH-PWAS in contact with different liquids in different density and viscosity. The EMIS of SH-PWAS with different fuels are also simulated by using 3-D coupled field finite element models in ANSYS. The material properties of fuels were published in the paper by Schaschke et-al. [20]. The published fuel material properties at room temperature ( $25^\circ\text{C}$ ) and at the atmospheric pressure (1 atm) are used in the simulations in order to obtain some preliminary results before the experimental studies. The trends of the E/M impedance and admittance simulation results are discussed by comparing the fuels with different viscosity and density. The experimental results will not be presented in this paper.

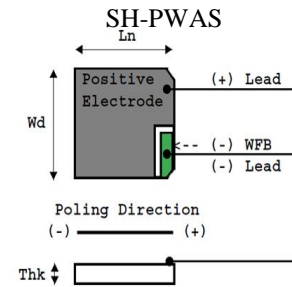


**Fig. 2** Schema of shear horizontal piezoelectric wafer active sensor under stress-free boundary condition

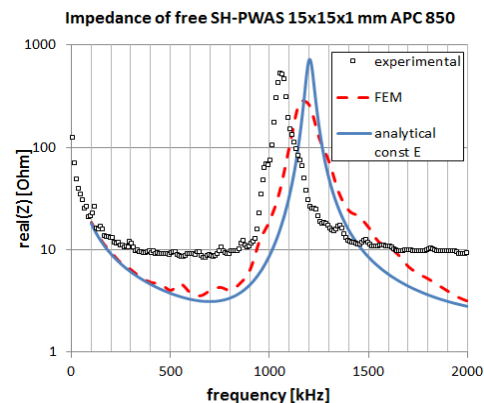


**Fig. 3** Real part of impedance for APC850 type free SH-PWAS in sizes of 15mmx15mmx1mm [13]

## 2. Analytical modelling of SH-PWAS in contact with a fuel layer

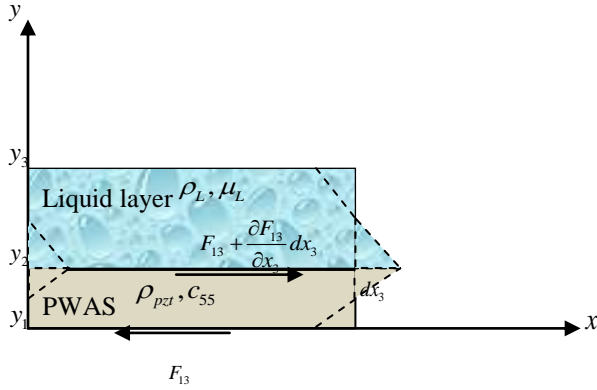


**Fig. 4** Schematic of piezo-wafer resonator deformed in shear horizontal  $d_{35}$  mode by induced  $T_s = T_{13}$  shear stress

**Table 1** Properties of APC 850 piezoelectric ceramic [22]

Property	$\rho$ kg/m <sup>3</sup>	$d_{33}$ m/V	$d_{31}$ m/V	$g_{33}$ Vm/N	$g_{31}$ Vm/N	$s_{33}^E$ m <sup>2</sup> /N
APC 850	7700	$400 \times 10^{-12}$	$175 \times 10^{-12}$	$26 \times 10^{-3}$	$12.4 \times 10^{-3}$	$17.3 \times 10^{-12}$
Property	$s_{11}^E$ m <sup>2</sup> /N	$\epsilon_{33}^T / \epsilon_0$	$\kappa_p$	$\kappa_{33}$	$\kappa_{31}$	$\nu$
APC 850	$15.3 \times 10^{-12}$	1750	0.63	0.72	0.36	0.35

In this section, the response of a piezo-resonator coupled with liquid layer (**Fig. 4**) is presented in terms of E/M impedance and admittance spectra. The shear horizontal waves and the corresponding piezoelectric constitutive equations were taken into account to derive the EMIS response of a SH-PWAS resonator in contact with liquid layer [21].

The 1-D analytical SH-PWAS EMIS model including the liquid layer effects was derived. The particle velocity of SH-PWAS along its thickness in contact with water can be seen in **Fig. 5(a)**. The particle velocity at the interface is 1.332  $\mu\text{m}/\text{sec}$  at electric field amplitude of 20 kV/m and SH-PWAS sizes are 15mmx15mmx1mm. The particle velocity of SH-PWAS along its thickness in contact with water and ethylene glycol can be seen in **Fig. 5(b)**, the particle velocity at the interface between PWAS and ethylene glycol is 0.4702  $\mu\text{m}/\text{sec}$ . This shows that the velocity continuity at the interface was satisfied. Piezoelectric material properties given in **Table 2** are used for the calculations.

The liquid particle velocity can be defined by

$$v_L = i\omega \left\{ \theta \psi - e^{-\phi_{SH}} \right\} \frac{u_{ISA}}{\phi_{SH}} e^{i\gamma_L(x_3 - y_2)} \quad (4)$$

PWAS particle displacement is

$$u_1(x_3) = \left\{ \theta \left( e^{-\phi_{SH} \left( \frac{x_3 - y_1}{h_p} + 1 \right)} + e^{\phi_{SH} \left( \frac{x_3 - y_2}{h_p} \right)} \right) - e^{-\phi_{SH} \left( \frac{x_3 - y_1}{h_p} \right)} \right\} \frac{u_{ISA}}{\phi_{SH}} \quad (5)$$

Where,

$$\begin{aligned} \theta &= \frac{[\lambda \omega h_p e^{-\phi_{SH}} - \phi_{SH} \chi]}{[\phi_{SH} \xi + \lambda \omega h_p \psi]} \\ \lambda &= s_{55}^E \eta_L \gamma_L \\ \xi &= -e^{-2\phi_{SH}} + 1 \\ \psi &= e^{-2\phi_{SH}} + 1 \\ \chi &= e^{-\phi_{SH}} - 1 \\ \phi_{SH} &= i\gamma h_p \end{aligned} \quad (6)$$

and the induced displacement is introduced as

$$u_{ISA} = d_{35} \hat{E}_3 h_p \quad (7)$$

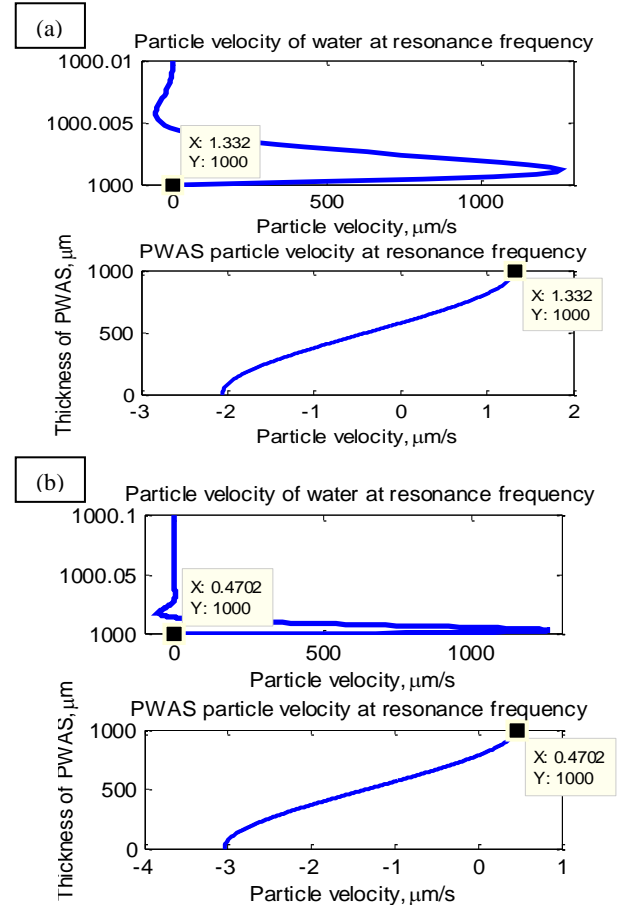


**Fig. 5** Liquid particle velocity change in the vicinity of PWAS-liquid interface at the first resonance frequency of 850.4kHz (a) for water with the density of 1000kg/m<sup>3</sup> and the dynamic viscosity of 8.9x10<sup>-4</sup> Pa.s (b) for ethylene glycol with the density of 1113kg/m<sup>3</sup> and the dynamic viscosity of 0.01 Pa.s. PWAS sizes 15mmx15mmx1mm

**Table 2** Material properties of fuels used in analytical simulations

Fuel Type	Density kg/m <sup>3</sup>	Viscosity x10 <sup>-3</sup> Pa.s
Fuel 1	725	2
Fuel 2	725	5
Fuel 3	925	2

$$Y = i\omega C_0 \left\{ 1 - \kappa_{35}^2 + \frac{\kappa_{35}^2}{\phi_{SH}} \left[ \theta \left( e^{-\phi_{SH} \left( \frac{x_2 - y_1}{h_p} + 1 \right)} + e^{\phi_{SH} \left( \frac{x_2 - y_2}{h_p} \right)} - e^{-\phi_{SH} \left( \frac{x_2 - y_1}{h_p} \right)} \right) \left( \xi - 2e^{-\phi_{SH}} \right) \right] \right\} \quad (8)$$

In the analytical simulation, first EMIS of SH-PWAS under stress-free boundary condition was simulated. Then two liquids with different density and viscosity are used as a layer on top of SH-PWAS such as water and fuel oil as seen in the model (Fig. 4) and derived as shown in Eq.(8).

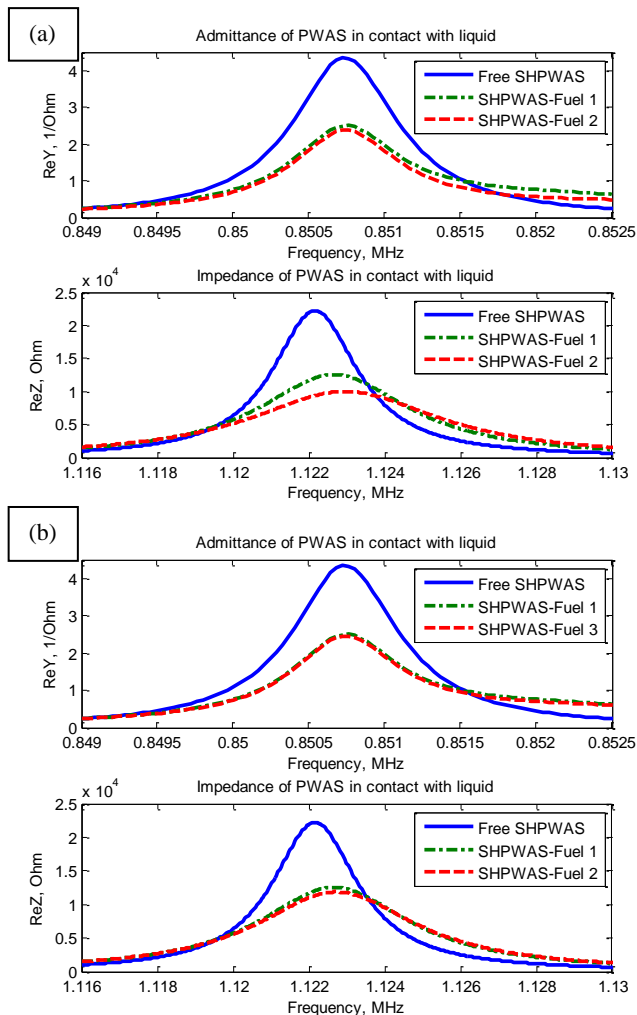


**Fig. 6** Analytical simulation results for real and imaginary parts of E/M impedance and admittance of SH-PWAS interacting with fuels (a) in different viscosity and (b) in different density

The density and the viscosity of fuels are listed in **Table 2**. The analytical simulation results at the first shear horizontal mode of SH-PWAS are presented in **Fig. 6(a)** in terms of real part of E/M impedance and admittance of SH-PWAS and SH-PWAS coupled with fuel 1 and fuel 2. The fuels 1 and 2 have the same density but different viscosity. The results presented in **Fig. 6(b)** are also EMIS of SH-PWAS and SH-PWAS coupled with fuel 1 and fuel 3. The fuels have the same viscosity but different density. In the E/M impedance results, one can observe that the amplitude shifts down whereas the anti-resonance frequency shifts up as the fuel viscosity increases; however as the density of the fuel layer is increased from 725 kg/m<sup>3</sup> to 925 kg/m<sup>3</sup>, the amplitude of impedance peak slightly decreases. Admittance results do not hold promise for good indication of parameters changes because only the amplitude of the real part of the admittance decreases when the liquid layer existed and as the viscosity was increased but the frequency did not noticeably change. Also, as the density of fuel was increased, we observed very little change in the amplitude of the admittance.

## 2. Coupled Field FEA Modelling of SH-PWAS in contact with a fuel layer

### 2.1. Free SH-PWAS

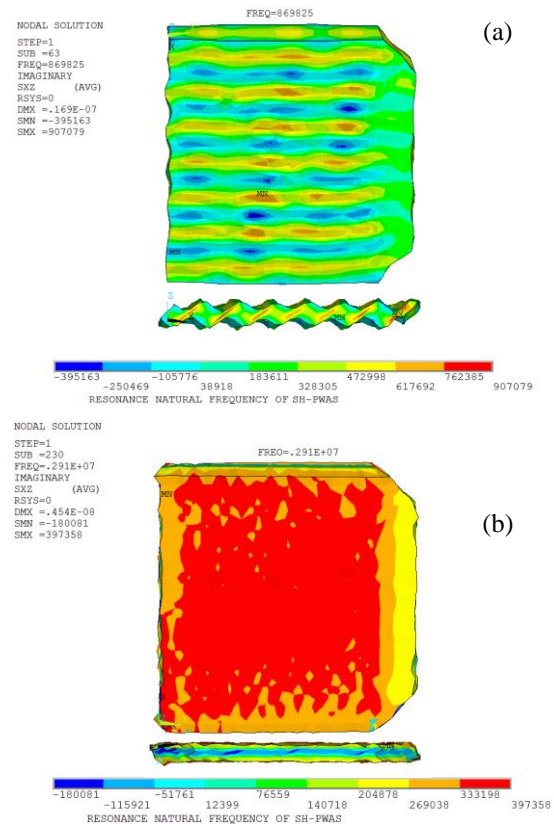


**Fig. 7 (a)** The first shear horizontal mode shape of SH-PWAS at the resonance frequency of 869 kHz. (b) The second shear horizontal mode shape of SH-PWAS at the resonance frequency of 2.91 MHz. The counter plots show  $T_{xz}$  shear stress distribution

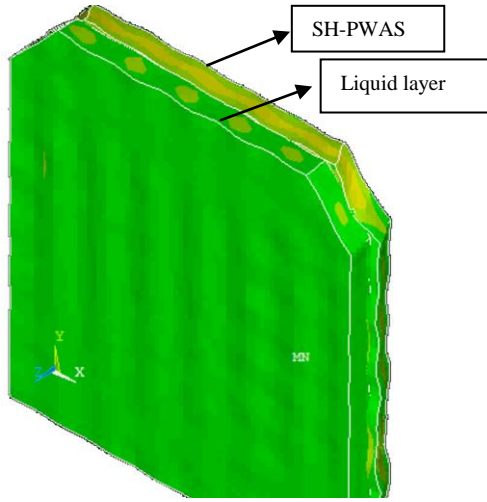


**Fig. 8** Coupled field FEA model of SH-PWAS with liquid layer vibrating in the first shear horizontal mode

We first modelled three dimensional (3-D) 15mmx15mmx1mm SH-PWAS under traction-free boundary conditions in ANSYS® without introducing the liquid layer; we used APC 850 ceramic piezoelectric material properties that were presented in **Table 2**. ANSYS multi-physics software with the implicit solver was used to perform EMIS computation in frequency domain. To perform the coupled stress and electric field analysis of PWAS transducers, coupled field piezoelectric elements were used. These coupled field finite elements consist of both mechanical and electrical fields. The elements that represent piezoelectric effects in our analysis are the 3-D coupled field solid elements i.e. SOLID5. The electrical charge  $Q$  is the electrical reaction corresponding to the voltage DOF. The charge  $Q$  is then used to calculate the admittance and impedance data. The admittance  $Y$  is calculated as  $I/V$ , where  $I$  is the current in ampere and  $V$  is the applied potential voltage in volts. The current comes from the charge accumulated on the PWAS surface electrodes and is calculated as

$$I = i\omega \sum Q_i \quad (9)$$

with  $\omega$  being the operating frequency,  $i$  is the complex number, and  $\sum Q_i$  is the summed nodal charge.

$$[C_p] = \begin{bmatrix} 97 & 49 & 49 & 0 & 0 & 0 \\ 49 & 97 & 44 & 0 & 0 & 0 \\ 49 & 49 & 84 & 0 & 0 & 0 \\ 0 & 0 & 0 & 24 & 0 & 0 \\ 0 & 0 & 0 & 0 & 22 & 0 \\ 0 & 0 & 0 & 0 & 0 & 22 \end{bmatrix} \text{ GPa} \quad (10)$$

$$[\epsilon_p] = \begin{bmatrix} 947 & 0 & 0 \\ 0 & 605 & 0 \\ 0 & 0 & 947 \end{bmatrix} \times 10^{-8} \text{ F/m} \quad (11)$$

$$[e_p] = \begin{bmatrix} 0 & 0 & 0 & 0 & 12.84 & 0 \\ 0 & 0 & 0 & 12.84 & 0 & 0 \\ -8.02 & -8.02 & 18.31 & 0 & 0 & 0 \end{bmatrix} \text{ C/m}^2 \quad (12)$$

where  $[C_p]$  is the stiffness matrix,  $[\epsilon_p]$  is the dielectric matrix, and  $[e_p]$  is the piezoelectric matrix. The density of the PWAS material is assumed to be  $\rho = 7700 \text{ kg/m}^3$ .

The first and second shear horizontal mode shapes are shown in **Fig. 7(a)** and **(b)** respectively. We also retained the electromechanical impedance and admittance results from the free SH-PWAS simulation.

## 2.2. SH-PWAS in contact with compressible and inviscid fluid

We introduced the liquid layer in the same geometric shape and sizes by using the FLUID30 element type for 3-D liquid layer modelling merged with the SH-PWAS elements (**Fig. 8**). One restriction that this fluid element has is that the dissipative effect due to the fluid viscosity was neglected. However, the sound absorption at the interface was taken into account by generating a damping matrix using the surface area and boundary admittance at the interface. The boundary admittance (MU) can be input as material property between 0 and 1. The reference pressure (PREF) was used to calculate the sound pressure level of element (defaults to  $20 \times 10^{-6} \text{ N/m}^2$ ). The speed of sound

$$c = \sqrt{k / \rho_0} \quad (13)$$

in the fluid can be input by SONC where  $k$  is the bulk modulus of the fluid and  $\rho_0$  is the mean fluid density (input as DENS) [23].

In order to show the effect of the existence of a liquid layer on EMIS of SH-PWAS, we illustrate the preliminary results in terms of a wide band impedance spectra by CF-FEA analysis including in-plane modes between 100kHz and 800kHz; thickness modes in relatively high frequency range of MHz; as well as three shear horizontal modes that appear at anti-resonance frequency of around 1MHz, 3MHz, and 4.5MHz (**Fig. 9**). It can be clearly observed that amplitude and frequency shift due to the presence of the water layer was accomplished in the FEA simulations. As seen in the analytical simulations in the preceding section, only amplitude shift occurs in admittance spectra due to the water layer existence but not frequency shift. In FEA, we adopted the fuel material properties from Reference [24] as provided in **Table 2**.



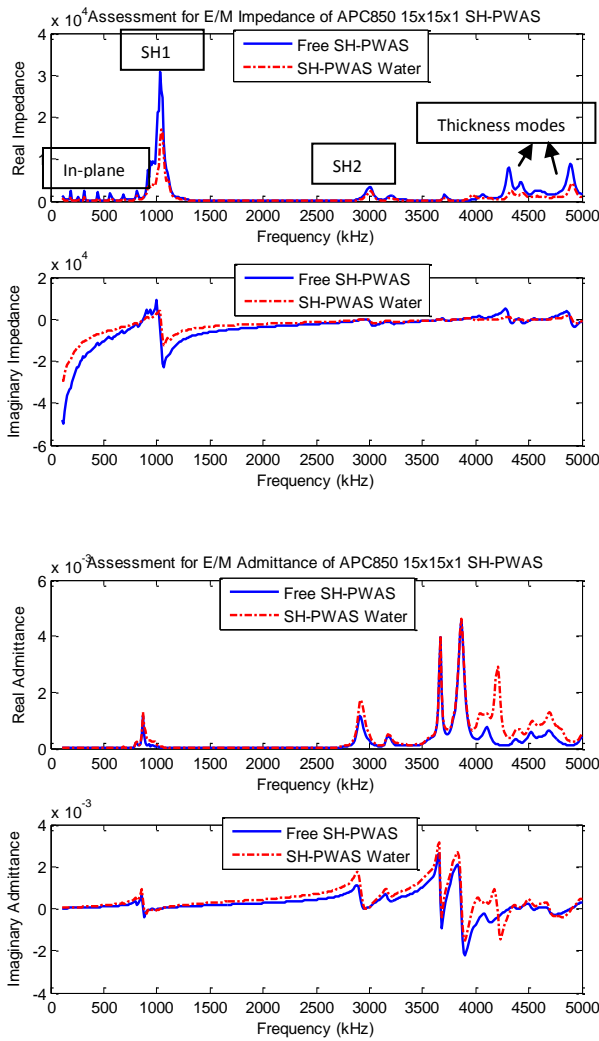


**Fig. 9** Electromechanical impedance (left) and admittance (right) spectra of 15mmx15mmx1mm SH-PWAS and SH-PWAS coupled with a 1mm thick layer of water (Please use two-column publishing format)

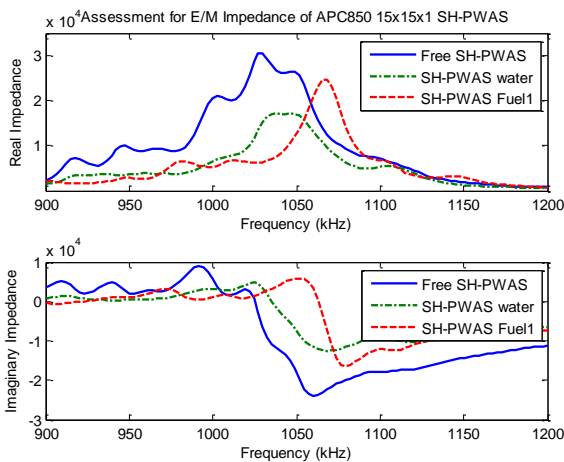


**Fig. 10** Electromechanical impedance spectra of 15mmx15mmx1mm SH-PWAS; SH-PWAS coupled with a 1mm thick layer of water; and SH-PWAS coupled with a 1mm thick layer of fuel-oil

The CF-FEA simulations also proves that E/M impedance spectrum is better indicator of presence of liquid layer and the changes in the liquid layer in comparison to the admittance spectrum. From this point of view, we focus on E/M impedance simulation results in our FEA analyses. The next results were found to be a good indicator of the liquid density effects on EMI spectrum. Since the fuel 1 is less dense ( $825 \text{ kg/m}^3$ ) than the water ( $1000 \text{ kg/m}^3$ ), the amplitude of impedance peak of SH-PWAS coupled with the fuel 1 is higher than that of the SH-PWAS with water.

### 3. Summary and Conclusion

In this paper, we presented the E/M impedance spectroscopy of piezoelectric wafer active resonator capable of being excited in shear horizontal modes (SH-PWAS) with relatively high electromechanical coupling coefficient. We developed and simulated one-dimensional analytical model and three dimensional coupled field finite element models for SH-PWAS coupled with liquid layer as well as SH-PWAS under stress-free boundary condition. We analysed the results from both analytical and CF-FEA simulations for both free SH-PWAS and SH-PWAS interacting with different liquids and fuel-oils. We aimed at developing new methodology for measuring the fuel-oil material properties such as viscosity and density by measuring the E/M impedance and admittance of SH-PWAS in contact with different liquids with different viscosity and density. The results from both simulations showed that E/M impedance is a good indicator to develop the new measurement technique. This paper presents preliminary study results and needs further developments and investigations to develop the complete methodology of fuel-oil parameter measurement.

### Acknowledgements

Acknowledgments are thankfully sent to Prof. Victor Giurgiutiu and Dr. Abdelrahman Kamal for their support to this research.

## References

- [1] V. Giurgiutiu, J. Bao, and W. Zhao, "Active Sensor Wave Propagation Health Monitoring of Beam and Plate Structures," in *Proc of SPIE's 8th International Symposium on Smart Structures and Materials*, 2001, no. March.
- [2] C. Liang, F. P. Sun, and C. a. Rogers, "Coupled Electro-Mechanical Analysis of Adaptive Material Systems -- Determination of the Actuator Power Consumption and System Energy Transfer," *J. Intell. Mater. Syst. Struct.*, vol. 5, no. 1, pp. 12–20, Jan. 1994.
- [3] F. P. Sun, C. Liang, and C. A. Rogers, "Structural modal analysis using collocated piezoelectric actuator/sensors: an electromechanical approach," in *Proc. SPIE 2190, Smart Structures and Materials 1994: Smart Structures and Intelligent Systems*, 238, 1994.
- [4] A. N. Zagrai and V. Giurgiutiu, "Electro-Mechanical Impedance Method for Damage Identification in Circular Plates," vol. 40, 2001.
- [5] G. Park, H. Sohn, C. R. Farrar, and D. J. Inman, "Overview of Piezoelectric Impedance-Based Health Monitoring and Path Forward," *Shock Vib. Dig.*, vol. 35, no. 6, pp. 451–463, Nov. 2003.
- [6] S. Bhalla, P. Kumar, A. Gupta, and T. K. Datta, "Simplified Impedance Model for Adhesively Bonded Piezo-Impedance Transducers," *J. Aerosp. Eng.*, vol. 22, no. 4, pp. 373–382, Oct. 2009.
- [7] H. A. Tinoco and A. L. Serpa, "Bonding influence on the electromechanical admittance of piezoelectric sensors bonded to structures based on EMI technique," 2011.
- [8] V. G. Annamdas and M. a. Radhika, "Electromechanical impedance of piezoelectric transducers for monitoring metallic and non-metallic structures: A review of wired, wireless and energy-harvesting methods," *J. Intell. Mater. Syst. Struct.*, vol. 24, no. 9, pp. 1021–1042, Mar. 2013.
- [9] S. Srivastava, S. Bhalla, A. Madan, and A. Gupta, "Biomedical Applications of Smart Piezoelectric Materials," in *9th International Symposium on Advanced Science and Technology in Experimental Mechanics*, 2014, pp. 9–12.
- [10] Y. Y. Lim and C. K. Soh, "Towards more accurate numerical modeling of impedance based high frequency harmonic vibration," *Smart Mater. Struct.*, vol. 23, no. 3, p. 035017, Mar. 2014.
- [11] T. Kamas, B. Lin, and V. Giurgiutiu, "Analytical modeling of PWAS in-plane and out-of-plane electromechanical impedance spectroscopy (EMIS)," in *SPIE Smart Structure and Materials + Nondestructive Evaluation and Health Monitoring 2013, Sensors and Smart Structures Technologies for Civil, Mechanical, and Aerospace Systems*, 2013, vol. 8692, p. 869227.
- [12] T. Kamas, V. Giurgiutiu, and B. Lin, "Modeling and Experimentation of Thickness Mode E/M Impedance and Rayleigh Wave Propagation for Piezoelectric Wafer Active Sensors on Thick Plates," in *Volume 1: Development and Characterization of Multifunctional Materials; Modeling, Simulation and Control of Adaptive Systems; Structural Health Monitoring; Keynote Presentation*, 2014, p. V001T05A003.
- [13] A. Kamal, V. Giurgiutiu, and B. Lin, "Predictive modeling of PWAS-coupled shear horizontal waves," in *SPIE 2013 Smart Structure/NDE, Health Monitoring and Smart NDE of Structural and Biological Systems*, 2013, p. 86950F.
- [14] K. K. Kanazawa and J. G. Gordon, "The oscillation frequency of a quartz resonator in contact with a liquid," *Anal. Chem. Acta*, vol. 175, pp. 99–105, 1985.
- [15] F. Josse and Z. Shana, "Analysis of shear horizontal surface waves at the boundary between a piezoelectric crystal and a viscous fluid medium," *J. Acoust. Soc. Am.*, pp. 978–984, 1988.
- [16] E. Nwankwo and C. J. Durning, "Mechanical response of thickness-shear mode quartz-crystal resonators to linear viscoelastic fluids," *Sensors Actuators A Phys.*, vol. 64, pp. 119–124, 1998.
- [17] S. J. Martin, H. L. Bandey, R. W. Cernosek, A. R. Hillman, M. J. Brown, and L. Le, "Equivalent-Circuit Model for the Thickness-Shear Mode Resonator with a Viscoelastic Film Near Film Resonance," vol. II, no. 1, pp. 141–149, 2000.
- [18] Y. K. Suh and Y. H. Kim, "Effect of Overlayer Viscoelasticity on Resonant Characteristics of a Quartz Crystal Resonator," *Jpn. J. Appl. Phys.*, vol. 49, no. 6, p. 065801, Jun. 2010.
- [19] F. L. Guo and R. Sun, "Propagation of Bleustein–Gulyaev wave in 6mm piezoelectric materials loaded with viscous liquid," *Int. J. Solids Struct.*, vol. 45, no. 13, pp. 3699–3710, Jun. 2008.
- [20] C. Schaschke, I. Fletcher, and N. Glen, "Density and Viscosity Measurement of Diesel Fuels at Combined High Pressure and Elevated Temperature," *Processes*, vol. 1, no. 2, pp. 30–48, 2013.
- [21] T. Kamas, "Behavior of Piezoelectric Wafer Active Sensor in Various Media," University of South Carolina, 2014.
- [22] "APC 850 material properties." [Online]. Available: [www.americanpiezo.com](http://www.americanpiezo.com). [Accessed: 29-Jun-2015].
- [23] "ANSYS Help." 2009.
- [24] C. Schaschke, I. Fletcher, and N. Glen, "Density and Viscosity Measurement of Diesel Fuels at Combined High Pressure and Elevated Temperature," *Processes*, vol. 1, pp. 30–48, 2013.

# Single Phase Series Active For Aircraft Applications

Mohamad H Taha\*†

\*Department of Electrical and Computer Engineering, College of Engineering Rafik Hariri University, Chouf 2010 Lebanon  
tahamh@rhu.edu.lb

† Corresponding author; Mohamad H Taha, Department of Electrical and Computer Engineering, College of Engineering Rafik Hariri University, Chouf 2010 Lebanon, tahamh@rhu.edu.lb

*Received: 04.06.2015 Accepted: 16.06.2015*

**Abstract**-The new electric power technology for modern aircraft is based on variable frequency generators typically ranges from 360 Hz at low speed to 800 Hz at high speed. Modern aircraft electric systems, including novel electrical distribution architectures, network interactions, protection, wiring and load management should be designed to operate with variable frequency source. A modern aircraft technology is moving toward what is known as More Electric Aircraft (MEA), this aims to increase the electrical power equipment rather than mechanical or hydraulic equipment. Power Electronics and motors drives are the major MEA components, these could produce harmonics on line current with poor power factor. This paper presents an analytical method of calculating reactive and harmonic current and using this current as a reference to feed a series active filter to compensate the harmonic currents generated by a nonlinear load.

**Keywords** Series active power filters (APF), harmonic and reactive current, more electric aircraft (MEA), variable frequency source.

## 1. Introduction

Aircraft nonlinear load such as rectifier circuit could have very bad effect on the other aircraft electric systems. This could cause current distortion and serious problems on electrical equipment such as:

1. Improper responding, interferences and degradation of the performance of devices or equipment.
2. Overheating and premature aging of the electric devices.

The new power electronics technology could eliminate these problems and make the electric system more efficient with high power density.

MEA loads will be designed to operate with variable frequency supply, usually from 360 to 800 Hz approximately, although there are some electrical loads that may require a DC supply or a traditional fixed frequency supply (400 Hz). Sophisticated electrical systems are usually multiple voltage systems using a combination of AC and DC buses to power various aircraft components. Figure 1 shows a block diagram for aircraft power system [1,2]. Here depending on the type of the load, the input supply could feed variable frequency load, fixed frequency load or DC load. However, as one essential part of the MEA electric systems are the AC/DC converters which are connected to a variable frequency AC bus and used to supply DC power for different loads. These converters are required to show

low volume, high reliability, and low current harmonics. The current harmonics will cause distortion in the line impedance and the terminal voltage of the load will be distorted. If linear loads are connected to the system they will absorb the distorted current which could cause serious problems on the system. A traditional and simple method to overcome and solve these problems is to use passive filters; however, as it is well known these types of filters operate at specified frequency, which means many filters should be tuned to cancel harmonics at different frequencies. Furthermore, resonances can occur, and the electrical system can start to operate with capacitive power factor [3,4].

In More Electric Aircraft, the power electronics technology represents a challenge for aeronautical application, which enhances power quality problems even at the lowest voltage level in distribution system. In recent technology, active filters have been widely used in to improve the power quality for More Electric Aircrafts. Good numbers of different active filters have been designed with a limited emphasis on single phase system.

This paper presents a control method for a series active power filter (APF) by using an analytical method of calculating the active and non-active and harmonics current and power for non-sinusoidal load current. The voltage injected by the series active filter is proportional to the harmonics and reactive components of the load current. [1,3].



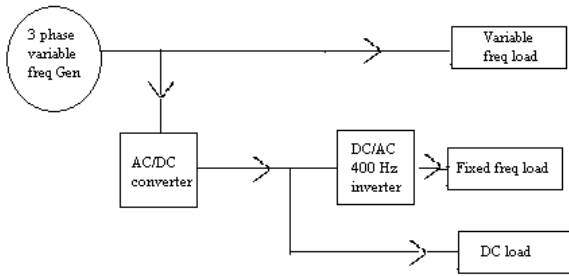


**Fig. 1.** Aircraft power system

The APF must comply with the regulations and standards of the aircraft power system such that:

1. The harmonics on the input current should be low and meet the required values.
2. Minimizing reactive power components that could be achieved by high input power factor.
3. Maximizing power density in order to minimize the weight. [1,2]

However, due to the wide ranging nature of the load and supply frequency variation, the design of this system poses significant challenges.

Furthermore, the choice of the hardware components such as semiconductor devices, capacitors, inductors and resistors is very important for aerospace industry. These components have to be selected so that normal service maintenance would ensure the retention of their specified characteristics through the full range of operational and environmental conditions likely to be encountered through the life of the aircraft, or support facility, in which they are installed. [1]

## 2. Power Calculation

Instantaneous active power is defined as the rate of change of the transfer or utilization of the energy generation. It is a physical quantity and satisfies the principles of conservation of energy.

Normally in the electric power system applications the voltage and current could be represented by:

$$v(t) = \sqrt{2} V_{rms} \sin \omega t \quad (1)$$

A sinusoidal current given by:

$$i(t) = \sqrt{2} I_{rms} \sin(\omega t - \phi). \quad (2)$$

The instantaneous power is the multiplication of the instantaneous voltage and current signals which is divided into two components namely the instantaneous active power and the instantaneous reactive power :

$$p(t) = v(t)i(t) = p_a + p_q \quad (3)$$

The active power is the time average of the instantaneous power over one periode of wave p(t):

$$P = \frac{1}{T} \int_0^T v(t)i(t)dt \quad (4)$$

Instantaneous reactive power is produced by the reactive components of the current and the related energy component oscillates between the source and the load where the net transfer energy to the load is zero. Furthermore reactive power can be thought of as the useless power that causes increased line current and losses.

When a nonlinear load is connected, the system no longer operates in sinusoidal condition due to the presence of the harmonics; in this case Fourier series is used to express the voltage and current [5,6,7]:

$$v(t) = V_0 + \sum_{n=1}^{\infty} \sqrt{2} V_{n,rms} \sin(n\omega t) \quad (5)$$

$$i(t) = I_0 + \sum_{n=1}^{\infty} \sqrt{2} I_{n,rms} \sin(n\omega t - \phi_n) \quad (6)$$

Where,  $V_0$  and  $I_0$  represent DC value;  $V_{n,rms}$  and  $I_{n,rms}$  represent RMS value for the nth harmonic and  $\phi_n$  represent phase between the voltage and current for the nth harmonic.

By assuming the DC voltage and current quantities equal to zero, the average active power is (8.9.10):

$$P = \sum_{n=1}^{\infty} I_{n,rms} V_{n,rms} \cos(\phi_n) \quad (7)$$

The nonsinusoidal single phase periodic voltage and current waveforms have two distinct components, the fundamental components and harmonics components bear in mind assuming the DC quantities for both voltage and current are zero.

$$i(t) = i_1(t) + i_h(t) \quad (8)$$

$$v(t) = v_1(t) + v_h(t) \quad (9)$$

$$v_1(t) = \sqrt{2} V_{rms} \sin(\omega t) \quad (10)$$

$$i_1(t) = \sqrt{2} I_{rms} \sin(\omega t - \phi_1) \quad (11)$$

$$v_h(t) = \sum_{n \neq 1}^{\infty} \sqrt{2} V_{n,rms} \sin(n\omega t) \quad (12)$$

$$i_h(t) = \sum_{n \neq 1}^{\infty} \sqrt{2} I_{n,rms} \sin(n\omega t - \phi_n) \quad (13)$$

In the IEEE Standard for non-sinusoidal voltage and current, the active power definition is the same as given in the equation (4) and :

$$P = P_I + P_h \quad (14)$$

$$P_I = V_I I_I \cos \phi_1 \quad (15)$$

$$P_h = P - P_I = \sum_{n \neq 1}^{\infty} I_{n,rms} V_{n,rms} \cos(\phi_n) \quad (16)$$

Similarly, the reactive power can be represented:

$$Q = Q_I + Q_h \quad (17)$$

Fundamental reactive power :

$$Q_{I1} = V_I I_I \sin \phi_1 \quad (18)$$

$$Q_h = Q - Q_I = \sum_{n \neq 1}^{\infty} I_{n,rms} V_{n,rms} \sin(\varphi_n) \quad (19)$$

Therefore the apparent power S is the sum of the fundamental and non-fundamental term:

Fundamental apparent power :

$$S_{I1} = V_I I_I = \sqrt{P_{11}^2 + Q_{11}^2} \quad (20)$$

Total apparent power:

$$S^2 = (VI)^2 = (V_I I_I)^2 + (V_I I_h)^2 + (V_h I_I)^2 + (V_h I_h)^2 \quad (21)$$

$$S^2 = S_I^2 + S_N^2 \quad (22)$$

$$S_I^2 = (V_I I_I)^2 = P_I^2 + Q \quad (23)$$

$$S_N^2 = (V_I I_h)^2 + (V_h I_I)^2 + (V_h I_h)^2 \quad (24)$$

As well known the total harmonic distortion for both voltage and current is defined as the ratio between rms value of harmonics to fundamental component:

$$THD_V = \frac{V_h}{V_1} \quad (25)$$

$$THD_I = \frac{I_h}{V I_1} \quad (26)$$

The distortion power factor due to the harmonic current is:

$$D_I = V_I I_h = S_I(THD_I) \quad (27)$$

The distortion power factor due to the harmonic voltage is:

$$D_V = V_h I_I = S_I(THD_V) \quad (28)$$

Harmonic apparent power

$$S_h = V_h I_h = S_I(THD_I)(THD_V) \quad (29)$$

Harmonic distortion power :

$$D_h = \sqrt{S_h^2 - P_h^2} \quad (30)$$

Apparent power becomes

$$S^2 = (VI)^2 = (S_{I1})^2 + (D_I)^2 + (D_V)^2 + (S_h)^2 \quad (31)$$

Nonfundamental apparent power:

$$S_N^2 = S^2 - S_I^2 = D_I^2 + D_V^2 + S_h^2 \quad (32)$$

Nonactive power :

$$N = \sqrt{S^2 - P^2} \quad (33)$$

The power factor of a sinusoidal AC system is equal to the cosine of the angle between the current and the voltage. This angle is called the displacement angle (power factor =  $\cos \varphi$ ). However, a rectifier draws a non-sinusoidal current from the AC system and the value  $\cos \varphi$  does not represent the power factor.

$$P.F = \frac{\text{Active power}}{V_{rms} I_{rms}} \quad (34)$$

The current contains harmonic components which result in an RMS value higher than the RMS value of its fundamental component. Thus, the power factor is less than the cosine of the displacement angle.

If the supply voltage of the rectifier is considered to be sinusoidal and consequently the mean power is:

$$P_{active} = V_{rms} I_{1rms} \cos \varphi_1 \quad (35)$$

Where the suffix 1 relates to the fundamental component of the current and  $\varphi_1$  is the phase angle between the voltage and the fundamental component of the current.

Therefore:

$$P.F = \frac{I_{1rms}}{I_{rms}} \cos \varphi_1 \quad (36)$$

Where,

$\frac{I_{1rms}}{I_{rms}}$  is defined as the input distortion factor,

$\cos \varphi_1$  is the input displacement factor.

Assume the input voltage is sinusoidal and has no distortion and the input current, which is distorted by the power factor and harmonics of the load, therefore the load current made up with the following terms:

$$i_L(t) = i_o(t) + i_a(t) + i_r(t) + i_h(t) \quad (37)$$

Where,

$i_o(t)$  Dc component

$i_a(t)$  Active current

$i_r(t)$  Reactive current

$i_h(t)$  Harmonic current

Equation (37) can be simplified by combining the reactive and harmonic currents and by assuming the dc component of the load current is zero because in practice this current is usually small or does not exist.

$$i_{rh}(t) = i_r(t) + i_h(t) \quad (38)$$

The harmonic and reactive current drawn by the load is extracted from the load current is given by:

$$i_{rh}(t) = i_L(t) - i_a(t) \quad (39)$$

By applying a low pass filter to the instantaneous load power the average active power can be obtained. Hence the instantaneous active current is:

$$i_a(t) = \frac{\sqrt{2}}{v_{rms}} p_{av} \times \sin \omega t \quad (40)$$

Combine equations (38), (39) and (40):

$$irh = il - \frac{\sqrt{2}}{v_{rms}} p_{av} \times \sin \omega t \quad (41)$$

To generate the reference current, the harmonic and reactive current drawn by the load is extracted from the load. Furthermore the voltage injected by the series active filter is proportional to the harmonic and reactive component of load current. Therefore :

$$V_{refer} = K (irh) \quad (42)$$

$V_{refe}$  is compared with the voltage injected from the active filter and a PI controller is used to control the PWM in turn control the power compensation to the load [11,12,13].

Figure 2 shows the APF circuit diagram and figure 3 control strategy of the series filter. The output stage of the diode rectifier could be connected to a DC or to 400 Hz inverter (Single or 3 phase inverter). In this case the system will be operated as variable to constant frequency inverter.

### 3. Simulation Results

Simulation has been done at different input frequency and different componsation ratio. The diode rectifier is connected to a resistive load, in this case the system will be used to feed DC load. Results are show in figures 4 to 17. It can be seen with good compensation, the power factor is unity and THD of the input current equal to 7%, with poor compensation the system operates with bad power factor and THD of the input current is high. The parameter values used for the simulation are shown in table 1.

**Table 1.** Simulation parameters.

RMS phase voltage	115 V
Input inductance , L1,2,3	L = 200uH
Dc Output capacitor	C <sub>dc</sub> = 500μF
Active filter capacitor	C = 500μF
Load	R = 1 Ω
Compensation ratio	K = 10
Switching frequency	20 KHz

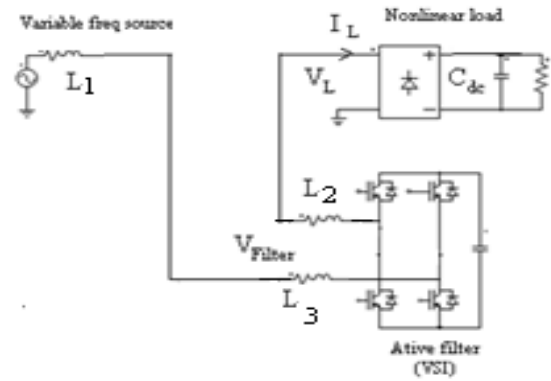


**Fig. 2.** Active filter circuit.

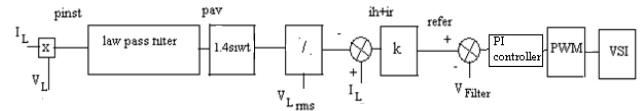


**Fig. 3.** Control strategy for the active filter.

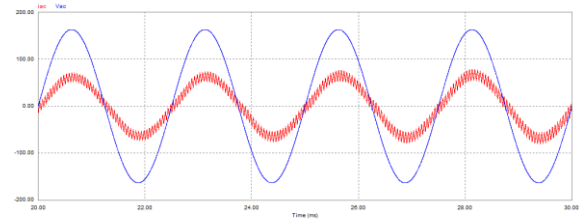


**Fig. 4.** Simulation results for 400 Hz input voltage and k=10 showing input voltage and current.

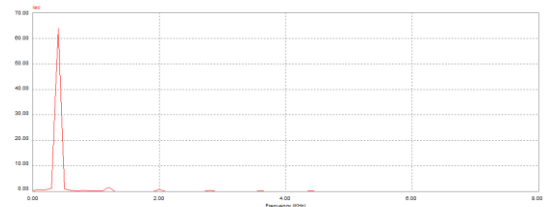


**Fig. 5.** Simulation results for 400 Hz input voltage and k =10 showing FFT for the input current. (THD = 7%)

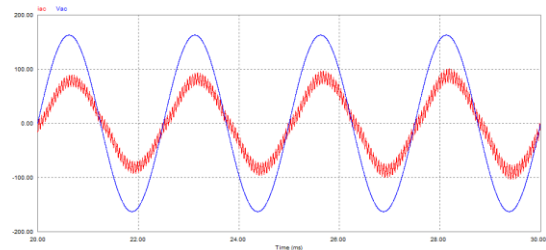


**Fig. 6.** Simulation results for 400 Hz input voltage and k = 5 showing input voltage and current.

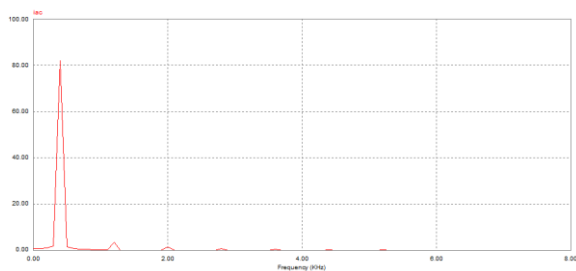


**Fig. 7.** Simulation results for 400 Hz input voltage and  $k = 5$  showing FFT for the input current. (THD = 11%)

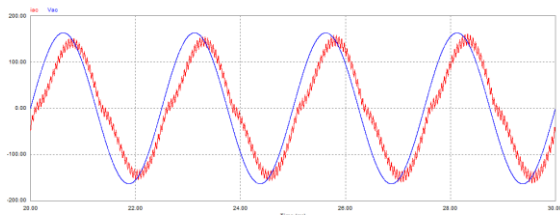


**Fig. 8.** Simulation results for 400 Hz input voltage and  $k = 1$  showing input voltage and current.

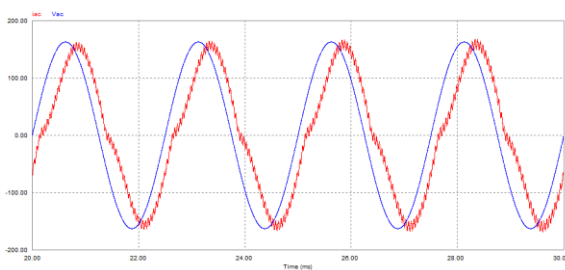


**Fig. 9.** Simulation results for 400 Hz input voltage and  $k=0.5$  showing input voltage and current.

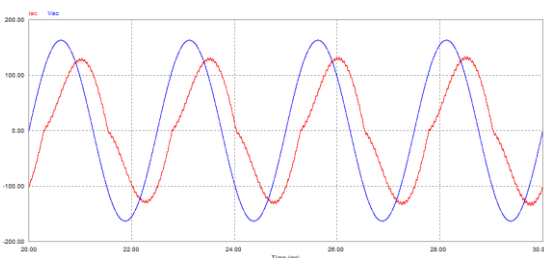


**Fig. 10.** Simulation results for 400 Hz input voltage and  $k=0.1$  showing input voltage and current.

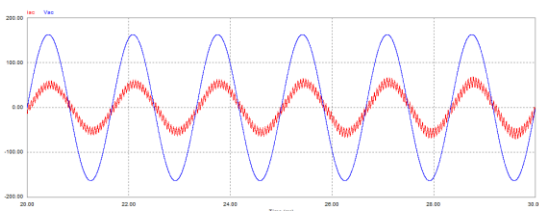


**Fig. 11.** Simulation results for 600 Hz input voltage and  $k=10$  showing input voltage and current.

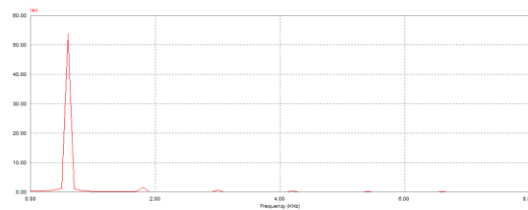


**Fig. 12.** Simulation results for 600 Hz input voltage and  $k=10$  showing FFT for the input current. (THD = 7%)

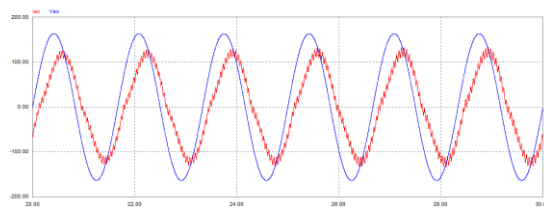


**Fig. 13.** Simulation results for 600 Hz input voltage and  $k=1$  showing input voltage and current.

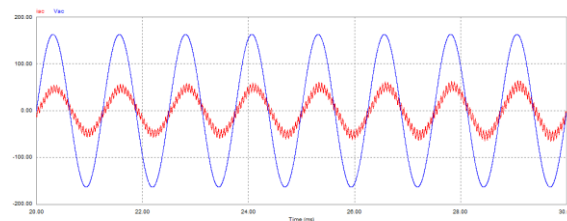


**Fig. 14.** Simulation results for 800 Hz input voltage and  $k=10$  showing input voltage and current.

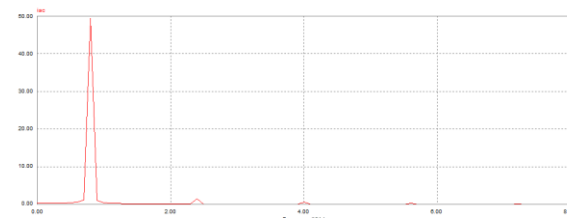


**Fig. 15.** Simulation results for 800 Hz input voltage and  $k=10$  showing FFT for the input current. (THD = 7%)

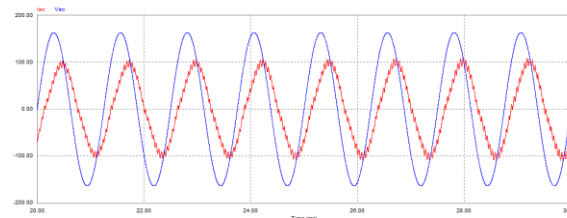


**Fig. 16.** Simulation results for 800 Hz input voltage and  $k=1$  showing input voltage and current.

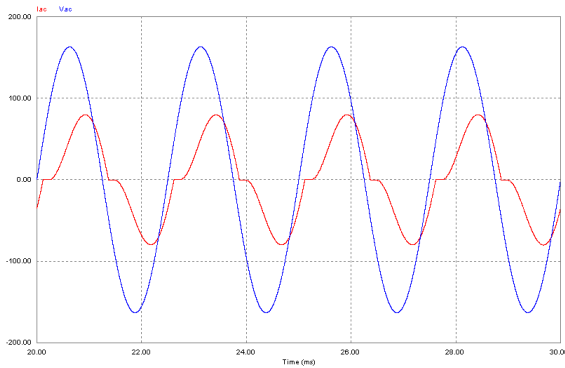


**Fig.17.** Simulation results for 400 Hz input voltage showing input voltage and current for  $K=0.5$

#### 4. Conclusion

In this paper a simple control strategy for single phase active filter y has been proposed. The system could be used in MEA to feed DC load from variable input source frequency.

The proposed active filter injects series voltage proportional to the sum of the harmonic and reactive current drawn by the nonlinear load. The simulation gave very encouraging results and shows that when the compensation ratio is low, high distortion appears on the input current and the power factor is not unity

Furthermore, this paper presents the definition and calculation of active and reactive power and power factor for sinusoidal and non-sinusoidal sources.

#### Acknowledgements

I would like to express my sincere appreciation and respect to the late prime minister Rafik Hariri who is entirely responsible for funding my studies in England.

#### References

- [1] M H Taha, "Active rectifier using DQ control for aircraft application" IEMDC 2007; PP 1306-1310.
- [2] M H Taha, S Skinner, S Gami, M Holme and G Raimondi " Variable frequency to constant frequency converter for aircraft application" PEMD 2002, PP235-240
- [3] Kamala Kant Mishra, Rajesh Gupta, " Load compensation for single phase using series active filter" IJEST Vol 3, No 3 , 2011 , pp 83-93
- [4] J. Sebastian Tepper, Juan W. Dixon, " A simple frequency – independent method for calculating the reactive and harmonics current in nonlinear load" IEEE Trans on Indust Elect, Vol. 43 No.6 Decem 1996. Pp 647-65

- [5] Marko Dimitrijevic and Vanco Litovski " Quantitative Analysis of reactive power calculation for small non-linear load" Proceeding of small system simulation symposium 2012, Nis
- [6] Juan Dixon, Luis Morán, José Rodríguez, Ricardo Domke, "Reactive Power Compensation Technologies, State of-the-Art Review", IEEE Proc. vol. 93, no. 12, pp. 2144-2164, 2005.
- [7] R. S. Herrera, P. Salmeron, and H. Kim, "Instantaneous reactive power theory applied to active power filter compensation: Different approaches, assessment, and experimental results", IEEE Trans. Ind. Electron., vol. 55, no. 1, pp. 184–196, Jan. 2008.
- [8] Kahraman Yumak, Omer Usta " A Controversial Issue: Power Components in Nonsinusoidal Single-Phase Systems", ELECO 2011 7th International Conference on Electrical and Electronic Engineering, 1-4 December, BURSA, Turkey, pp 158-162, 2011
- [9] A. E. EMANUEL, "Summary of IEEE Standard 1459: Definition for Measurement of Electric Power Quantities Under Sinusoidal, Nonsinusoidal, Balanced, or Unbalanced Conditions" IEEE Trans Ind Appl., vol. 40, no 3, pp869-878, May/jun, 2004
- [10] A, E, Emanuel, " Power Definitions and the physical Mechanism of power flow", John Wiley & Sons Ltd, UK 2010
- [11] L. Hongda and K. Cao, "Active power filter simulation based on instantaneous reactive power theory and the PWM hysteresis control mode", 978-1-4244-8161-3/11/ IEEE, 2011.
- [12] Roger C. Dugan, Mark F. McGranaghan, Surya Santoso and H. Wayne Beaty, "Electrical Power Systems Quality", 2nd edition, McGraw-Hill Companies, 2004.
- [13] J. L. Afonso, H. R. Silva and J. S. Martins, "Active Filters for Power Quality Improvement", IEEE Porto Power Tech'2001, Porto, Portugal, 10-13 Set.

# Original Solutions for Structural and Functional Rehabilitation of Masonry Buildings

Kubilay Kaptan\*<sup>‡</sup>

\* International Blue Crescent Relief and Development Foundation, Center for Humanitarian Studies, Bagdat Caddesi Dorsan Apt. No:467/9, Suadiye – Kadıkoy Istanbul Turkiye 34740

kaptankubilay@gmail.com

<sup>‡</sup> Kubilay Kaptan, Bagdat Caddesi Dorsan Apt. No:467/9, Suadiye – Kadıkoy Istanbul Turkiye 34740, Tel : +90 216 384 14 86-87, Fax : +90 216 361 57 45, kaptankubilay@gmail.com

*Received: 11.05.2015 Accepted:20.06.2015*

**Abstract-** The paper presents strengthening solutions and elements of functional rehabilitation for a certain class of 2-4 storied historical buildings of masonry structure. In order to protect the ornamental plastering of the ceiling, an original technology of rehabilitation for large spanned timber slab structures was performed. The worked out technical solution was applied on several buildings. It is presented on the case of a historical building from the 19<sup>th</sup> century. This case also gives the opportunity to emphasizing the functional improvement of the building.

**Keywords** Structural rehabilitation, masonry buildings, historical buildings, strengthening, ornamental plastering.

## 1. Introduction

At the time of 17th to 19th centuries, from Baroque to Eclectic era, a large number of 2-4 storied masonry buildings were performed all across Middle-East Europe. Most of them public buildings are functioning even today. So there are the Palace of Justice in Odorheiu-Secuiesc (Figure 1) and the Palace of Justice in Miercurea-Ciuc (Figure 2), both in Transilvania.

Generally, the supporting structure of these buildings consists of: brick or/and stone-walls and pillars as vertical supporting elements, respectively brick and/or stone bridging elements like masonry arches and vaults, barrel vaults with metal beams or timber slabs as horizontal bearing structures [1], [2] and [3]. Many of these buildings present serious damages today, influencing the reliability of them concerning serviceability limit state and even ultimate limit state requirements [4].

In previous studies [5], [6] different types of historical masonry vaults and slab structures were defined and classified. Their characteristic deficiencies and damages were also put into evidence. A convenient and objective approach of the technical state of the building was proposed and solutions of strengthening were presented [7], [8].

At this time, the purpose is to present some special strengthening techniques corroborated with architectural

and functional demands in the frame of the general rehabilitation of the building [9]. The necessity of functional improvement of the old buildings has to be also discussed. These purposes are developed through a significant case (Figure 1).

## 2. Description of the Building

### 2.1. Historical considerations

The Palace of Justice in Odorheiu-Secuiesc is a representative example of many administrative buildings constructed in Transilvania during the 19th century [10], [11]. These buildings responded to the main process of reorganizing and developing the whole system of justice. In this order, the Palace of Justice in Odorheiu-Secuiesc was finished and put in function in 1835 [12].

### 2.2. Structural and architectural description

The palace initially housed not only the trials, but also the prison. Consequently, the organization of the interior spaces corresponded to the functional requirements of that time. It is a two-storied building with basement (Figure 1).





**Fig. 1.** Palace of Justice in Odorheiu-Secuiesc



**Fig. 2.** Palace of Justice in Miercurea-Ciuc



**Fig. 3.** Masonry stone walls, brick arch and vault

The structure of the cellar is of masonry stone walls sustaining brick arches and vaults (Figure 3).

The structure of the ground floor and first floor consists in brick masonry walls and timber slabs. The roof structure is of main timber trusses of Eclectic type. The whole building can be classified as Eclectic, with late Baroque influence [13], [14], [15].

### 3. The General Rehabilitation Process

The rehabilitation of the Palace of Justice was carried out in the years 1999 – 2003. The diagnosis of the building put into evidence the necessity of a capital repair and also consolidation of some subassemblies of the structure in

order to reassure the resistance and serviceability of the building [16]. On the other hand, actual demands of functionality imposed its extension, by adding a new block to the old building.

#### *3.1. Consolidation of the masonry vault system over the basement*

The masonry vault system of the basement is supported by masonry arches and walls (Figure 3). It is to be mentioned the pronounced flatness of the brick arches.

The examination of the masonry vaults and arches put into evidence two main aspects: cracks and breaks with detached bricks on the one hand and important vertical displacements on the other hand. Obviously, the vault system had to be discharged [17], [18]. For this purpose, a new independent slab system was performed over the initial bearing system (Figure 4). It consists in a reinforced concrete slab on metal beams leaning on the stone walls. So, the vaults and arches have to carry only their own weight. The detached and destroyed pieces of brick were replaced with new ones and the masonry joints were filled with lime mortar with powdered brick as hydraulic additive.

#### *3.2. Consolidation of the timber slab system over the first floor*

The ordinary timber slab over the ground floor and first floor consists in wooden beams bridging the shorter opening between the supporting masonry walls. Their diagnostic, repair and consolidation represented usual engineering tasks. The strengthening solution was: discovering the timber beams, replacing or repairing them, their treatment with antiseptic and fire protection substances, using them as shuttering for the new reinforced concrete slab [19]. The ventilation of the old timber slab was assured by providing a slit between the lower face of the old timber slab and the false ceiling attached to it. Holes of ventilation were provided along the perimeter and around the lamps.

The main technical problem was the rehabilitation of the slab system over the Great Judgement Hall on the first floor. Originally, it is a timber slab system covering a surface of 11.50 x 10.50 m<sup>2</sup>. The slab system consists in a girder network of main and secondary timber beams supported by the perimeter walls. A number of three main beams crosses a span of 10.50 m, placed at a distance of approximately 2.80 m one from the other, thus creating a number of four 2,80 m long openings for the secondary beams. Double boarding is fixed on the upper, respectively on the bottom face of the grid. The original ceiling was realized by a decorative plastering on a reed sheet fixed to the inferior boarding. On its upper side the slab structure was completed with thermal slag insulation and brick covering.

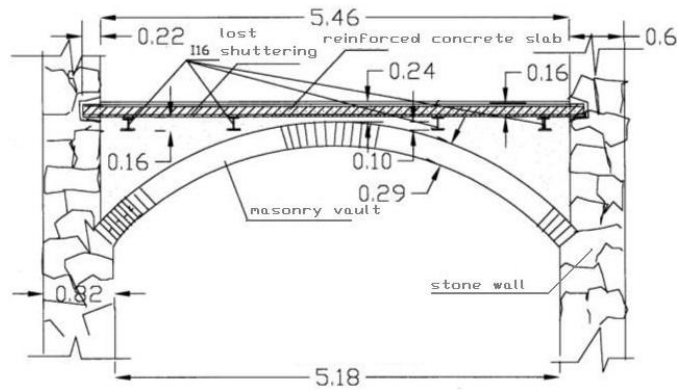


**Fig. 4.** Consolidation of the slab system over the basement



**Fig. 5.** Plastering in stucco of the ceiling

The most inconvenient phenomenon was the great deflection of the slab, respectively of the main beams. The measured vertical displacements at the middle of the beams were between 11 and 14 cm. This phenomenon caused serious damages, i. e. visible cracks in the ornamental stucco plastering of the ceiling (Figure 5).

The aim was to find a technique of intervention to diminish the deflections saving the ornamental plastering of the ceiling too. For this purpose it was necessary to bring the timber slab back near to its initial form [20], [21]. In this respect, at first, the slab has been discharged taking away the vertical loading given by the floor (thermal insulation and bricks). Secondly, the middle of the main beams had to be lifted for diminishing the vertical deflections. The solution was to build over each main timber beam an independent reinforced concrete girder (Figure 6) supported by the marginal walls.

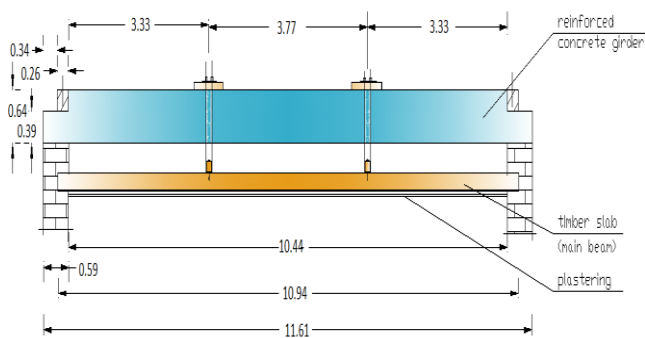


**Fig. 6.** Lifting girder

An additional temporary sustaining system was conceived to sustain the shuttering, the reinforcement and the cast concrete of the lifting girder. It consists in a triangular timber structure with a tie-rod (Figure 7 and Figure 8) to which the vertical loading is transferred by a series of vertical metal bars.

A transverse section of the whole lifting system, after striking the reinforced concrete girder, is presented in Figure 9.

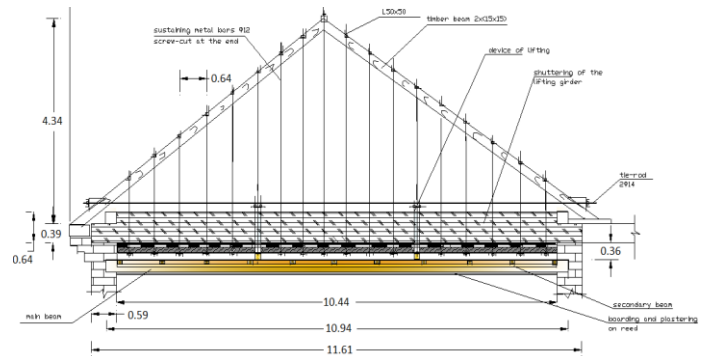


**Fig. 7.** Additional supporting structure of the lifting girder-design



**Fig. 8.** Additional supporting structure of the lifting girder- photo

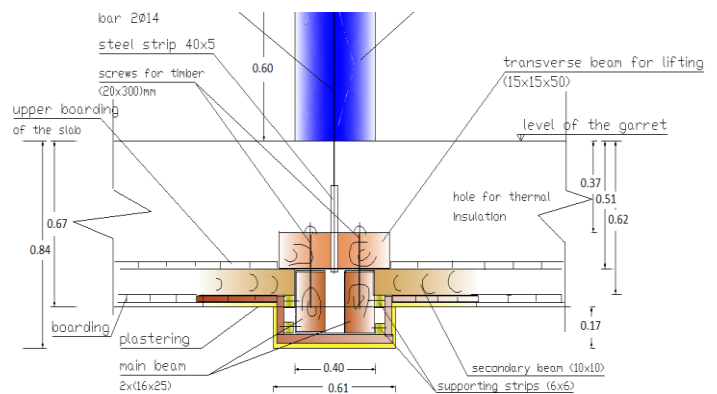


**Fig. 9.** Transverse section of the lifting system



The operation of lifting can be performed in two ways:

(a) Lifting the slab before casting the girder, using the additional timber structure for lifting; in this way the bottoming of the two lifting bars is made automatically by the concrete hardening; a relatively short time for the operation can be assured (7-8 days);

(b) Lifting after the execution of the reinforced concrete girder; the lifting bars pass through the girder by former embedded tubes; it has the advantage of a perfectly controlled way of lifting and bottoming the lifting bars on the girder surface by screwed devices; the time of operation is relatively long because of the hardening time of the concrete;

In this way the middle of the main beams could be lifted with 8 – 9 cm without displacements of the supports. This rising of the axes of the beams was enough to close the cracks of the ornamental plastering and finally permitted a proper restoration of the ceiling.

### 3.3. Functional rehabilitation

For improving the circulation flux in the building and also responding to the actual requirements concerning emergency evacuation, a new staircase was added to the old building [22], [23]. The originality of the solution consists in the fact that the architect didn't try to take again the initial style of the building [24], [25]. On contrary, aiming to a maximum functional and structural efficiency, a very modern solution in reinforced concrete and glass was adopted (Figure 10, Figure 11).



Fig. 10. New staircase - interior view



Fig. 11. New staircase - exterior view

## 4. Conclusions

The study put into evidence one of the major dilemma of the rehabilitation process: the necessary balance between preserving the valuable historical characteristics of an old building and today's requirements concerning the safety, serviceability and functionality of the building.

The paper presents an original technical solution for consolidating large spanned timber slab structures saving architectural values as well. The solution consists in diminishing the vertical deflection of the slab by using a special lifting system.

Modern architectural solutions can be successfully used in order to improve the functionality of the historical buildings, without disturbing, on the contrary, emphasizing their historical character.

## References

- [1] Ahmad Hamid, 2012, Design and Retrofit of unreinforced Masonry Structures, FUNDEC course on. Lisbon, February 6, 2012.
- [2] Appleton J, 2009, Técnicas de reabilitação de estruturas de alvenaria, Seminar "Patologia, Inspeção e Reabilitação de Edifícios tradicionais" (in Portuguese).
- [3] Appleton, J., Reabilitação de Edifícios Antigos Patologias e tecnologias de intervenção, Edições Orion, 1ª Edição, Setembro de 2003 [in Portuguese].
- [4] Amadio C., Gattesco N., Dudine A., Franceschinis R., Rinaldin G., 2012, Structural performance of spandrels in stone masonry buildings, Proc. of the 15th World conference on Earthquake Engineering, pp 5077, Lisbon, Portugal.
- [5] Bucur-Horváth, I., Popa, I., Tanasoiu, I. 2000, "Study on old masonry structures in brick vaults", 2nd International Congress on Studies on Ancient Structures, Istanbul, pp. 311-322.
- [6] Bucur-Horváth, I., Popa, I., Bacsó, Á., Puskás, A. 2001, "Approaches of the technical state and behaviour for old structures in brick vaults", 3rd International Seminar on Historical Constructions. Possibilities of numerical and experimental techniques. Guimarães, Portugal, pp. 283-291.
- [7] Arifuzzaman S. and Saatcioglu M., 2012, Seismic Retrofit of Load Bearing Masonry Walls by FRP Sheets and Anchors, Proc. of the 15th World conference on Earthquake Engineering, pp 4501, Lisbon, Portugal.
- [8] Córias e Silva V (2007) Reabilitação Estrutural de Edifícios Antigos—Alvenaria, Madeira—Técnicas pouco intrusivas. Ed. Argumentum & Gecorpa, Lisbon, Portugal (in Portuguese).
- [9] Costa A., 2008, Notes from the post9 graduation course on rehabilitation of constructions – Stone Masonry structures.

- [10] Cruz H., FUNDEC course on Rehabilitation techniques of constructions, wood structures, IST 9 23 Jan to 3 Feb 2012.
- [11] Ingham, J., 2012, FUNDEC one day lecture on the "Seismic assessment and improvement of unreinforced masonry buildings", IST.
- [12] Kabir M. Z., Kalali A., Shahmoradi R., 2012, Cyclic Behavior of Perforated Masonry Walls
- [13] Strengthened with Fiber Reinforced Polymers, Proc. of the 15th World conference on Earthquake Engineering, pp 3734, Lisbon, Portugal.
- [14] Lourenço, P. "Reabilitação de edifícios de alvenaria e adobe". Lectures on the rehabilitation of masonry structures, University of Minho.
- [15] Ma R., Jiang L., He M., Fang C., Liang F., 2012, Experimental investigations on masonry structures using external prestressing techniques for improving seismic performance, Engineering Structures 42 (2012) 297–307.
- [16] Magenes G., Penna A., Rota M., Galasco A., Senaldi I., 2012, Shaking table test of a full scale stone masonry building with stiffened floor and roof diaphragms, Proc. of the 15th World conference on Earthquake Engineering, pp 5320, Lisbon, Portugal.
- [17] Mahdizadeh A., Borzouie J., Raessi M., 2012, New Approach to seismic Rehabilitation of Masonry School Buildings, Proc. of the 15th World conference on Earthquake Engineering, pp 2851, Lisbon, Portugal.
- [18] Mayorka P. and Meguro K, 2008, "A step towards the formulation of a simple method to design PP9Band mesh retrofitting for Adobe/Masonry houses", 14th World Conference on Earthquake Engineering, Beijing, October 2008.
- [19] Meireles, HA, 2012, Seismic vulnerability of Pombalino buildings, PhD Thesis, IST, Portugal (in English).
- [20] Parisi M.A., Chesi C., Tardini C., 2012, The Role of Timber Roof Structures in the Seismic Response of Traditional Buildings, Proc. of the 15th World conference on Earthquake Engineering, pp 2394, Lisbon, Portugal.
- [21] Robinson L, Bowman I, 2000, Guidelines for Earthquake Strengthening, New Zealand, Historic Places Trust, Wellington, NZ.
- [22] Roque, J. A., 2002, "Reabilitação Estrutural de Paredes Antigas de Alvenaria". Master Thesis University of Minho, Setembro 2002. ([www.civil.uminho.pt/masonry](http://www.civil.uminho.pt/masonry)) (in Portuguese).
- [23] Santos S.P. (reporter), 2010, Guide for the Structural Rehabilitation of Heritage Buildings, CIB Publication 335, June 2010.
- [24] Santos, S.P., 2003, "Structural Rehabilitation of Historic Buildings", 40th Meeting of Commission CIB W023, Padova, Italy, (in CD9ROM).
- [25] Shrestha H., Pradhan S., Guragain R., 2012, Experiences on Retrofitting of Low Strength Masonry Buildings by Different Retrofitting Techniques in Nepal, Proc. of the 15th World conference on Earthquake Engineering, pp 2012, Lisbon, Portugal.

# Calculation of Aerodynamic Performance Characteristics of Airplane Wing and Comparing with the Experimental Measurement

Haci Sogukpinar\*<sup>‡</sup> and Ismail Bozkurt\*\*

\*Department of Energy Systems Engineering, Faculty of Technology, University of Adiyaman, Adiyaman 02040, Turkey,

\*\*Department of Mechanical Engineering, Faculty of Engineering, University of Adiyaman, Adiyaman 02040, Turkey.

(hsogukpinar@adiyaman.edu.tr, ibozkurt@adiyaman.edu.tr)

<sup>‡</sup> Corresponding Author; Haci Soğukpinar, Department of Energy Systems Engineering, Faculty of Technology, University of Adiyaman, Adiyaman 02040, Turkey, Tel: +90 416 223 38 00/2840, hsogukpinar@adiyaman.edu.tr

*Received: 11.06.2015 Accepted: 21.06.2015*

**Abstract-** With the flight of Wright brothers with the first airplane, it has been begun to design different wing section. With the beginning of the new industrial process, hundreds of aerofoils were designed and implemented in the aviation sector. In this study, aerodynamic performance of airplane NACA 2415 aerofoils was numerically investigated to understand effect of angle of attack on the aerodynamic performance. The lift and drag coefficient, lift to drag ratio and power coefficients around NACA 2415 aerofoil were calculated with SST turbulence model and are compared with two different experimental data to validate simulation accuracy of Computational Fluid Dynamics approach. Result indicates that at the low angle of attack, the lift coefficient of NACA 2415 aerofoil obtained in the present study is in a good agreement with experimental results but after zero degree, agreement is not good with experimental results.

**Keywords-** Airplane, airfoil, aerodynamic performance

## 1. Introduction

It is right to claim that airfoil section of plane is the second most important parameters after wing planform area. The lower and upper surfaces are responsible for creating the ideal pressure distribution. The main task of the wing is to create a lifting force. There is a need for specially designed wing shape to the formation of this force and these are called airfoil. Airfoil design is complex and requires significant expertise because it is a very time consuming process. That's why companies like Boeing and Airbus are designed individually for each aircraft airfoil with their own expert staff. But smaller companies are generally use currently available airfoil shape. Airfoils in many different structures were designed by NACA. National advisory Committee for Aeronautics (NACA)- predecessor of present National Administration for Aeronautics and Astronautics (NASA). They are currently available in several books and websites. These airfoils are used as helicopter blades, propeller blades, hydrofoils, and wind turbine blades are just some examples. Efficiencies of all of these blades rely heavily on the airfoil section. With the advent of high speed and powerful computer, there has been developed airfoil design code that is based on conformal mapping. One of the oldest and most

reliable of these codes is Eppler code. That is the reason why two reliable airfoil resources are NACA and Eppler.

Sogukpinar et. al [1] simulated air flow around inclined NACA 632-215 airfoil using SST turbulence model. Lift, drag coefficient, lift to drag ratio and power coefficient around the airfoil were calculated and compared with different velocity. With the increasing of wind velocity, lift and drag coefficient increases, after reaching maximum lift to drag ratio at 4 degree lift to drag ratio starts to decrease again. Mehrdad Ghods [2] experimentally observed lift and drag coefficients of the NACA 2415 airfoil in a wind tunnel. According to the test results, lift coefficient increases as the angle of attack increases between -5 and +17 degrees and at +17 degrees maximum lift was generated. If the angle of attack is increased any further, drag becomes the dominant factor and the wing enters the stall mode. As comparing the theoretical data with experiment, it was observed experimentally a higher drag coefficient. This is because imperfection around airfoil section and experimental inaccuracies. Rajakumar et. al [3] investigated aerodynamic performance characteristics of horizontal-axis wind turbines. The airfoils NACA 4410 and NACA 2415 are taken into consideration for evaluating this proposed approach. It was shown that the approach used in calculation is efficient and

time saving as compared with the commonly used iterative procedures. The results of computational fluid dynamics (CFD) simulations in two and three spatial dimensions were compared to pressure measurements and particle image velocimetry (PIV) flow surveys to assess the suitability of numerical models for the simulation of deep dynamic stall experiments carried out on a pitching NACA 23012 airfoil [4]. The comparison of the airloads curves and of the pressure distribution over the airfoil surface shows that a three-dimensional numerical model can better reproduce the flow structures and the airfoil performance for the deep dynamic stall regime. A NACA 4415 airfoil model was tested in the Ohio State University Aeronautical and Astronautical Research Laboratory 3x5 subsonic wind tunnel under steady state and unsteady conditions [5]. Steady state results of the NACA 4415 testing at Reynolds number of 1 million showed a baseline maximum lift coefficient of 1.35 at 14.3° angle of attack. The numerical simulation of horizontal axis wind turbines (HAWTs) with untwisted blade was performed to determine the optimal angle of attack that produces the highest power output [6]. The power outputs reach maximum at pitch angles: 4.12°, 5.28°, 6.66° and 8.76° for the wind speeds 7.2, 8.0, 9.0 and 10.5 m/s, respectively.

In this study, NACA 2415 airfoil was simulated with low speed airflow to determine optimal angle of attack for airplane wing. Numerical results of original airfoil were compared with experimental data to validate the calculation accuracy of the CFD. Numerical experiment were conducted by varying the pitch angles: -4°, -2°, 0°, 2°, 4°, 6°, 8°, 10° for the wind speed 19.6 m/s. this study indicates that maximum lift to drag ratio reaches at the angle of 4°.

## 2. Materials and methods

The equations solved by the Turbulent Flow, SST interface are the Navier-Stokes equation for conservation of momentum and the continuity equation for conservation of mass. The SST model is a so-called low-Reynolds number model, which means that it resolves the flow all the way down to the wall. SST turbulence model is expressed in terms of  $k$  and  $\omega$  with equation (1) and (2) [7].

$$\rho \frac{\partial k}{\partial t} + \rho u \cdot \nabla k = P - \rho \beta_0^* k \omega + \nabla \cdot ((\mu + \sigma_k \mu_T) \nabla k) \quad (1)$$

$$\rho \frac{\partial \omega}{\partial t} + \rho u \cdot \nabla \omega = \frac{\rho \gamma}{\mu_T} P - \rho \beta \omega^2 + \nabla \cdot ((\mu + \sigma_\omega \mu_T) \nabla \omega) + 2(1 - f_{v1}) \frac{\rho \sigma_\omega \omega^2}{\omega} \nabla \omega \cdot \nabla k \quad (2)$$

Where,  $\rho$  is density,  $u$  is velocity field of wind,  $k$  is turbulent kinetic energy,  $\mu$  is dynamic viscosity of air,  $\omega$  is specific dissipation rate,  $\beta_0^*$ ,  $\sigma_k$ ,  $\beta$ ,  $\sigma_\omega$  are turbulence model parameters.  $P$  is the static pressure and expressed with the equation (3):

$$P = \min(P_k, 10\rho\beta_0^* k\omega) \quad (3)$$

Where,  $P_k$  is production term. The interpolation functions  $f_{v1}$  and  $f_{v2}$  are represented with the equation (4) and (5):

$$f_{v1} = \tanh \left( \min \left[ \max \left( \frac{\sqrt{k}}{\beta_0^* \omega l_\omega}, \frac{500\mu}{\rho \omega l_\omega^2} \right), \frac{4\rho \sigma_\omega^2 k}{\max(\frac{2\rho \sigma_\omega^2}{\omega} \nabla \omega \cdot \nabla k, 10^{-10}) l_\omega^2} \right] \right) \quad (4)$$

$$f_{v2} = \tanh \left( \max \left( \frac{\sqrt{k}}{\beta_0^* \omega l_\omega}, \frac{500\mu}{\rho \omega l_\omega^2} \right)^2 \right) \quad (5)$$

Where  $I$  is intensity and COMSOL default model constants are given by,

$$\beta_1 = 0.075, \gamma_1 = \frac{5}{9}, \sigma_{k1} = 0.85, \sigma_{\omega1} = 0.5, \beta_2 = 0.0828, \gamma_2 = 0.44, \sigma_{k2} = 1.0, \sigma_{\omega2} = 0.856, \beta_0^* = 0.09, \sigma_1 = 0.31.$$

As shown in Figure 1, computational domain consist of a semicircle and rectangular domain which is created with COMSOL. The inlet port is set as a velocity inlet and values are given in Table 1. Outlet port is set as open boundary and no-slip condition is applied for the blade surface. The computational conditions are shown in Table 1.

Table 1. Computational condition

Density	1.20 kg/m <sup>3</sup>
Wind speed	25 m/s, 19.6 m/s
Angle of attack (Deg)	-4,-2,0,2,4,6,8,10
Turbulent kinetic energy	2.090E-7m <sup>2</sup> /s <sup>2</sup>
Specific dissipation rate	1.3889 1/s
Chord lengths	1.8 m, 27 cm
Temperature	193 K
Reference pressure	1 atm
Reference Length	0.2 m
Reynolds number	3,000,000; 341,400

COMSOL is used to generate mesh topology. Due to advantage of minimizing the skewness of a near wall mesh, C-grid mesh is adopted to discrete flow field. A boundary layer mesh is applied with dense element distribution. Domain is optimized based on the number of cells and final mesh distribution which is used for this calculation is shown in Figure 2.

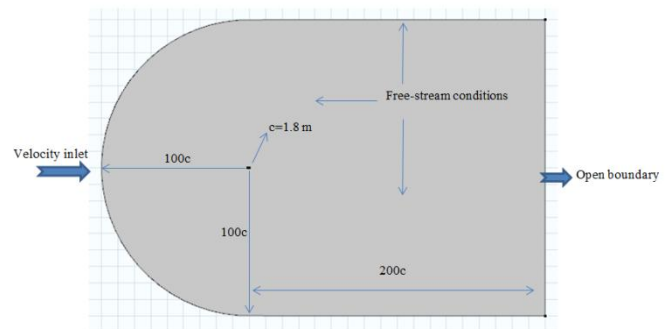


Fig. 1. Computational domain.



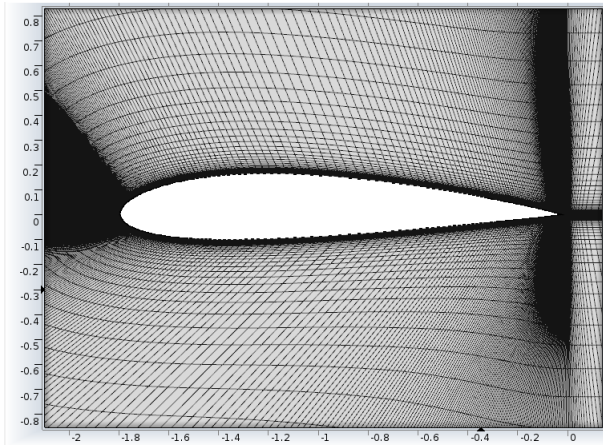


Fig. 2. Mesh distribution around airfoil.

### 3. Results and Discussion

The design of an efficient airplane requires careful balancing many conflicted requirement. This statement is especially true for airplane wing. To find optimum airfoil, NACA designed many different types of airfoil and tested 68 airfoils in wind tunnel in 1931 and published the result as a report [8]. The results were presented in the standard graphic form. Experimental test were conducted at the Reynolds numbers of 3,000,000. Another experiment was conducted in 2001 [2]. For the second experiment related with NACA 2415 airfoil was conducted at open circuit wind tunnels which pull the air from the environment into the tunnel and release the air back into the environment. Airfoil with 1.8 m and 26 cm chord length and 25 m/s and 19.6 m/s airflow speed were chosen for experiments with Reynolds numbers of 3,000,000 and 341,466. Experimental results are available as table data [2] and as a graph [8]. With the numerical simulation method, aerodynamic performance of NACA 2415 airfoil was analyzed to determine optimum angle of attack for maximum lift to drag ratio. Computational results were compared with the field experimental data of ref [2] and ref [8] for turbulent condition. Velocity magnitude and the streamlines for steady flow around the NACA 2415 airfoil at the angle of attack  $10^\circ$  is shown in Figure 3. A location where the air flow speed increases is shown in red color in the graph. This means that low pressures are generated at the upper surface compared with bottom surface of airfoil and upwardly lift force is generated. The blue regions are the region where the lowest air flow dominates. These portions are also the location of turbulent flow. When the flow rate is increased, eddy current occurs in these areas.

Lift coefficients with different angle of attack and experimental results [2,8] are shown in Figure 4 and Figure 5. With the increasing angle of attack lift coefficient increases linearly. There is discernible difference between the computational and experimental results. The agreement between the computational and experimental results is very good at the low angle but at high angles agreement is not good. This may be due to imperfection around airfoil section

and experimental inaccuracies. A fully smooth blade profile in the experimental work is not always possible. But during theoretical calculations, all conditions are considered ideal in the framework of the parameters entered. Drag coefficient with different angle of attack were calculated and is shown in Figure 6. With the increasing angle, drag coefficient starts to decrease and reach minimum at zero angle of attack after then it starts to increase again and continue to increase with the angle.

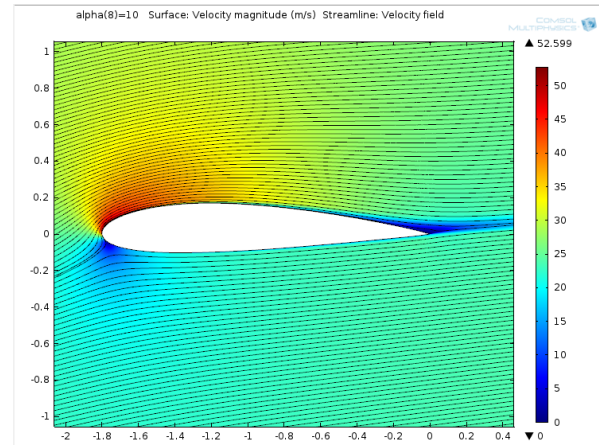


Fig. 3. Velocity magnitude and streamlines for the flow around a NACA 2415 airfoil.

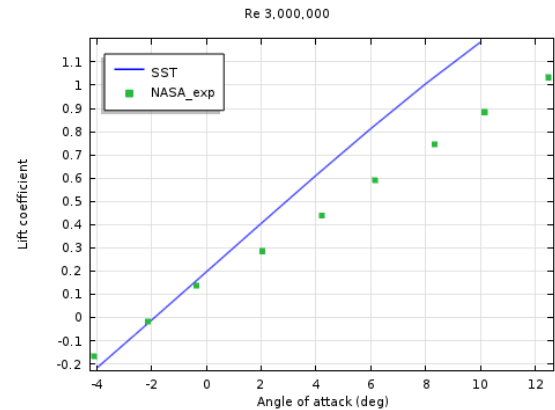


Fig. 4. Lift coefficient vs. angle of attack with NASA experimental data.

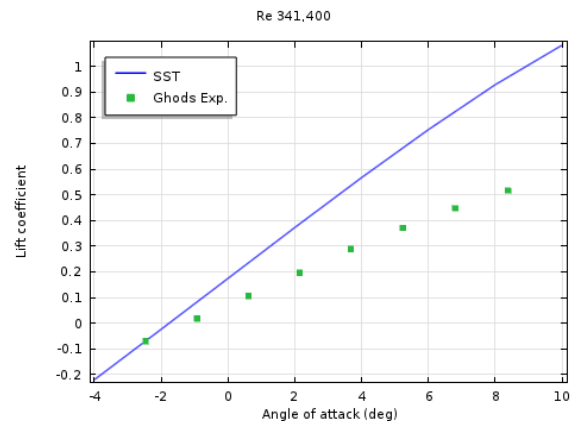
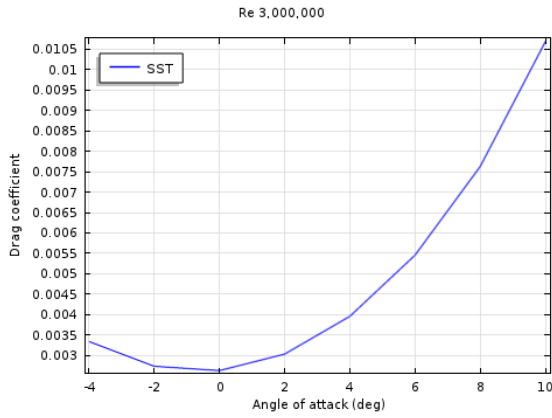
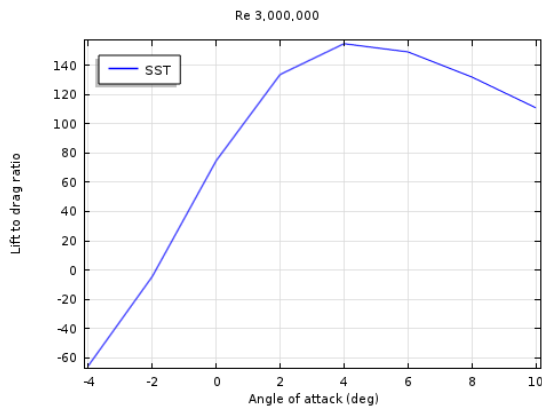


Fig. 5. Lift coefficient vs. angle of attack with Ghods experimental data.



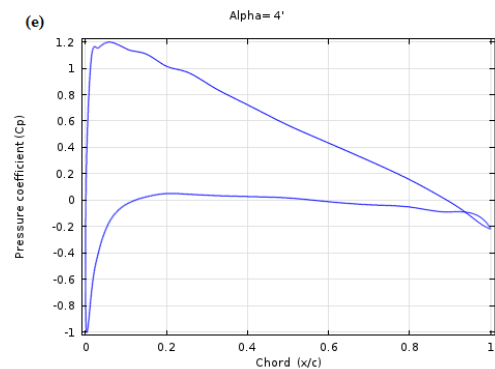
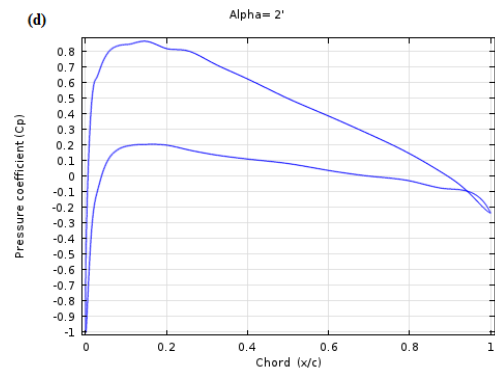
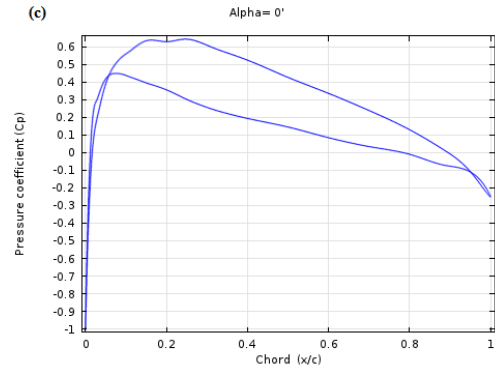
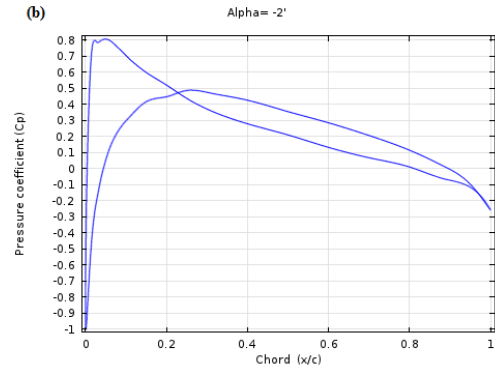
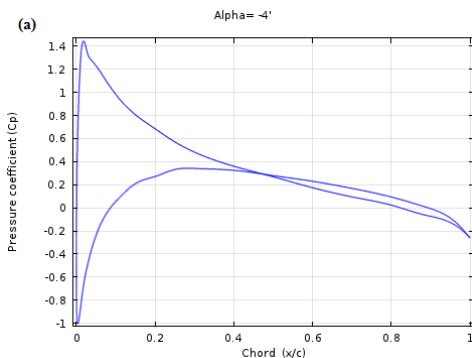
**Fig. 6.** Drag coefficient vs. angle of attack.

Lift to drag ratio was calculated by using SST turbulent model and is shown in Figure 7. Lift to drag ratio increases from  $-4^\circ$  and becomes maximum at the angle of attack 4 degree then it start to decrease again. This figure indicates that optimum angle of attack for NACA 2415 airfoil is  $4^\circ$  at low speed.



**Fig. 7.** Lift to drag ratio vs. angle of attack.

Pressure coefficient for NACA 2415 airfoil at the Reynolds numbers of 3,000,000 were calculated and are shown in Figure 8 for the angle of attack from  $-4^\circ$  to  $10^\circ$ . With the increasing angle of attack from  $-4^\circ$  to  $10^\circ$ , pressure difference between upper and lower surface increases. With the increasing angle, pressure decrement at the upper surface increases more quickly and pressure increment at the lower surface becomes slower.



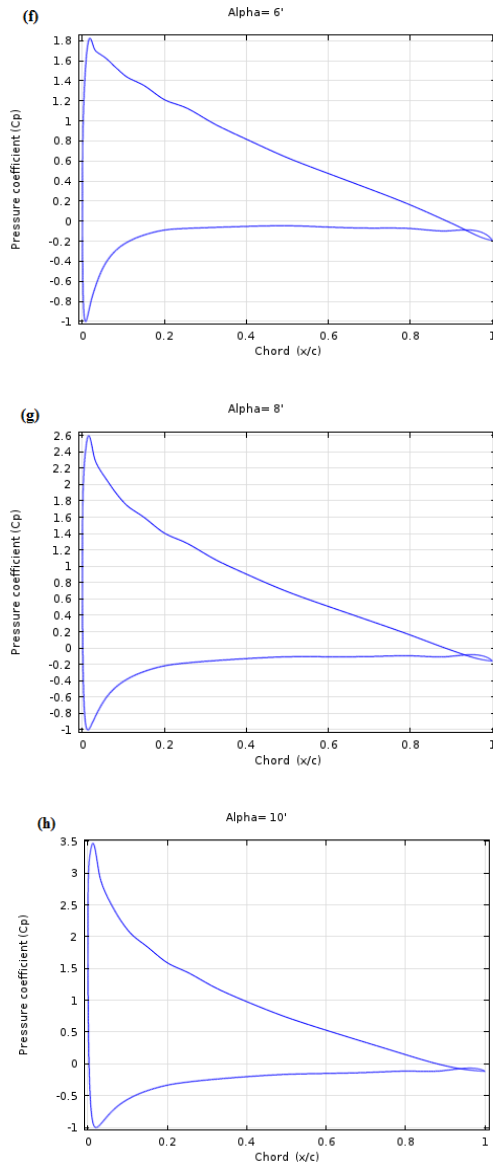


**Fig. 8.** Pressure coefficients of airfoil with different angle of attack.

#### 4. Conclusion

Aircraft wings' horizontal and vertical stabilizers are built up with airfoil-shaped cross sections, as are helicopter rotor blades. Airfoils are also used in propellers, fans, compressors, wind turbines and almost all objects in returning. Sails are also made with the shape of airfoils, and the underwater surfaces of sailboats, are stand in cross-section and actuate on the same principles as airfoils. Swimming and flying creatures employ airfoils, such as bird wings, the bodies of fish etc. People first have made sharing information from birds to fly. In this study, effect of angle of attack on aerodynamic performance of airplane wing airfoil was conducted by CFD with SST turbulence model. Airfoil

NACA 2415 was simulated and results were compared with those two different wind tunnel experiment. The comparison shows good agreement at the low angle of attack but at high angle, agreement is not good with the experiment. Next, drag coefficient were calculated for different angle of attack and minimum drag coefficient were obtained at the angle of  $0^\circ$ . After then drag coefficient increases more quickly with the angle. Then, lift to drag ratios were calculated for different angle of attack from  $-4^\circ$  to  $10^\circ$  and maximum lift to drag ratio was found at the angle of attack  $4^\circ$ . Finally, pressure coefficient for the angle of attack from  $-4^\circ$  to  $10^\circ$  were calculated and analysed. With the increasing angle of attack, pressure difference between upper and lower surface increases with angle.

#### Acknowledgment

I thank Middle East Technical University, allowing me to this work in there with their facility.

#### References

- [1] H.Sogukpinar, I. Bozkurt, "Calculation of Optimum Angle of Attack to Determine Maximum Lift to Drag Ratio of NACA 632-215 Airfoil", Journal of Multidisciplinary Engineering Science and Technology, Vol. 2, pp. 1103-1108, 2015.
- [2] M. Ghods, "Theory of Wings and Wind Tunnel Testing of A NACA 2415 Airfoil, Technical Communication for Engineers", The University of British Columbia, July 23, 2001.
- [3] S. Rajakumar, D. Ravindran, "Iterative approach for optimizing coefficient of power, coefficient of lift and drag of wind turbine rotor", Renewable Energy, Vol. 38, pp. 83-93, 2012.
- [4] A. Zanotti, R. Nilifard, G. Gibertini, A. Guardone, G. Quaranta, "Assessment of 2D/3D numerical modeling for deep dynamic stall experiments", Journal of Fluids and Structures, Vol. 51, pp. 97-115, 2014.
- [5] M. J. Hoffmann, R. Reuss Ramsay, G.M. Gregorek, "Effects of Grit Roughness and Pitch Oscillations on the NACA 4415 Airfoil", Airfoil Performance Report, NREL/TP-442-7815, 1996.
- [6] C. Thumthae, T. Chitsomboon, "Optimal angle of attack for untwisted blade wind turbine", Renewable Energy, Vol. 34, pp. 1279-1284, 2009.
- [7] COMSOL CFD module user guide <http://www.comsol.com>, 2015.
- [8] N.J. Eastman, E.W. Kenneth, R.M Pinkerton, "The characteristics of 78 related airfoil sections from test in the variable-density wind tunnel", NACA report no: 460,1932.

# Seismic Fragility Curves for 1 And 2 Stories R/C Buildings

Muhammed Tekin\*, Ali Gurbuz \*\*

\*Department of Civil Engineering, Faculty of Engineering, Gelisim University, Istanbul

\*\* Department of Civil Engineering, Faculty of Engineering, Recep Tayyip Erdogan University, Rize

mtekin@gelisim.edu.tr, ali.gurbuz@erdogan.edu.tr

‡ Corresponding author; Muhammed Tekin, Department of Civil Engineering, Faculty of Engineering, Gelisim University, Istanbul, mtekin@gelisim.edu.tr

*Received: 20.04.2015 Accepted:23.06.2015*

**Abstract-** In this study, the fragility curves were formed for 1 and 2 stories reinforced concrete (RC) residential buildings. The information regarding the structures was taken from projects of the buildings. Nonlinear pushover (NP) analyze was performed to 84 RC buildings which were divided to 2 groups. The buildings built 1998 and later were called Group-A. The building built before 1998 was called Group B. As for nonlinear analysis, a 3D computer model was drawn for each building and nonlinear analyses were applied to these models. Each building was analysed for 2 dimensions (X and Y). Totally 168 NP analysis were performed for each building. 4 damage limits (slight, moderate, heavy and complete) and 5 damage zones (undamaged, slight, medium, extensive and collapse) were determined according to maximum interstorey drift ratio. Fragility curve parameters were obtained at the result of the NP analysis. Probability density functions were calculated with the help of lognormal mean and lognormal standard deviation values of limit states. The fragility curves were generalized for the buildings in Group A and Group B. At the conclusion of this work; 8 fragility curves obtained for 1 and 2 stories reinforced concrete buildings in. Using these 8 curves; damage possibility can be estimated for RC buildings which have same features.

**Keywords** Fragility curves, regional earthquake risk, low rise reinforced concrete structures

## 1. Introduction

Seismic evaluation of the existing building stock has become a recognized priority after damage and collapse of many reinforced concrete (RC) structures during recent earthquakes [1]. Turkey is frequently exposed to destructive earthquakes. Besides, it is one of several countries in which earthquakes causing loss of lives occur with the shortest return period [2], [3]. It is known that more than 80% of the land of the country is under high seismic risk [4].

Considerable heavy damages have happened because of the earthquakes during the last 10 years [5]. RC buildings built before the modern codes have either collapsed or sustained extensive damage during the past earthquakes because of low quality concrete, poor confinement of the end regions of columns and beams, weak column–strong beam behavior, short column behavior, inadequate splice lengths and improper hooks of the stirrups [4], [6], [7]. ]

There are several study about earthquake damages and loss estimation methods for RC buildings. On the other hand, low rise RC structures are not considered as fragile. Especially one and two-storey buildings are usually ignored. However low rise reinforced concrete (RC) structures are not considered as fragile, there has been

several collapse case in recent earthquakes. The paper aims to develop useful damage estimation tools for 1 and 2 stories RC structures.

## 2. Earthquake Hazard for Turkey

Turkey is located on active faults. The country has hazardous earthquake zones. Turkey earthquake zoning map is shown in Figure 1 [8]. Istanbul is the largest city in Turkey, constituting the country's economic, cultural, and historical center. Istanbul is located on the North Anatolian Fault Line. The city and its surrounding areas have been hit by an estimated above 100 earthquakes over the last years according to the Istanbul municipality's disaster coordination center. More than 110,000 deaths, 250,000 hospitalizations and 600,000 destroyed housing units were recorded across turkey as a result of earthquakes in the 20th century [26], [27].

Many earthquakes have been recording every year in the country. Table 1 shows that four and above magnitude earthquakes which were occurred between 30 days in Turkey and its surrounding areas. Likewise; more than 1800 earthquakes were recorded around the country just over the 30 days according to Republic of Turkey, Disaster and Emergency Management Presidency [9]. Table 1 and Figure 2 show that four and above magnitude earthquakes



occurred between last 30 days (14 March – 15 April 2015) in Turkey and its surrounding areas.

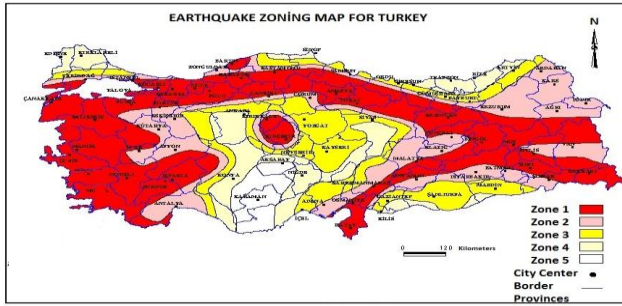


Fig. 1. Earthquake zoning map [8].

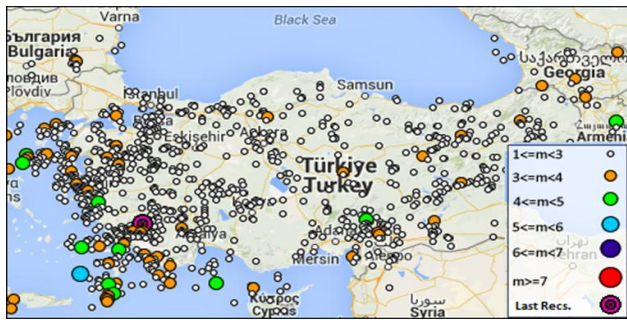


Fig. 2. Earthquake data records for Turkey and its surrounding areas [9].

13 records are shown in table 1. The biggest magnitude earthquake is 5.0 in the table. It was occurred in Aegean Sea, the latitude of 35.7295 and longitude of 26.5760.

**Table 1.** Four and above magnitude earthquakes occurred between 14 March – 15 April 2015 in Turkey and its surrounding areas [9].

DATE (GMT)	LATITUDE	LONGITUDE	DEPTH	RMS	MAGNITUDE	LOCATION
20/06/2015 19:52:47	34.7483	26.3781	7.33	0.77000	4.5	- AKDENIZ-DOGU BASINI
18/06/2015 01:52:58	35.0610	26.6098	20.93	0.90000	4.1	- GIRIT
13/06/2015 01:03:15	38.6620	40.1986	25.11	0.56000	4	Turkey BINGOL
09/06/2015 21:49:50	35.1771	26.8226	12.74	0.87000	5.1	- AKDENIZ-DOGU BASINI
09/06/2015 01:09:03	38.7675	23.4230	5.56	0.48000	5	Greece Greece
09/06/2015 22:20:59	35.3550	26.9141	38.73	0.77000	4.4	ONIKI ADA ONIKI ADA
03/06/2015 09:35:41	40.7560	49.4020	15	0.80000	4.6	Azerbaijan Azerbaijan
01/06/2015 14:54:16	37.5080	43.8820	12.69	0.64000	4	Turkey HAKKARI
30/05/2015 01:56:17	40.2100	21.7920	16.20	0.40000	4	Greece Greece
29/05/2015 08:02:51	36.8703	27.5928	17.01	0.25000	4.1	GOKOVA GOKOVA
29/05/2015 00:03:48	34.9566	26.7278	15.85	0.82000	4.1	AKDENIZ AKDENIZ
28/05/2015 12:59:21	35.0620	26.7396	6.44	0.68000	4.2	GIRIT -

The loss estimation is based on the damage states of the structures. There are several models which can be used to quantify the damages, characterization of damage state and estimation of losses after the earthquakes [11]. Fragility analysis is one of the key components in seismic risk assessment and more specifically in regional seismic risk assessment [12].

For instance, Federal Emergency Management Agency (FEMA) has developed HAZUS methodology for Estimating Potential Losses from Disasters. HAZUS uses a systematic approach for probabilistic damage assessment of structures [13], [14]. As part of these procedures, fragility curves are employed in order to estimate the damage of a building after various intensities of ground motion shaking [15]. Fragility curves express the

probability of the structure reaching or exceeding various damage states as a function of a specific earthquake intensity measure. The function of fragility curves can be assumed as a cumulative distribution function, such as a normal distribution, lognormal distribution or beta distribution [10], [14], [16], [25].

### 3. Fragility Curves

Fragility curve is a useful tool for predicting earthquake risk of buildings with similar characteristics such as material, height and design code level [12]. The curves can be formed using one of three kinds of procedures: (a) the experimental procedure, (b) the nonlinear static analysis based procedure, (c) the dynamic analysis based procedure [17]. The principle of the analytical method which is preferred in this study is to analyze the damage state of structures.

On the other side, fragility curves are cumulative distribution functions that probability of reaching or exceeding a damage state as demand parameters such as story drift ratio (SDR), peak ground acceleration (PGA), spectral acceleration ( $S_a$ ) or spectral displacement ( $S_d$ ) [10], [15], [18], [19]. It has been widely accepted that spectral displacement can be closely correlated with seismic damage of structures [18], [19]. Probability density function of a random variable with lognormal distribution is as follows equation-1:

$$f(x) = \frac{1}{x\sigma_Y\sqrt{2\pi}} \exp \left[ -\frac{(\ln x - \mu_Y)^2}{2\sigma_Y^2} \right], (0 < x < +\infty) \quad (1)$$

In this distribution;  $\mu_Y$  is lognormal mean of variable  $Y$  and  $\sigma_Y$  is lognormal standard deviation of variable  $Y$ .  $\mu_X$  ve  $\sigma_X$  are associated with  $\mu_Y$  ve  $\sigma_Y$  by equation-2 and equation-3.

$$\mu_Y = \ln \left[ \mu_X / \sqrt{\left( \frac{\sigma_X^2}{\mu_X^2} + 1 \right)} \right] \quad (2)$$

$$\sigma_Y = \sqrt{\ln \left( \frac{\sigma_X^2}{\mu_X^2} + 1 \right)} \quad (3)$$

Probability distribution of earthquake damage is assumed to be lognormal distribution. Thus, the analytical expression of fragility curve for a damage level is written as the follows equation-4

$$Pd \geq (d_{s_i} | S_d) = \varphi \left( \frac{\ln(S_d) - \overline{S_{d_{s_i}}}}{\beta_{d_{s_i}}} \right) \quad (4)$$

$Pd$  is probability of damage.  $S_d$  is modal displacement.  $d_{s_i}$  is modal displacement for damage level “i”.  $\overline{S_{d_{s_i}}}$  is mean modal displacement for damage level “i”.  $\beta_{d_{s_i}}$  is lognormal standard deviation of modal displacement values for damage level “i”.  $\varphi$  is cumulative distribution function.

In this study, analytical parameters of fragility curves were obtained by nonlinear static pushover (NP) analysis. In the newly developed performance-based seismic design, NP analysis is one of the useful methods for determining the patterns and levels of damage for assessing a structure's inelastic behavior [20]. NP analysis uses lateral external static forces at floor levels, in combination with inelastic response spectra [21], [22]. Generally, the first mode response of the structures is considered in NP analysis [23]. In case, fundamental mode of vibration is the predominant response of structures [20]. There is a relatively good statistical correlation observed between the earthquake-induced displacement and the extent of structural damage contributed [24, [12]. NP analysis was performed on 3D computer models of the buildings by CSI SAP2000 computer program.

#### 4. Building Stock

1 and 2 stories 84 RC residential buildings discussed within earthquake damage risk. The buildings were selected by random sampling method from municipal archives. Total 84 structures were divided to 2 groups which are Group A and Group B. the buildings built 1998 and later were called Group-A and the building built before 1998 was called Group B. NP analysis was performed to all structures in 2 directions. Parameters of the buildings in Group A and Group B have given in Table 2.

Concrete and reinforcement bar classifications were made according to Turkish Standards TS500 and TS708. A lot of similarities were observed between the buildings built 1998 and later as shown in table 2. Concrete class was usually observed as C16 and reinforcement bars were usually observed as S420.

As for Group B; concrete class was usually observed as C14 and reinforcement bars were usually observed as S220 for Group A. Column and beam sizes were almost similar with Group A. In addition to table 2 and table 3, the slab thickness are usually 10cm, story highness of the buildings are observed between 2,60 and 2,80m for both 2 groups. Stirrups diameter was 8mm in all columns and beams.

#### 5. Modeling and Analysis

In this study; 3D computer models was occurred for buildings to analyze the damage state of structures. As for the modeling issues; columns defined as R/C elements which work for axial load, M2 and M3 moment. Beams also defined as R/C element which working M3 moment. Soil-structure interaction was not considered. All translations and rotations are highlighted for lower ends of the columns at the bottom floor. Otherwise, "Mander model" was used for the stress-strain relation of concrete model (Mander 1988, Ersoy and Ozcebe 2010).

The shear capacity of the section was evaluated based on the code of ATC 32 recommendations. According to ATC – 32, the shear strength of the hoops is determined as:

$$V_s = \frac{A_s f_y d'}{s} \quad (5)$$

Where  $A_s$  is the cross-sectional area of the transverse reinforcement,  $f_y$  is the steel yield strength;  $d'$  is effective depth and  $s$  is the vertical hoops spacing.

The shear strength provided by the concrete is taken as:

$$V_c = 2 \left[ 1 + \frac{P_e}{2000 A_g} \right] \sqrt{f'_c} A_e \quad (6)$$

Where  $P_e$  is the axial compressive force on the column,  $A_g$  is the gross shaft area and  $A_e$  is the effective shear area of column.

3.8 kN/m<sup>2</sup> load was assigned to exterior beams due to brick wall but 2.5 kN/m<sup>2</sup> assigned on the interior beams. The rigid diaphragm effect was modeled using "joint constrains" properties. Plastic hinges were defined on the both upper and lower ends of columns and beams to idealize the nonlinear behavior. Plastic hinge length was considered as half of cross sections.

Nonlinear pushover analyze was applied for each building in two dimensions. Totally, 120 modal capacity curves were obtained at the result of NP analysis. Figure 4 shows that the highest and the lowest capacity curves as an example.

The building B07 (from group B) has the lowest capacity and the building A12 (form goup A) has the higher capacity as shown in figure 3. In addition; general performance of the buildings in group A is higher than the buildings in group B.

After the obtaining modal capacity curves, it was described the damage levels according interstory drift ratio. Table 4 shows that damage levels for low story reinforced concrete frame buildings according to interstory drift ratios.

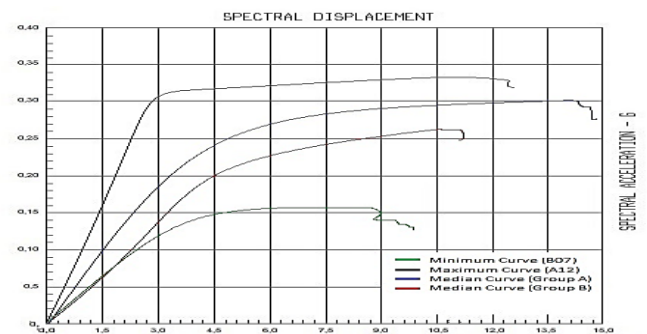


**Fig. 3.** 3D model and Modal Capacity Curve of Building A01 as an example.

**Table 2** Building Parameters of Group A.

Building Code	Project Year	Number of Story	Majority Column Size (cm)	Majority Beam Size (cm)	Concrete Material	Bar Mat.	Soil Type	Plan Irregularity	Short Column
A01	2004	1	25x40	25x50	C16	S420	Z2	No	No
A02	2005	1	30x50	25x50	C16	S420	Z3	No	No
A03	2008	1	30x50	25x50	C16	S420	Z3	No	No
A04	2008	1	40x40	30x50	C14	S220	Z3	No	No
A05	1998	1	25x40	25x50	C16	S420	Z4	No	No
A06	1998	1	30x30	30x50	C16	S220	Z3	No	No
A07	1998	1	30x40	30x60	C20	S420	Z3	No	No
A08	1999	1	25x40	30x50	C16	S420	Z2	Yes	No
A09	1999	1	30x30	30x50	C20	S420	Z3	No	No
A10	1999	1	30x40	30x50	C16	S420	Z3	No	No
A11	1999	1	25x40	25x50	C20	S220	Z4	No	No
A12	1999	1	30x50	30x50	C16	S220	Z3	No	No
A13	1999	1	30x50	30x50	C20	S420	Z4	Yes	No
A14	2000	1	25x40	25x50	C16	S420	Z3	No	No
A15	2000	1	30x40	30x50	C16	S420	Z4	No	No
A16	2001	2	25x50	25x50	C16	S420	Z4	No	No
A17	2001	2	30x30	25x50	C16	S420	Z3	No	No
A18	2001	2	30x50	25x50	C16	S420	Z2	No	No
A19	2001	2	30x30	25x50	C20	S420	Z3	No	No
A20	2002	2	25x40	30x50	C16	S420	Z3	No	No
A21	2002	2	30x40	25x50	C16	S420	Z3	No	No
A22	2002	2	30x40	30x50	C16	S420	Z3	No	No
A23	2003	2	25x40	30x50	C16	S420	Z3	No	Yes
A24	2003	2	30x30	25x50	C16	S420	Z3	Yes	No
A25	2003	2	40x40	30x50	C16	S420	Z2	Yes	No
A26	2003	2	30x30	30x50	C16	S420	Z3	No	No
A27	2003	2	25x40	25x50	C16	S420	Z2	No	No
A28	2003	2	25x40	25x50	C18	S420	Z3	No	No
A29	2003	2	30x40	30x50	C16	S420	Z4	No	No
A30	2003	2	30x30	25x50	C14	S420	Z3	No	No
A31	2003	2	40x40	25x50	C16	S420	Z3	No	No
A32	2004	2	25x40	30x60	C16	S420	Z3	No	No
A33	2004	2	40x40	25x50	C16	S420	Z3	No	No
A34	2004	2	25x40	25x50	C20	S420	Z2	No	No
A35	2004	2	25x40	30x60	C16	S420	Z2	No	Yes
A36	2004	2	30x30	25x50	C16	S420	Z3	No	Yes
A37	2004	2	30x30	30x50	C16	S420	Z4	No	No
A38	2005	2	40x40	25x50	C16	S420	Z3	No	No
A39	2005	2	25x40	30x50	C16	S420	Z4	Yes	No
A40	2005	2	25x40	25x50	C20	S420	Z4	No	No
A41	2006	2	40x40	30x60	C20	S420	Z3	Yes	No
A42	2006	2	30x30	30x50	C20	S420	Z3	Yes	No
A43	2006	2	25x30	30x60	C20	S420	Z4	No	No
A44	2006	2	25x40	25x50	C20	S420	Z3	No	No
A45	2007	2	40x40	30x60	C20	S420	Z2	No	No
A46	2008	2	30x30	30x50	C20	S420	Z3	No	No
A47	2008	2	25x30	25x50	C20	S420	Z3	No	Yes
A48	2008	2	25x40	30x50	C20	S420	Z3	Yes	No
A49	2008	2	25x30	25x50	C20	S420	Z2	No	No
A50	2008	2	25x30	25x50	C20	S420	Z2	No	No
A51	2008	2	30x30	25x50	C20	S420	Z3	No	No
A52	2009	2	40x40	30x60	C20	S420	Z4	No	No
A53	2009	2	25x40	25x50	C20	S420	Z4	No	No
A54	2009	2	25x40	30x50	C20	S420	Z3	No	No
A55	2009	2	30x30	25x50	C20	S420	Z3	No	No
A56	2009	2	25x40	30x50	C20	S420	Z3	No	No
A57	2009	2	25x40	25x50	C20	S420	Z2	No	No
A58	2009	2	25x40	30x60	C20	S420	Z3	No	No
A59	2010	2	30x30	30x50	C20	S420	Z4	No	No

A60	2010	2	40x40	25x50	C20	S420	Z3	Yes	No
A61	2010	2	25x40	30x60	C20	S420	Z3	No	No
A62	2010	2	25x40	30x50	C20	S420	Z4	No	No
A63	2011	2	30x30	25x50	C20	S420	Z3	No	No

**Table 3** Building Parameters of Group B.

Building Code	Project Year	Number of Story	Majority Column Size (cm)	Majority Beam Size (cm)	Concrete Material	Bar Mat.	Soil Type	Plan Irregularity	Short Column
B01	1973	2	30x30	25x50	C16	S220	Z2	Yes	No
B02	1974	2	25x40	25x50	C16	S220	Z3	No	No
B03	1977	2	30x30	25x50	C16	S220	Z3	No	No
B04	1978	2	40x40	30x50	C16	S220	Z3	No	No
B05	1984	1	25x40	25x50	C14	S220	Z3	No	No
B06	1985	2	30x30	25x50	C14	S220	Z3	No	Yes
B07	1986	1	25x40	30x60	C14	S220	Z4	Yes	Yes
B08	1986	2	25x40	25x50	C14	S220	Z3	No	No
B09	1987	2	25x40	25x50	C16	S220	Z3	No	No
B10	1988	2	30x30	25x50	C16	S220	Z3	No	No
B11	1989	2	25x40	25x50	C16	S220	Z2	No	No
B12	1989	2	30x50	25x50	C16	S220	Z3	No	No
B13	1993	2	25x40	25x50	C14	S220	Z3	Yes	No
B14	1995	2	30x30	25x50	C16	S420	Z3	No	No
B15	1995	2	25x40	30x50	C16	S220	Z3	No	No
B16	1996	1	30x50	30x60	C14	S220	Z4	No	No
B17	1996	2	25x40	25x50	C16	S220	Z2	No	No
B18	1997	1	30x30	25x50	C20	S420	Z4	No	Yes
B19	1997	1	30x50	25x50	C16	S220	Z3	Yes	No
B20	1997	2	30x40	25x50	C16	S220	Z3	No	No
B21	1997	2	25x50	25x50	C20	S420	Z2	No	No

**Table 4.** Damage levels according to FEMA HAZUS MH MR 5.

Design Code	Slight Damage (%)	Medium Damage (%)	Heavy Damage (%)	Collapse (%)
Low Code	0,005	0,008	0,02	0,05
Moderate Code	0,005	0,0087	0,0233	0,06

The buildings in Group A were assumed as “moderate code” and the buildings in Group B “were assumed as “low code” in the table.

At the final step of calculations; lognormal mean modal displacement and lognormal standard deviation of modal displacement values were utilized as parameters of fragility curves. All parameters of fragility curves are shown in table 5 for Group A and Group B.

**Table 5.** Parameters of Fragility Curves.

Groups	Sd1 (Slight )		Sd2 (Moderate)		Sd3 (Heavy)		Sd4 (Collapse)	
	LM	LS	LM	LS	LM	LS	LM	LS
A	1,09	0,32	1,66	0,39	2,24	0,39	2,94	0,39
B	0,83	0,37	1,30	0,39	2,31	0,46	3,08	0,40

4 fragility curves were calculated for each group using the parameters in table 5. Figure 5 and Figure 6 show the fragility curves of slight, moderate, heavy and complete damage level for Group A and Group B.

In the literature; the best value for the damage estimation is 50 percent corresponding to the mid-point of fragility curve. Then the Group A buildings would be situated in undamaged zone with more than % 50 probabilities for 3cm modal displacement. Similarly, there is more than %50 probabilities for the buildings to be situated in slight damage zone between 3 and 5,30cm. There is %51 possibility to be in moderate damage zone between 5,30 and 13cm spectral displacement. As for

heavy damage zone, this value changed between 13cm and 19cm. Finally, the buildings have more than %50 possibilities being in collapse zone for above 19cm spectral displacement value.

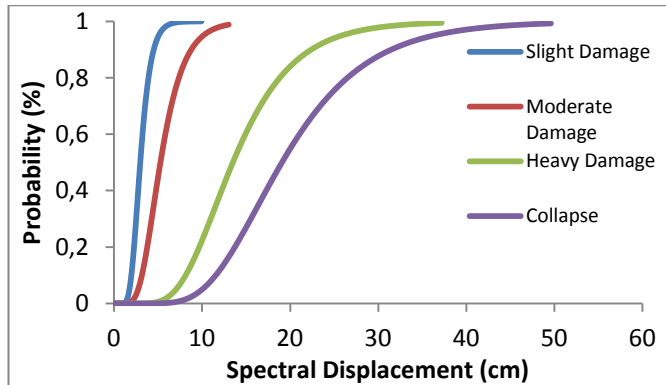


Fig. 4. Fragility curves for Group A.

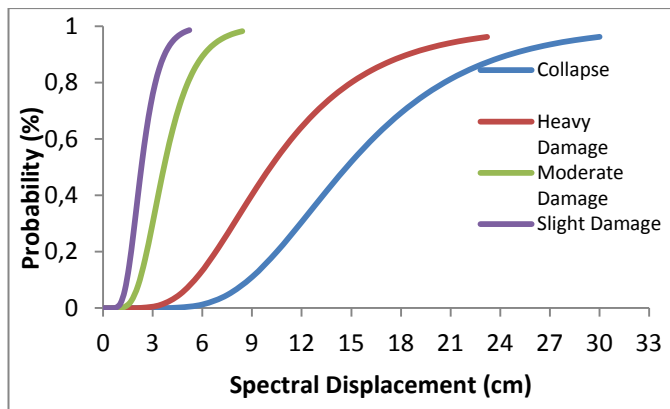


Fig. 5. Fragility curves for Group B.

The Group B buildings would be situated in undamaged zone with more than % 50 probabilities for 2,30cm modal displacement. Then, there is more than %50 probabilities for the buildings to be situated in slight damage zone between 2,30 and 3,65cm. There is %51 possibility to be in moderate damage zone between 3,65 and 10cm spectral displacement. As for extensive damage zone, these values changed between 10cm and 15cm. Finally, the buildings have more than %50 possibilities being in collapse zone for above 15cm spectral displacement value.

## 6. Conclusions

This paper aims at using numerical simulation to develop fragility curves for 1 and 2 stories RC frame structures. Fragility curves were formed for 84 RC residential buildings. The buildings were divided into 2 groups according to year of Turkish Earthquake Code 1998. A 3D computer model was drawn for each building and analysis was applied to these models. 4 damage limits (slight, moderate, extensive and complete) and 5 damage zones (undamaged, slight, medium, heavy and collapse) were determined according to interstory drift ratios of the buildings. Cumulative probability functions were calculated with the help of lognormal mean and lognormal standard deviation values of limit states. Then, fragility

curves that show probability of the damages were generalized.

According to pushover results; the buildings in Group B have lower lateral capacity compared to the buildings in Group A. However modal capacity curves give information about the current status of the buildings, analyses need long time. Therefore, regional studies and rapid risk assessment methods are required. Therewith, a general assessment can be made by the results of the fragility curves.

In this study, it has been observed that fragility curves were close to each other for slight and moderate levels. The Group A buildings would be situated in undamaged zone with more than % 50 probabilities in the range of 0-3cm modal displacement. Similarly, there is more than %50 probabilities for the Group A buildings to be situated in slight damage zone in the range of 3,00-5,30cm, moderate damage zone in the range of 5,30-13cm, heavy damage zone in the range of 13-19cm and collapse zone above 19cm.

Likewise, The Group B group buildings would be situated in undamaged zone with more than % 50 probabilities in the range of 0-2,30cm modal displacement. There is more than %50 probabilities for the Group B buildings to be situated in slight damage zone in the range of 2,30-3,65cm, moderate damage zone in the range of 3,65-10cm, extensive damage zone in the range of 20-15cm and collapse zone above 15cm.

In conclusion; the buildings in Group A have more ductile behavior as compared to Group B. The difference between fragility curves of Group A and Group B was compared for midpoint of the curves. The buildings in Group A have higher displacement capacity than the buildings in Group B. The difference is approximately %30 for slight, heavy and collapse damage states. Nevertheless, the difference is increased to approximately %45 for moderate damage state.

## References

- [1] Thermou, Georgia E., Pantazopoulou, Stavroula J., Elnashai, Amr S. "Design Methodology for Seismic Upgrading of Substandard Reinforced Concrete Structures." *Journal of Earthquake Engineering*, 11 (4), 582-606. 2007. DOI: 10.1080/13632460601031573.
- [2] Doğangün, A., "Performance of reinforced concrete buildings during the May 1, 2003 Bingöl Earthquake in Turkey." *Engineering Structures*, 26 (6), 841-856. 2004. DOI: 10.1016/j.engstruct.2004.02.005
- [3] Yilmaz, S., Tama, Y. S., Bilgin, H., "Seismic performance evaluation of unreinforced masonry school buildings in Turkey." *Journal of Vibration and Control*, 19 (16), 2421-2433. 2012. DOI: 10.1177/1077546312453190
- [4] Kaplan, H., Yilmaz, S., Binici, H., Yazar, E., Çetinkaya, N., "May 1, 2003 Turkey-Bingöl earthquake: damage in reinforced concrete structures." *Engineering Failure Analysis*, 11 (3), 279-291. 2004. DOI: 10.1016/j



- [5] Kaltakci, M. Y., Arslan, M. H., Yilmaz, U. S., Arslan, U. S., "A new approach on the strengthening of primary school buildings in Turkey: An application of external shear wall." *Building and Environment*, 43 (6), 983-990. 2008. DOI: 10.1016/j.buildenv.2007.02.009
- [6] Erdik, M., Şeşetyan, K., Demircioğlu, M. B., Hancılar, U., Zulfikar, C., "Rapid earthquake loss assessment after damaging earthquakes" *Soil Dynamics and Earthquake Engineering*, 31 (2), 247-266. 2011. DOI: 10.1016/j.soildyn.2010.03.009
- [7] Görgülü, T., Tama, Y., S., Yilmaz, S., Kaplan, H., Ay, Z., "Strengthening of reinforced concrete structures with external steel shear walls" *Journal of Constructional Steel Research*, 70, 2012. DOI: 10.1016/j.jcsr.2011.08.010
- [8] Özmen, B., Nurlu, M., Güler, H., "Examination of the earthquake zone with geographic information system" in *The Ministry of Public Works and Settlement Headquarter of Disaster*, pp:9. 1997. URL:deprem.gazi.edu.tr/posts/download?id=43390
- [9] Republic of Turkey, Disaster and Emergency Management Presidency, "Earthquake Database", 2015.URL:<http://www.deprem.gov.tr/sarbis/Shared/Default.aspx>
- [10] Hsieh, M.H., Lee, B. J., Lei, T. C., Lin, J. Y., "Development of medium and low-rise reinforced concrete building fragility curves based on Chi-Chi Earthquake data." *Natural Hazards*, 69 (1), 695-728. 2013. DOI: 10.1007/s11069-013-0733-8
- [11] Hamid, N. H. A., Mohamad, N. M., "Seismic Assessment of a Full-Scale Double-Storey Residential House using Fragility Curve." *Procedia Engineering*, 54, pp: 207-221. 2013. DOI: 10.1016/j.proeng.2013.03.019
- [12] Abo-El-Ezz, A., Nollet, M. J., Nastev, M. "Seismic fragility assessment of low-rise stone masonry buildings." *Earthquake Engineering and Engineering Vibration*, 12(1), 87-97. 2013. DOI: 10.1007/s11803-013-0154-4
- [13] HAZUS, "Earthquake Loss Estimation Methodology." HAZUS Technical Report Federal Emergency Agency and National Institute 4(4). Updated 2014.
- [14] Park, J., Towashiraporn, P., Craig, J. I., Goodno, B. J. "Seismic fragility analysis of low-rise unreinforced masonry structures." *Engineering Structures*, 31(1), 125-137. 2009. DOI: 10.1016/j.engstruct.2008.07.021
- [15] Lignos, D. G., Karamanci, E. "Drift-based and dual-parameter fragility curves for concentrically braced frames in seismic regions." *Journal of Constructional Steel Research*, 90, 209-220. 2013. DOI: 10.1016/j.engstruct.2008.07.021
- [16] Bessason, B., Bjarnason, J. Ö., Gudmundsson, A., Sólmes, J., Steedman, S. "Probabilistic Earthquake Damage Curves for Low-Rise Buildings Based on Field Data." *Earthquake Spectra*, 28 (4), 1353-1378. 2012. DOI: 10.1193/1.4000082
- [17] Wu, D., Tesfamariam, S., Stierner, S. F., and Qin, D. "Seismic fragility assessment of RC frame structure designed according to modern Chinese code for seismic design of buildings." *Earthquake Engineering and Engineering Vibration*, 11 (3), 331-342. 2012. DOI: 10.1007/s11803-012-0125-1
- [18] Su, R. K. L. and Lee, C. L. "Development of seismic fragility curves for low-rise masonry infilled reinforced concrete buildings by a coefficient-based method." *Earthquake Engineering and Engineering Vibration*, 12 (2), 319-332. 2013. DOI: 10.1007/s11803-013-0174-0
- [19] Kircil, M. S., Polat, Z. "Fragility analysis of mid-rise R/C frame buildings." *Engineering Structures*, 28 (9), 1335-1345. 2006. DOI: 10.1016/j.engstruct.2006.01.004
- [20] Zou, X. K., Chan, C. M. "Optimal seismic performance-based design of reinforced concrete buildings using nonlinear pushover analysis." *Engineering Structures*, 27 (8), 1289-1302. 2005. DOI: 10.1016/j.engstruct.2005.04.001
- [21] Makarios, T. K. "Optimum definition of equivalent non-linear SDF system in pushover procedure of multistory r/c frames." *Engineering Structures*, 27 (5), 814-825. 2005. DOI: 10.1016/j.engstruct.2005.01.005
- [22] Belletti, B., Damoni, C., Gasperi, A. "Modeling approaches suitable for pushover analyses of RC structural wall buildings." *Engineering Structures*, 57, 327-338. 2013. DOI: 10.1016/j.engstruct.2013.09.023
- [23] Chopra, A. K., Goel, R. K., Chintanapakdee, C., "Evaluation of a Modified MPA Procedure Assuming Higher Modes as Elastic to Estimate Seismic Demands." *Earthquake Spectra*, 20 (3), 757-778. 2004. DOI: <http://dx.doi.org/10.1193/1.1775237>
- [24] García, R. J., Negrete, M., "Drift-based fragility assessment of confined masonry walls in seismic zones." *Engineering Structures*, 31 (1), 170-181. 2009. DOI: 10.1016/j.engstruct.2008.08.010
- [25] Bessason, B., J. Ö. Bjarnason, A. Gudmundsson, J. Sólmes and S. Steedman (2012). "Probabilistic Earthquake Damage Curves for Low-Rise Buildings Based on Field Data." *Earthquake Spectra* 28(4): 1353-1378.
- [26] Kestler-D'Amours, J. "Turkey Braces for Next Major Earthquake." *Al Jazeera, News (Middleeast)*. (19 Apr 2014). URL: <http://www.aljazeera.com/news/middleeast/2014/03/turkey-braces-next-major-earthquake-201431182932518813.html>
- [27] Istanbul Büyükşehir Belediyesi, "Deprem Master Plan for Istanbul." *Planlama ve İmar Mudurluğu*. (2003).

## **Guide for Authors**

---

The *International Journal of Engineering Technologies (IJET)* seeks to promote and disseminate knowledge of the various topics of engineering technologies. The journal aims to present to the international community important results of work in the fields of engineering such as imagining, researching, planning, creating, testing, improving, implementing, using and asking. The journal also aims to help researchers, scientists, manufacturers, institutions, world agencies, societies, etc. to keep up with new developments in theory and applications and to provide alternative engineering solutions to current.

The *International Journal of Renewable Energy Research* is a quarterly published journal and operates an online submission and peer review system allowing authors to submit articles online and track their progress via its web interface. The journal aims for a publication speed of **60 days** from submission until final publication.

The coverage of IJET includes the following engineering areas, but not limited to:

All filed of engineering such as;

### **Chemical engineering**

- Biomolecular engineering
- Materials engineering
- Molecular engineering
- Process engineering

### **Civil engineering**

- Environmental engineering
- Geotechnical engineering
- Structural engineering
- Transport engineering
- Water resources engineering

### **Electrical engineering**

- Computer engineering
- Electronic engineering
- Optical engineering
- Power engineering

### **Mechanical engineering**

- Acoustical engineering



- Manufacturing engineering
- Thermal engineering
- Vehicle engineering

#### **Systems (interdisciplinary) engineering**

- Aerospace engineering
- Agricultural engineering
- Applied engineering
- Biological engineering
- Building services engineering
- Energy engineering
- Railway engineering
- Industrial engineering
- Mechatronics
- Military engineering
- Nano engineering
- Nuclear engineering
- Petroleum engineering

Types of Articles submitted should be original research papers, not previously published, in one of the following categories,

- Applicational and design studies.
- Technology development,
- Comparative case studies.
- Reviews of special topics.
- Reviews of work in progress and facilities development.
- Survey articles.
- Guest editorials for special issues.

## Editorial Board

---

### ***Editor-in-Chief:***

***Professor ILHAMI COLAK***

### ***Associate Editors:***

***Dr. Selin ÖZCIRA***

***Dr. Mehmet YESILYAPRAK***

## Ethic Responsibilities

---

The publication of an article in peer-reviewed “*International Journal of Engineering Technologies*” is an essential building block in the development of a coherent and respected network of knowledge. It is a direct reflection of the quality of the work. Peer-reviewed articles support and embody the scientific method. It is therefore important to agree upon standards of expected ethical behavior for all parties involved in the act of publishing: the author, the journal editor, the peer reviewer, the publisher and the society of society-owned or sponsored journals.

All authors are requested to disclose any actual or potential conflict of interest including any financial, personal or other relationships with other people or organizations within three years of beginning the submitted work that could inappropriately influence, or be perceived to influence, their work.

Submission of an article implies that the work described has not been published previously that it is not under consideration for publication elsewhere. The submission should be approved by all authors and tacitly or explicitly by the responsible authorities where the work was carried out, and that, if accepted, it will not be published elsewhere in the same form, in English or in any other language, including electronically without the written consent of the copyright-holder.

Upon acceptance of an article, authors will be asked to complete a “Copyright Form”. Acceptance of the agreement will ensure the widest possible dissemination of information. An e-mail will be sent to the corresponding author confirming receipt of the manuscript together with a “Copyright Form” form or a link to the online version of this agreement.

### ***Author Rights***

As a journal author, you retain rights for a large number of author uses, including use by your employing institute or company. These rights are retained and permitted without the need to obtain specific permission from *IJER*. These include:

- ❖ The right to make copies (print or electronic) of the journal article for your own personal use, including for your own classroom teaching use;
- ❖ The right to make copies and distribute copies (including via e-mail) of the journal article to research colleagues, for personal use by such colleagues for scholarly purposes;
- ❖ The right to post a pre-print version of the journal article on internet web sites including electronic pre-print servers, and to retain indefinitely such version on such servers or sites for scholarly purposes

- ❖ the right to post a revised personal version of the text of the final journal article on your personal or institutional web site or server for scholarly purposes
- ❖ The right to use the journal article or any part thereof in a printed compilation of your works, such as collected writings or lecture notes.

## Article Style

---

Authors must strictly follow the guide for authors, or their articles may be rejected without review. Editors reserve the right to adjust the style to certain standards of uniformity. Follow Title, Authors, Affiliations, Abstract, Keywords, Introduction, Materials and Methods, Theory/Calculation, Conclusions, Acknowledgements, References order when typing articles. The corresponding author should be identified with an asterisk and footnote. Collate acknowledgements in a separate section at the end of the article and do not include them on the title page, as a footnote to the title or otherwise.

### ***Abstract and Keywords:***

Enter an abstract of up to 250 words for all articles. This is a concise summary of the whole paper, not just the conclusions, and is understandable without reference to the rest of the paper. It should contain no citation to other published work. Include up to six keywords that describe your paper for indexing purposes.

### ***Abbreviations and Acronyms:***

Define abbreviations and acronyms the first time they are used in the text, even if they have been defined in the abstract. Abbreviations such as IEEE, SI, MKS, CGS, sc, dc, and rms do not have to be defined. Do not use abbreviations in the title unless they are unavoidable.

### ***Text Layout for Peer Review:***

Use single column layout, double spacing and wide (3 cm) margins on white paper at the peer review stage. Ensure that each new paragraph is clearly indicated. Present tables and figure legends in the text where they are related and cited. Number all pages consecutively; use 12 pt font size and standard fonts; Times New Roman, Helvetica, or Courier is preferred.

Research Papers should not exceed 12 printed pages in two-column publishing format, including figures and tables.

Technical Notes and Letters should not exceed 2,000 words.

Reviews should not exceed 20 printed pages in two-column publishing format, including figures and tables.

### ***Equations:***

Number equations consecutively with equation numbers in parentheses flush with the right margin, as in (1). To make equations more compact, you may use the solidus ( / ), the exp function, or appropriate exponents. Italicize Roman symbols for quantities and variables, but not Greek symbols. Use an dash (–) rather than a hyphen for a minus sign. Use parentheses to avoid ambiguities in denominators. Punctuate equations with commas or periods when they are part of a sentence, as in

$$C = a + b$$

(1)

Symbols in your equation should be defined before the equation appears or immediately following. Use “Eq. (1)” or “equation (1),” while citing.

### ***Figures and Tables:***

All illustrations must be supplied at the correct resolution:

- \* Black and white and colour photos - 300 dpi
- \* Graphs, drawings, etc - 800 dpi preferred; 600 dpi minimum
- \* Combinations of photos and drawings (black and white and color) - 500 dpi

In addition to using figures in the text, upload each figure as a separate file in either .tiff or .eps format during submission, with the figure number.

Table captions should be written in the same format as figure captions; for example, “Table 1. Appearance styles.”. Tables should be referenced in the text unabbreviated as “Table 1.”

### ***References:***

Please ensure that every reference cited in the text is also present in the reference list (and viceversa). Any references cited in the abstract must be given in full. Unpublished results and personal communications are not recommended in the reference list, but may be mentioned in the text. Citation of a reference as “in press” implies that the item has been accepted for publication. Number citations consecutively in square brackets [1]. Punctuation follows the bracket [2]. Refer simply to the reference number, as in [3]. Use “Ref. [3]” or Reference [3]” at the beginning of a sentence: “Reference [3] was ...”. Give all authors’ names; use “et al.” if there are six authors or more. For papers published in translated journals, first give the English citation, then the original foreign-language citation.

#### ***Books***

- [1] J. Clerk Maxwell, *A Treatise on Electricity and Magnetism*, 3rd ed., vol. 2. Oxford:Clarendon Press, 1892, pp.68-73.

#### ***Journals***

- [2] Y. Yorozu, M. Hirano, K. Oka, and Y. Tagawa, “Electron spectroscopy studies on magneto-optical media and plastic substrate interface”, *IEEE Transl. J. Magn. Japan*, vol. 2, pp. 740-741, August 1987.

#### ***Conferences***

- [3] Çolak I., Kabalci E., Bayindir R., and Sagiroglu S, “The design and analysis of a 5-level cascaded voltage source inverter with low THD”, *2nd PowerEng Conference*, Lisbon, pp. 575-580, 18-20 March 2009.

#### ***Reports***

- [4] IEEE Standard 519-1992, Recommended practices and requirements for harmonic control in electrical power systems, *The Institute of Electrical and Electronics Engineers*, 1993.

### ***Text Layout for Accepted Papers:***

A4 page margins should be margins: top = 24 mm, bottom = 24 mm, side = 15 mm. Main text should be given in two column. The column width is 87mm (3.425 in). The space between the two columns is 6 mm (0.236 in). Paragraph indentation is 3.5 mm (0.137 in). Follow the type sizes specified in Table. Position figures and tables at the tops and bottoms of columns. Avoid placing them in the middle of columns. Large figures and tables may span across both columns. Figure captions should be centred below the figures; table captions should be centred above. Avoid placing figures and tables before their first mention in the text. Use the abbreviation “Fig. 1,” even at the beginning of a sentence.

Type size (pts.)	Appearance		
	Regular	<b>Bold</b>	<i>Italic</i>
10	Authors’ affiliations, Section titles, references, tables, table names, first letters in table captions, figure captions, footnotes, text subscripts, and superscripts	<b>Abstract</b>	
12	Main text, equations, Authors’ names, <sup>a</sup>		<i>Subheading (1.1.)</i>
24	Paper title		

### **Submission checklist:**

It is hoped that this list will be useful during the final checking of an article prior to sending it to the journal's Editor for review. Please consult this Guide for Authors for further details of any item. Ensure that the following items are present:

- ❖ One Author designated as corresponding Author:
  - E-mail address
  - Full postal address
  - Telephone and fax numbers
- ❖ All necessary files have been uploaded
- Keywords: a minimum of 4
- All figure captions (supplied in a separate document)
- All tables (including title, description, footnotes, supplied in a separate document)
- ❖ Further considerations
  - Manuscript has been "spellchecked" and "grammar-checked"
  - References are in the correct format for this journal
  - All references mentioned in the Reference list are cited in the text, and vice versa

- Permission has been obtained for use of copyrighted material from other sources (including the Web)
- Color figures are clearly marked as being intended for color reproduction on the Web (free of charge) and in print or to be reproduced in color on the Web (free of charge) and in black-and-white in print.

# Article Template Containing Author Guidelines for Peer-Review

First Author\*, Second Author\*\*‡, Third Author\*\*\*

\*Department of First Author, Faculty of First Author, Affiliation of First Author, Postal address

\*\*Department of Second Author, Faculty of First Author, Affiliation of First Author, Postal address

\*\*\*Department of Third Author, Faculty of First Author, Affiliation of First Author, Postal address

(First Author Mail Address, Second Author Mail Address, Third Author Mail Address)

‡Corresponding Author; Second Author, Postal address, Tel: +90 312 123 4567, Fax: +90 312 123 4567,corresponding@affl.edu

*Received: xx.xx.xxxx Accepted:xx.xx.xxxx*

**Abstract-** Enter an abstract of up to 250 words for all articles. This is a concise summary of the whole paper, not just the conclusions, and is understandable without reference to the rest of the paper. It should contain no citation to other published work. Include up to six keywords that describe your paper for indexing purposes. Define abbreviations and acronyms the first time they are used in the text, even if they have been defined in the abstract. Abbreviations such as IEEE, SI, MKS, CGS, sc, dc, and rms do not have to be defined. Do not use abbreviations in the title unless they are unavoidable.

**Keywords-** Keyword1; keyword2; keyword3; keyword4; keyword5.

## 2. Introduction

Authors should any word processing software that is capable to make corrections on misspelled words and grammar structure according to American or Native English. Authors may get help by from word



processor by making appeared the paragraph marks and other hidden formatting symbols. This sample article is prepared to assist authors preparing their articles to IJET.

Indent level of paragraphs should be 0.63 cm (0.24 in) in the text of article. Use single column layout, double-spacing and wide (3 cm) margins on white paper at the peer review stage. Ensure that each new paragraph is clearly indicated. Present tables and figure legends in the text where they are related and cited. Number all pages consecutively; use 12 pt font size and standard fonts; Times New Roman, Helvetica, or Courier is preferred. Indicate references by number(s) in square brackets in line with the text. The actual authors can be referred to, but the reference number(s) must always be given. Example: "..... as demonstrated [3, 6]. Barnaby and Jones [8] obtained a different result ...."

IJRER accepts submissions in three styles that are defined as Research Papers, Technical Notes and Letter, and Review paper. The requirements of paper are as listed below:

- Research Papers should not exceed 12 printed pages in two-column publishing format, including figures and tables.
- Technical Notes and Letters should not exceed 2,000 words.
- Reviews should not exceed 20 printed pages in two-column publishing format, including figures and tables.

Authors are requested write equations using either any mathematical equation object inserted to word processor or using independent equation software. Symbols in your equation should be defined before the equation appears or immediately following. Use “Eq. (1)” or “equation (1),” while citing. Number equations consecutively with equation numbers in parentheses flush with the right margin, as in Eq. (1). To make equations more compact, you may use the solidus ( / ), the exp function, or appropriate exponents. Italicize Roman symbols for quantities and variables, but not Greek symbols. Use an dash (–) rather than a hyphen for a minus sign. Use parentheses to avoid ambiguities in denominators. Punctuate equations with commas or periods when they are part of a sentence, as in

$$C = a + b \tag{1}$$

Section titles should be written in bold style while sub section titles are italic.

### 3. Figures and Tables

#### 3.1. *Figure Properties*

All illustrations must be supplied at the correct resolution:

- Black and white and colour photos - 300 dpi
- Graphs, drawings, etc - 800 dpi preferred; 600 dpi minimum
- Combinations of photos and drawings (black and white and colour) - 500 dpi

In addition to using figures in the text, Authors are requested to upload each figure as a separate file in either .tiff or .eps format during submission, with the figure number as Fig.1., Fig.2a and so on. Figures are cited as “Fig.1” in sentences or as “Figure 1” at the beginning of sentence and paragraphs. Explanations related to figures should be given before figure. Figures and tables should be located at the top or bottom side of paper as done in accepted article format.



Figure 1. Engineering technologies.

Table captions should be written in the same format as figure captions; for example, “Table 1. Appearance styles.”. Tables should be referenced in the text unabbreviated as “Table 1.”

Table 1. Appearance properties of accepted manuscripts

Type size (pts.)	Appearance		
	Regular	<b>Bold</b>	<i>Italic</i>
10	Authors’ affiliations, Abstract, keywords, references, tables, table names, figure captions, footnotes, text subscripts, and superscripts	<b>Abstract</b>	
12	Main text, equations, Authors’ names, Section titles		<i>Subheading (1.1.)</i>
24	<b>Paper title</b>		

#### 4. Submission Process

The *International Journal of Engineering Technologies* operates an online submission and peer review system that allows authors to submit articles online and track their progress via a web interface. Articles that are prepared referring to this template should be controlled according to submission checklist given in “Guide f Authors”. Editor handles submitted articles to IJET primarily in order to control in terms of compatibility to aims and scope of Journal.

Articles passed this control are checked for grammatical and template structures. If article passes this control too, then reviewers are assigned to article and Editor gives a reference number to paper. Authors registered to online submission system can track all these phases.

Editor also informs authors about processes of submitted article by e-mail. Each author may also apply to Editor via online submission system to review papers related to their study areas. Peer review is a critical element of publication, and one of the major cornerstones of the scientific process. Peer Review serves two key functions:

- Acts as a filter: Ensures research is properly verified before being published
- Improves the quality of the research

## 5. Conclusion

The conclusion section should emphasize the main contribution of the article to literature. Authors may also explain why the work is important, what are the novelties or possible applications and extensions. Do not replicate the abstract or sentences given in main text as the conclusion.

## Acknowledgements

Authors may acknowledge to any person, institution or department that supported to any part of study.

## References

- [1] J. Clerk Maxwell, *A Treatise on Electricity and Magnetism*, 3rd ed., vol. 2. Oxford:Clarendon Press, 1892, pp.68-73. (Book)
- [2] H. Poor, *An Introduction to Signal Detection and Estimation*, New York: Springer-Verlag, 1985, ch. 4. (Book Chapter)
- [3] Y. Yorozu, M. Hirano, K. Oka, and Y. Tagawa, "Electron spectroscopy studies on magneto-optical media and plastic substrate interface", *IEEE Transl. J. Magn. Japan*, vol. 2, pp. 740-741, August 1987. (Article)
- [4] E. Kabalcı, E. Irmak, I. Çolak, "Design of an AC-DC-AC converter for wind turbines", *International Journal of Energy Research*, Wiley Interscience, DOI: 10.1002/er.1770, Vol. 36, No. 2, pp. 169-175. (Article)
- [5] I. Çolak, E. Kabalci, R. Bayindir R., and S. Sagiroglu, "The design and analysis of a 5-level cascaded voltage source inverter with low THD", *2nd PowerEng Conference*, Lisbon, pp. 575-580, 18-20 March 2009. (Conference Paper)
- [6] IEEE Standard 519-1992, Recommended practices and requirements for harmonic control in electrical power systems, *The Institute of Electrical and Electronics Engineers*, 1993. (Standards and Reports)

# Article Template Containing Author Guidelines for Accepted Papers

First Author\*, Second Author\*\*<sup>‡</sup>, Third Author\*\*\*

\*Department of First Author, Faculty of First Author, Affiliation of First Author, Postal address

\*\*Department of Second Author, Faculty of First Author, Affiliation of First Author, Postal address

\*\*\*Department of Third Author, Faculty of First Author, Affiliation of First Author, Postal address

(First Author Mail Address, Second Author Mail Address, Third Author Mail Address)

<sup>‡</sup>Corresponding Author; Second Author, Postal address, Tel: +90 312 123 4567,

Fax: +90 312 123 4567,corresponding@affl.edu

*Received: xx.xx.xxxx Accepted:xx.xx.xxxx*

**Abstract-** Enter an abstract of up to 250 words for all articles. This is a concise summary of the whole paper, not just the conclusions, and is understandable without reference to the rest of the paper. It should contain no citation to other published work. Include up to six keywords that describe your paper for indexing purposes. Define abbreviations and acronyms the first time they are used in the text, even if they have been defined in the abstract. Abbreviations such as IEEE, SI, MKS, CGS, sc, dc, and rms do not have to be defined. Do not use abbreviations in the title unless they are unavoidable.

**Keywords** Keyword1, keyword2, keyword3, keyword4, keyword5.

## 1. Introduction

Authors should any word processing software that is capable to make corrections on misspelled words and grammar structure according to American or Native English. Authors may get help by from word processor by making appeared the paragraph marks and other hidden formatting symbols. This sample article is prepared to assist authors preparing their articles to IJRER.

Indent level of paragraphs should be 0.63 cm (0.24 in) in the text of article. Use single column layout, double-spacing and wide (3 cm) margins on white paper at the peer review stage. Ensure that each new paragraph is clearly indicated. Present tables and figure legends in the text where they are related and cited. Number all pages consecutively; use 12 pt font size and standard fonts; Times New Roman, Helvetica, or Courier is preferred. Indicate references by number(s) in square brackets in line with the text. The actual authors can be referred to, but the reference number(s) must always be given. Example: "..... as demonstrated [3,6]. Barnaby and Jones [8] obtained a different result ...."

IJRER accepts submissions in three styles that are defined as Research Papers, Technical Notes and Letter, and Review paper. The requirements of paper are as listed below:

➤ Research Papers should not exceed 12 printed pages in two-column publishing format, including figures and tables.

➤ Technical Notes and Letters should not exceed 2,000 words.

➤ Reviews should not exceed 20 printed pages in two-column publishing format, including figures and tables.

Authors are requested write equations using either any mathematical equation object inserted to word processor or using independent equation software. Symbols in your equation should be defined before the equation appears or immediately following. Use "Eq. (1)" or "equation (1)," while citing. Number equations consecutively with equation numbers in parentheses flush with the right margin, as in Eq. (1). To make equations more compact, you may use the solidus ( / ), the exp function, or appropriate exponents. Italicize Roman symbols for quantities and variables, but not Greek symbols. Use an dash (-) rather than a hyphen for a minus sign. Use parentheses to avoid ambiguities in denominators. Punctuate equations with commas or periods when they are part of a sentence, as in

$$C = a + b \quad (1)$$

Section titles should be written in bold style while sub section titles are italic.

## 6. Figures and Tables

### 6.1. Figure Properties

All illustrations must be supplied at the correct resolution:

- Black and white and colour photos - 300 dpi
- Graphs, drawings, etc - 800 dpi preferred; 600 dpi minimum
- Combinations of photos and drawings (black and white and colour) - 500 dpi

In addition to using figures in the text, Authors are requested to upload each figure as a separate file in either .tiff or .eps format during submission, with the figure number as Fig.1., Fig.2a and so on. Figures are cited as “Fig.1” in sentences or as “Figure 1” at the beginning of sentence and paragraphs. Explanations related to figures should be given before figure.



**Fig. 1.** Engineering technologies.

Figures and tables should be located at the top or bottom side of paper as done in accepted article format. Table captions should be written in the same format as figure captions; for example, “Table 1. Appearance styles.”. Tables should be referenced in the text unabbreviated as “Table 1.”

**Table 1.** Appearance properties of accepted manuscripts

Type size (pts.)	Appearance		
	Regular	<b>Bold</b>	<i>Italic</i>
10	Main text, section titles, authors’ affiliations, abstract, keywords, references, tables, table names, figure captions, equations, footnotes, text subscripts, and superscripts	<b>Abstract-</b>	<i>Subheading (1.1.)</i>
12	Authors’ names,		
24	<b>Paper title</b>		

### 6.2. Text Layout for Accepted Papers

A4 page margins should be margins: top = 24 mm, bottom = 24 mm, side = 15 mm. The column width is 87mm (3.425 in). The space between the two columns is 6 mm (0.236 in). Paragraph indentation is 3.5 mm (0.137 in). Follow the type sizes specified in Table. Position figures and tables at the tops and bottoms of columns. Avoid placing them in the middle of columns. Large figures and tables may span across both columns. Figure captions should be centred below the figures; table captions should be centred above. Avoid placing figures and tables before their first mention in the text. Use the abbreviation “Fig. 1,” even at the beginning of a sentence.

## 7. Submission Process

The International Journal of Renewable Energy Research operates an online submission and peer review system that allows authors to submit articles online and track their

progress via a web interface. Articles that are prepared referring to this template should be controlled according to submission checklist given in “Guide f Authors”. Editor handles submitted articles to IJRER primarily in order to control in terms of compatibility to aims and scope of Journal. Articles passed this control are checked for grammatical and template structures. If article passes this control too, then reviewers are assigned to article and Editor gives a reference number to paper. Authors registered to online submission system can track all these phases. Editor also informs authors about processes of submitted article by e-mail. Each author may also apply to Editor via online submission system to review papers related to their study areas. Peer review is a critical element of publication, and one of the major cornerstones of the scientific process. Peer Review serves two key functions:

- Acts as a filter: Ensures research is properly verified before being published
- Improves the quality of the research

## 8. Conclusion

The conclusion section should emphasize the main contribution of the article to literature. Authors may also explain why the work is important, what are the novelties or possible applications and extensions. Do not replicate the abstract or sentences given in main text as the conclusion.

## Acknowledgements

Authors may acknowledge to any person, institution or department that supported to any part of study.

## References

- [7] J. Clerk Maxwell, A Treatise on Electricity and Magnetism, 3rd ed., vol. 2. Oxford:Clarendon Press, 1892, pp.68-73. (Book)
- [8] H. Poor, An Introduction to Signal Detection and Estimation, New York: Springer-Verlag, 1985, ch. 4. (Book Chapter)
- [9] Y. Yorozu, M. Hirano, K. Oka, and Y. Tagawa, "Electron spectroscopy studies on magneto-optical media and plastic substrate interface", IEEE Transl. J. Magn. Japan, vol. 2, pp. 740-741, August 1987. (Article)
- [10] E. Kabalcı, E. Irmak, I. Çolak, "Design of an AC-DC-AC converter for wind turbines", International Journal of Energy Research, Wiley Interscience, DOI: 10.1002/er.1770, Vol. 36, No. 2, pp. 169-175. (Article)
- [11] I. Çolak, E. Kabalci, R. Bayindir R., and S. Sagiroglu, "The design and analysis of a 5-level cascaded voltage source inverter with low THD", 2nd PowerEng Conference, Lisbon, pp. 575-580, 18-20 March 2009. (Conference Paper)
- [12] IEEE Standard 519-1992, Recommended practices and requirements for harmonic control in electrical power systems, The Institute of Electrical and Electronics Engineers, 1993. (Standards and Reports)



# INTERNATIONAL JOURNAL OF ENGINEERING TECHNOLOGIES (IJET)

## COPYRIGHT AND CONSENT FORM

This form is used for article accepted to be published by the IJET. Please read the form carefully and keep a copy for your files.

**TITLE OF ARTICLE (hereinafter, "The Article"):**

.....

.....

.....

**LIST OF AUTHORS:**

.....

.....

.....

**CORRESPONDING AUTHOR'S ("The Author") NAME, ADDRESS, INSTITUTE AND EMAIL:**

.....

.....

.....

### COPYRIGHT TRANSFER

The undersigned hereby transfers the copyright of the submitted article to International Journal of Engineering Technologies (the "IJET"). The Author declares that the contribution and work is original, and he/she is authorized by all authors and/or grant-funding agency to sign the copyright form. Author hereby assigns all including but not limited to the rights to publish, distribute, reprints, translates, electronic and published derivatives in various arrangements or any other versions in full or abridged forms to IJET. IJET holds the copyright of Article in its own name.

Author(s) retain all rights to use author copy in his/her educational activities, own websites, institutional and/or funder's web sites by providing full citation to final version published in IJET. The full citation is provided including Authors list, title of the article, volume and issue number, and page number or using a link to the article in IJET web site. Author(s) have the right to transmit, print and share the first submitted copies with colleagues. Author(s) can use the final published article for his/her own professional positions, career or qualifications by citing to the IJET publication.

Once the copyright form is signed, any changes about the author names or order of the authors listed above are not accepted by IJET.

**Authorized/Corresponding Author**

**Date/ Signature**